APPLICATION OF ERROR CORRECTION CODES FOR ENHANCING DATA INTEGRITY IN POWER LINE CHANNELS

Thesis

Submitted in partial fulfillment of the requirements for the degree of

Doctor of Philosophy

In Engineering

by

Rajeshwari L Itagi
(EE04P4)

DEPARTMENT OF ELECTRICAL AND ELECTRONICS ENGINEERING
NATIONAL INSTITUTE OF TECHNOLOGY KARNATAKA, SURATHKAL,
SRINIVASNAGAR, MANGALORE -575025

August 2012

NATIONAL INSTITUTE OF TECHNOLOGY KARNATAKA, SURATHKAL

D E C L A R A T I O N

by the Ph.D. Research Scholar

I hereby *declare* that the Research Thesis entitled **"APPLICATION OF ERROR CORRECTION CODES FOR ENHANCING DATA INTEGRITY IN POWER LINE CHANNELS"** which is being submitted to the **National Institute of Technology Karnataka, Surathkal** in partial fulfillment of the requirements for the award of the Degree of Doctor of Philosophy in Power and Energy Systems, Department of Electrical and Electronics Engineering is a *bonafide report of the research work carried out by me*. The material contained in this Research Thesis has not been submitted to any University or Institution for the award of any degree.

Rajeshwari L Itagi

EE04P4

Department of Electrical and Electronics Engineering

Place: NITK-Surathkal

Date: 17-05-2013

NATIONAL INSTITUTE OF TECHNOLOGY KARNATAKA, SURATHKAL

C E R T I F I C A T E

This is to *certify* that that the Research Thesis entitled "Application of error correction codes for enhancing data integrity in power line channels**"** submitted by **Mrs. Rajeshwari L Itagi (Register Number: EE04P4)** as the record of the research work carried out by her, is accepted as the Research Thesis submission in partial fulfillment of the requirements for the award of the degree of **Doctor of Philosophy.**

Dr. Vittal K. P.
Prof.& H.O.D.,E&E Engg.
National Institute of Technology,
Karnataka, Surathkal, Mangalore.

Dr. U. Sripati
Prof. & H.O.D., E&E Engg
National Institute of Technology,
Karnataka, Surathkal, Mangalore.

Research Guides

Acknowledgements

"All power is within you, you can do anything and everything, do not believe that you are weak, and show the divinity within you" said by great saint Swami Vivekananda is preached by my respectable guides *Dr. Vittal K. P.* and *Dr. U. Sripati*, not by words, but by their disciplined guidance towards completion of my thesis. True that it was an impossible task made possible with the kind cooperation, help and guidance by my dignified guides and I feel that these words express my respect towards them.

This is indeed a great pleasure and a moment of great satisfaction for me to express my sense of profound gratitude and indebtedness to my guides, respected *Dr. Vittal K. P.*, Professor and Head of the Department of Electrical and Electronics Engineering, NITK, Surathkal and *Dr. U. Sripati*, Associate Professor, Department of Electronics and Communication Engineering, NITK, Surathkal, whose zeal and enthusiasm were the source of inspiration for me, giving me necessary platform for conducting my experiments. Their immense help and perfect knowledge has helped me a lot in this endeavor. At the same time they were kind enough to understand my difficulties and guided me properly.

I truly and wholeheartedly convey my gratitude to *Dr. Shubhaga*, DRPC, Department of E&E, NITK, Surathkal, for providing critical progress tips and timely guidance. I also express my gratitude to *Prof. Dr. S. M. Kulkarni,* Department of Mechanical Engineering, NITK, Surathkal, for his kind support and guidance as a member of DRPC, Department of E&E, NITK, Surathkal.

I thank the then Head of the Department of E&E Department, NITK, Surathkal, Late *Dr. Shridhar* , who bestowed kindness and provided support.

I express my sincere thanks to *Prof. Dr. Muralidhar Kulkarni*, Head of the Department of E&C Engg., NITK, Surathkal, for supporting with technical guidance and also supporting with the laboratory facilities.

I am sincerely thankful to *Prof. Dr. D. H. Rao*, former Principal of Gogte Institute of Technology, Belgaum for enlightening the importance of research work and support during my course work.

My sincere thanks to *Prof. Dr. B. S. Anami*, Principal, K. L. E. Institute of Technology, Hubli, for constant support. His encouragement and good wishes helped me to proceed with this difficult task. I convey my thanks to Management of K.L.E.Society's KLEIT, Hubli, for being kind to provide study leave to complete the course.

I also express my sincere thanks for the moral support given by *Prof. R. R. Burbure*, Dean Academics, KLEIT, Hubli. My special thanks to *Prof. Manu T. M.* H.O.D. E&C, KLEIT, Hubli, for his support and kind cooperation.

I take this opportunity to convey my gratitude to *Dr. Basavraj Humbarwadi* and *Dr. Shreelata B. Humbarwadi*, Bangalore and Prof. Dr. A. C. Hegde and Mrs. Sunanda Hegde, NITK, Surathkal for their encouragement towards the completion of my thesis writing.

I acknowledge the priceless all time support received from my sister *Leelavati A. Ashtagi* and thank for her novel understanding. I also convey my gratitude to Late *Mr. Ashok Astagi* for the concern and support shown towards completion of my doctorate degree. I acknowledge the infinite love and affection showered and support received by my dear sister Late *Mrs. Mahadevi G.,* who left us in 2011. I express my sincere thanks to my brothers Shrikant and Shivanand for their wishes and encouragement. I also acknowledge the good wishes received by Shri. S. S. Itagi, Mrs. Sulochana Itagi, Mrs. Shridevi Shrikant and Mrs. Geeta Shivanand. I dedicate this work to my father *D. B. Vanaki* and my mother *Anasuya*, a source of inspiration for me.

Thanks to my husband *Lingraj S. Itagi,* for his unparalleled support for the entire duration of completion of this course, without which the task would be impossible. I thank the Management of Punjab National Bank for their kind cooperation in my endeavor. I specially thank my children *Tejaswini* and *Vinaykumar* for their invaluable support, extraordinary understanding, cooperation and patience during long hours of my work. The deprival of mother's care at times I was away from home is the sacrifice from their side towards the completion of this course, which I respectfully acknowledge and I feel blessed to have such wonderful children. And last but not the least I thank Almighty God.

Rajeshwari L Itagi

Abstract

The use of existing power lines for home/industry/substation automation has drawn the attention of many researchers in the recent years because this infrastructure is easily available everywhere. However, the Power Line channel has been primarily designed for power transfer at low frequencies. Hence, the propagation characteristics of this channel are not well suited to support high speed data transmission and ensuring reliable high speed and error free data transmission on this channel is a very challenging task. Many researchers have been attracted to this challenging field in recent years and a variety of techniques from the domain of Digital Signal Processing and Communication Engineering have been applied to solve some of the challenges posed by this application.

The three critical channel parameters namely noise, impedance and attenuation are found to be highly unpredictable and variable with time, frequency and location. Further, the regulatory standards designed to prevent spurious radiation restrict the carrier power that can be used for digital modulation.

In this work, we have concentrated on the use of Medium Voltage (MV) Power Line (< 30 kV) for narrow band applications. After a study of relevant literature and an understanding of mathematical models used to describe the variation of channel parameters, a suitable model has been simulated in MATLAB® platform. Simulation results presented by the channel model have been obtained for different channel conditions such as line length, noise variations and variations in transfer function (attenuation) of the channel and for different data size. The frequency band employed in narrowband power line communication is restricted to a value less than 500 kHz.

An effort is made in the thesis to devise a powerful error correcting code which can eliminate the errors caused by channel impairments. Power line channel is modeled using multipath model. As noise experienced on power line channels is a mixture of Gaussian and Impulsive varieties, it is modeled by using the Middleton Class-A pdf. Taking into account the channel behavior; two channel coding strategies were deployed. In the first approach a four state Turbo code was combined with a 32-carrier OFDM modulator and the performance of this combination was studied under various channel conditions. In the second approach, a Bose-Choudhari-Hocquenghem (BCH)

code was concatenated with the Alamouti Space-Time Block code and the performance of the channel was similarly evaluated.

To realize the Turbo coded OFDM scheme, a four state Turbo code using Recursive Systematic Convolutional (RSC) encoder/decoder pair was designed. The output of the encoder was modulated by 32 sub carrier OFDM (designed using IFFT and FFT). The efficacy of this arrangement in ensuring data integrity over the MV power line channel was tested.

To realize the second approach, a BCH code with parameters $n = 63, k = 36, t = 5$ was designed and encoding/decoding processes were implemented. BCH code in concatenation with Alamouti 2x1 space time code (with PSK modulation) was tested. A partial hardware implementation was realized by employing a Digital Signal Processor TMS 320C6713 for encoding/decoding and MATLAB® for simulating the power line channel. Data input present in text form encoded and decoded after transmission through the channel. This process allows the visualization of the power of error correction algorithms.

Performance evaluation of the two proposed schemes for channel code and modulation design namely Turbo coded OFDM and BCH coded space time code were carried out. The performance criteria for the evaluation include the bit error rate (BER) at a specific signal to noise ratio (SNR). The reflections at branching points (load locations) vary the attenuation profile of the link. As a result, the effect of different parameters on the channel attenuation was observed based on the number of loads and length of the link. A BER analysis was performed to compare the performance of the channel under impulsive noise conditions under three impulsive scenarios. The first scenario was specified as $A = 0.1,\ T = 0.1$. The second scenario was specified as $A = 0.1,\ T = 0.01$ and the the third scenario was specified as $A = 0.1,\ T = 0.001$.

A comparison of the relative performance of uncoded and coded schemes reveals the following:

- Scheme 1 achieves BER of 10^{-5} at SNR=55 dB for $A = 0.1, T = 0.1$(case 1 impulse noise), with channel attenuation varying between 10 dB to 50 dB. Scheme 2 achieves BER of 10^{-5} at SNR=50dB for $A = 0.1, T = 0.1$(case 1 impulse noise), with channel attenuation on two paths varying between 18 dB and 6 dB.

- Both schemes have achieved a BER of 10^{-5} at SNR=66 dB for $A = 0.1, T = 0.01$(case 2 impulse noise), with 10dB to 50 dB channel attenuation for scheme 1 and with 16 dB and 34 dB channel attenuation on two paths for scheme 2.

  Following remark can be made with reference to the discussion on results:

Both schemes 1 and 2 have given equivalent performance under similar channel conditions (attenuation and noise), when the error correcting capacity of channel code used in scheme 2 is $t = 5$.

After a thorough study and implementation of both approaches, it was observed that both schemes exhibit equivalent performance under similar channel conditions (attenuation and noise levels). With enhanced error correction capacity with t=11, a BCH coded space time code will require lesser SNR to give the same performance as OFDM under similar channel conditions.

Keywords:

Power line Communication (PLC), Impulsive noise, Turbo code, Bose-Choudhari-Hocquenghem (BCH) code, Orthogonal Frequency Division Multiplexing (OFDM), Space Time Coding, Signal to Noise Ratio (SNR), Bit Error Rate (BER).

CONTENTS

4 MODELING POWER LINE COMMUNICATION CHANNEL

5 RESULTS AND CONCLUSION

LIST OF FIGURES Page Number

LIST OF TABLES Page Number

LIST OF ABBREVIATIONS

APP - A Posteriori Probability

AWGN - Additive White Gaussian Noise

BCH - Bose-Chaudhuri-Hocquenghen

BCJR - Bahl Cocke Jelinek Raviv

BER - Bit Error Rate

BM - Baerley kamp Massey

BPL - Broadband over Power Lines

CP - Cyclic Prefix

CSI - Channel State Information

DSP - Digital Signal Processing

FEC - Forward Error Correction

GF - Galois Field

LLR - Log Likelihood Ratio

Mbit/s - Mega bits per second

MHz - Mega Hertz

MIMO - Multiple Input Multiple Output

MV - Medium Voltage

NBPLC - Narrowband Power Line communication

OFDM - Orthogonal Frequency Division Modulation

PDF - Probability Density Function

PLC - Power Line Communication

PSK - Phase Shift Keying

PSD - Power Spectral Density

RSC - Recursive Systematic Convolutional

SNR - Signal to Noise Ratio

STBC - Space Time Block Code

XOR - Exclusive OR

NOMENCLATURE

A	impulsive index of Middleton Class-A pdf
g_i	weighting factor
d_{in}	length of path i
τ_i	delay time for path i
$\in_r$	dielectric constant of the insulating material
c_0	speed of light
v_p	speed on the transmission line
α (f)	attenuation factor
a_0 and a_1	attenuation parameters
k	exponent of the attenuation factor
[n, k]	size of BCH encoder
n	code length
k	message length
d_{min}	minimum Hamming distance
t	error-correction capability
T	Gaussian to impulsive noise power ratio

CHAPTER 1

INTRODUCTION

The use of existing power lines for substation automation has drawn the attention of many researchers in recent years. This is because of several reasons.

- The increasing use of sub-station automation has resulted in the need for reliable exchange of enormous amounts of data in real time.
- Power lines constitute the built up infrastructure that is available everywhere. Laying additional cables for communicating data is not practically feasible. Hence, there is an urgent need to design algorithms and protocols which will enable high speed data communication across existing power lines.
- It is expected that with the development of robust modulation and error control protocols, high speed internet traffic can be carried on power lines. If properly designed and implemented, this has the potential of significantly mitigating the last mile problem.

Despite these potential advantages that Power Line Communication systems (PLC) possess, they have not been widely adopted for high speed data communication. This is because of the fact that there are still problems associated with this mode of communication that have not been properly resolved. It is a well known fact that three critical channel parameters namely attenuation, impedance and noise are found to be highly unpredictable and variable with time, frequency and location. Thus the propagating signal encounters unpredictable reflections due to random impedance variations and signal fading due to multiple randomly varying paths set up in the channel in addition to ever-present channel noise. This leads to a situation in which data signals propagating over the line encounter very harsh propagation conditions. In addition, regulatory standards restrict the carrier power used for digital modulation to prevent spurious radiation and meet electromagnetic compatibility (EMC) regulations.

Thus, we have a situation in which channel propagation conditions are harsh, channel bandwidth is limited and there is a constraint on the power that can be launched from the input end. Hence, several advanced digital modulation and coding schemes have been proposed to ensure the integrity of information conveyed over these channels. These schemes are designed to mitigate the effects of channel fading and noise. A number of new developments in the field of Communication Theory and Systems such as Turbo and LDPC (Low Density Parity Check) codes (which are capacity approaching), Multiple Input-Multiple Output (MIMO) systems (which have been proven to be very efficient in combating channel fading effects) have been proposed by many researchers for use in PLC systems. Hence, PLC systems provide researchers working in the field of Communication Systems, an extremely challenging environment in which to design and test efficient modulation and coding schemes.

The primary motivation of this thesis is to derive an efficient combination of error control code and MIMO scheme that will enable the use of existing medium voltage (MV) power line as communication medium for substation automation. Despite the existence of wireless and telephone line modems which can be used for communicating substation automation information, a number of researchers have concentrated on the problem of ensuring reliable communication with reduced carrier power on the power line. This is because this approach has the advantage of using existing infrastructure and is very cost effective for power system communication in sub-station environment.

Many factors can affect how the substation components are linked:

(i) The wide range of temperatures encountered in substation operations requires very robust communication equipment that can withstand harsh environmental conditions.

(ii) Existing conduits, if any, are usually filled to capacity with existing wiring, and hence adding additional wires is usually not possible.

(iii) Running hard wire cables out to the transformers to read monitoring equipment is difficult to accomplish due to underground high voltage wiring.

(iv) With a substation's field consisting of gravel and concrete, trenching is also extremely expensive and time-consuming.

(v) Where a suitable right-of-way between the control house and remote sensors exists, the fiber media converters for SCADA (Supervisory Control and Data Acquisition) are prohibitively expensive and not cost effective.

(vi) The magnetic and electrical fields, along with the high voltage equipment, can interfere with wireless signals, resulting in unknown signal strength and reliability. In addition, lack of security can also be a concern.

Utility substations represent a critical environment, requiring highly precise, real-time monitoring to ensure that catastrophic failures are avoided. Advances in PLC technology have enabled the design and implementation of cost-effective, reliable and real time remote monitoring platforms which can perform monitoring and proper data communication to ensure that substation equipment is kept at the optimum performance levels.

The internationally accepted value for EMC/EMI (Electromagnetic compatibility/Electromagnetic interference) level for Narrowband Power Line Communication (PLC) is 134 dBμV. While meeting this essential requirement (which requires that the data signal launched into the transmission line does not exceed 5V in amplitude), the communication scheme used should provide error free transmission in the presence of significant time and frequency variant channel attenuation, varying channel characteristics and time variant channel noise. Many state of the art technologies such as Spread Spectrum, OFDM (Orthogonal Frequency Division Multiplexing), Channel Codes such as Turbo codes, LDPC codes and Space Time Codes and various combinations of these are being actively considered to enhance the reliability of signals propagating through power lines in sub-station environments.

In the present work, the use of Turbo coded OFDM scheme and BCH (Bose Choudhari Hocquenghem) coded space time code for enhancing data integrity levels in sub-station environments have been studied. Study conducted in this research work indicates that BCH coded space time code can also be a suitable technology that can be

employed to design efficient communication schemes used for narrowband power line communication.

1.1 Scope of research work

The scope of research work has been modularized into the following four phases:

Phase 1: After extensive study of relevant literature, the channel model to be used to represent impairments experienced over a PLC channel was finalized. Power Line Channel is modeled to take into account multi-path effects and impulsive noise in addition to omnipresent Gaussian noise. The applicability of these models to Power Line Channels has been understood by conducting simulation studies.

Phase 2: After understanding the nature of Power Line Channels, several Error Control Codes for possible use in this application were synthesized. After conducting simulation studies to gauge effectiveness of the error control algorithms, the choice of codes to be used was narrowed down to Turbo codes combined with OFDM (Orthogonal Frequency Division Multiplexing) and a concatenated coding arrangement comprising of an inner Alamouti code and an outer BCH code. The Alamouti code was the first Space-Time code to be introduced and is widely deployed in wireless communication (3G) systems. This is an example of a code that has been designed to work in conjunction with Multiple-Input Multiple-Output (MIMO) systems. This code has the following features. It is the only orthogonal STBC that achieves rate-1. This is accomplished without any feedback from the receiver to the transmitter and with small computation complexity. This scheme requires no bandwidth expansion, as redundancy is applied in space across multiple antennas. It can improve the error performance, data rate, or capacity of wireless communication systems. BCH codes have been in continuous deployment since the past four decades. They have been used in information storage systems as well as in communication systems for protecting the information integrity. They are versatile in the sense that they have good random error correcting capability and the encoders/decoders required for their deployment can be easily designed. Hence, they have been deployed in applications as diverse as Flash memories and deep space communication systems.

The encoder and decoder for these approaches were designed and tested on different platforms.

Phase 3: In this phase, efficacy of data transmission was tested using the two schemes (Turbo coded OFDM and concatenated code employing a BCH code combined with Alamouti), on channels perturbed by impairments commonly experienced on PLC channels. The operation of OFDM was implemented using IFFT (Inverse Fast Fourier Transform) and FFT (Fast Fourier Transform) and space time code was realized using Alamouti's 2x1 scheme.

Phase 4: In this phase, a partial hardware implementation was attempted to realize the BCH code along with MIMO system that performed well in simulation studies. To do this, the BCH/Alamouti encoders and decoders were implemented on DSP processor, while the channel model was simulated on a computer running MATLAB®. The performance of the system under various conditions of impulsive noise and channel SNR was studied by sending text information through the system.

It is well known that if perfect Channel State Information (CSI) is available, Space Time codes have the potential to provide very reliable data transfer over fading channels [Vahid Tarokh et al. 1999]. Thus, the use of a Turbo code followed by a Space Time code was tested. However simulations carried out in the present research work indicate that the overall coding gain provided by this scheme as compared to un-coded transmission is not very promising. Ultimately, it was found that the combination of BCH code followed by a space time code gives good results in simulation, yielding good Bit Error Rates (BER) at moderate values of Signal to Noise Ratios (SNR). Thus, looking at all issues, including enhancement of information integrity, throughput and complexity of implementation, it was concluded that the BCH coded Space Time code constitutes a good choice for adoption to preserve and enhance the reliability of information transfer over power lines.

1.1.1 Definition of Power Line Communication (PLC)

Power line communication refers to communication of information with power line as the channel for communication. Digital communication has replaced the former analog PLC. Digital data corresponding to information is encoded first with a suitable channel code (for protecting information integrity) and then modulated using digital modulation schemes. The modulated data being continuous in time is coupled to the high voltage power line by means of a coupling transformer in series with a capacitor. A similar capacitor transformer arrangement at the receiver point is used to collect the distorted and attenuated data. Useful information is sought to be extracted from this waveform by employing suitable algorithms that can compensate for the disturbances introduced by the channel.

1.1.2 Classification of PLC

Power line channels used for data transmission are classified into two categories:

(i) Wideband or Broadband power line communication (BPLC), to transmit and receive internet data which are further classified as:

a) Low voltage (<1 kV) high speed BPLC (>2 Mbps) for internet application.

b) High voltage (>36 kV) high speed BPLC (>2 Mbps) for internet application.

(ii) Narrowband power line communication (NPLC) intended for supervisory or control data transmission on power line for automation application. This is further classified as:

a) Low voltage low speed NPLC for home automation (<100 kbps).

b) Medium voltage (1 kV-30 kV) low speed NPLC for industry automation.

In this work, an attempt has been made to design and validate (with MATLAB® simulation as well as partial hardware implementation) error control schemes that can ensure successful information transfer over medium voltage (1kV-30 kV) low speed NPLC for industry automation.

1.1.3 Limit on the carrier signal level in PLC

The high frequency carrier signal carrying digital data information is coupled to the line carrying power with 50 Hz frequency. Information signal when coupled to the line gets superimposed on 50 Hz line. The transmission line tends to act as antenna and radiate electromagnetic (EM) waves. This feature of the line is undesirable, as the EM radiations may cause interference in other receivers operating in the same frequency range in the immediate vicinity and thus limit their usefulness. A well known and strong opponent of PLC deployment is the association of Radio Amateur Operators. Their opposition is based on their experience that deployment of PLC systems has resulted in severe interference in the frequency bands allotted to them. This is because of non-adherence to the regulatory standards. In the present work, efforts are made to ensure that signal levels in the simulation exercises would be well within the upper limit specified by regulatory authorities. Non adherence to signal strength limits specified by regulators has complicated the widespread setting services of PLC services. This is a negative development because the available infrastructure is not made use of. We cannot afford to have such wastage in a world that is increasingly concerned about inefficient use of resources and the impact of this waste on the environment. Thus it is very important to minimize the signal level so as to prevent spurious radiation and comply with regulatory standards. This gives the motivation to the research and industry community to design, synthesize and deploy transceivers with state of the art channel codes to match the customer requirements of information integrity (quantified by Bit Error Rate (BER) specification) with signal strength limitations imposed by regulatory bodies. In literature, schemes proposing the combination of Reed Solomon codes (RS) concatenated with Turbo codes, followed by Orthogonal Frequency Division Modulation (OFDM) have been suggested. A coding gain of nearly 4 to 5 dB with BER of 10^{-5} at 17 dBs is shown in performance analysis of uncoded and coded OFDM broadband transmission over low voltage power-line channels with impulsive noise [Pouyan Amirshahi et.al. 2006]. In the study of Linear block code with OFDM for power line communication, three channels good (attenuation< 20 dB), average (attenuation 30 to 40 dB) and below average (35 to 60 dB) are considered. BER of 10^{-4} is reached at 14 dB for below average channel and at

12 dB for good channel. The calculated power of carrier signal is given as 4.8 mW for below average channel. Perfect knowledge of the transfer function is assumed at the receiver [Riccardo Pighi 2002]. Performance of OFDM for broadband PLC (frequency range < 20 MHz) is conducted to evaluate the performance by varying path length and BER of the order of 10^{-4} is found at 14 dB of SNR. But in this simulation study, channel noise is not considered [Aminuddin B et al. 2011].

Internationally accepted regulatory bodies such as European Committee for Electrotechnical Standardization (CENELEC), (Federal Communication Commission (FCC) have set the limit for narrow band PLC. General instructions for PLC specified for narrowband PLC is that output signal should be < 134 dBμV (5 V at the signal launching point) [Gotz et al. 2004]. IEEE (Institution of Electrical and Electronic Engineers) standard IEEE 1901.2 is presently active to set the standard for narrowband power line communication.

It is the responsibility of the research community to develop schemes that are simple, practical and effective which can be enthusiastically adopted by industry to unlock the potential of this technique. The creation of this infrastructure will go a long way to make smart grids which require reliable real time transfer of critical information a future reality.

1.1.4 Modulation Schemes used in PLC communication

A variety of digital modulation schemes can be employed for data communication on PLCs. These can range from Amplitude Shift Keying (ASK), Frequency Shift Keying (FSK), Phase Shift Keying (PSK) [Klaus M. Dostert 2003], and it's variants (Q-PSK and M-ary PSK), Quadrature Amplitude Modulation (QAM) to Orthogonal Frequency Division Multiplexing (OFDM) [Ezio Biglieri et al. 2003]. A careful study of the channel model is required before an optimum combination of modulation scheme and error control code can be chosen. In this thesis, two different combinations of channel code and modulation scheme have been studied. In the first part the performance of OFDM combined with a Turbo code was analyzed. In the second part, the performance of PSK with a concatenated code comprising of a BCH code and the Alamouti Space Time code has been studied.

1.1.5 Advantages of Medium Voltage PLC

It has been stated in literature that Power line communication on medium voltage lines is more immune to switching disturbance as compared to low voltage lines [Antti Kosonen 2008], [A. Cataliotti et.al. 2008], [A. Cataliotti et al 2009], [Antonio Cataliotti et al. 2010]. This is because low voltage lines are connected to domestic loads which are switched on and off quite often. Hence the magnitude of impulse noise on these lines is less as compared to low voltage lines. In addition, the frequency band used for communication on medium voltage lines lies outside the AM radio range (frequency band of 3-148.5 kHz governed by Committee European de Normalization Electro technique Regulation-CENELEC in Europe, 10-490 kHz governed by Federal Communication Commission-FCC in USA, 10-450 kHz governed by ARIB (Association of Radio Industries and Businesses) in Japan and 3-500 kHz governed by EPRI (Electric Power Research Institute) in China. The attenuation offered by the power line is a function of frequency; typically, these lines offer less attenuation at lower frequencies than at higher frequencies.

1.1.6 Power line channel model

The power line is characterized by distributed taps (representing users or loads) at different locations. These loads are switched on and off at random. Thus the impedance seen looking into is time variant and can change randomly from instant to instant. As a result of random impedance variation, multiple reflections can be set up at various locations along the line. Thus the signal at any location can be viewed as the superposition of several wave fronts, sometimes combining constructively and sometimes destructively. This phenomenon is similar to multi-path communication in wireless channels which manifests as signal fading (random fluctuation of signal strength with time at a point). Hence, researchers have attempted to describe the power line channel using mathematical models developed for multipath wireless channels. It has been shown that the magnitude response of channel varies with respect to time as well as with frequency [K H Zuberi 2003], [Halid Hrasnica et al. 2004], [Suljanovic N. et al. 2004], [Stephen Robson et al. 2009], [Antonio Cataliotti et al. 2010].

Thus, any mathematical model used to describe the channel must be able to convey variations with respect to both time and frequency. In our study, we have used a model that exhibits random variations with time as well as frequency to accurately mimic the functioning of the channel.

1.1.7 Impulse noise on power line

A distinctive feature of the power line channel is the presence of strong and time-varying nonwhite noise arising due to random connection and disconnection of loads. Researchers have demonstrated that the Middleton Class-A noise is well suited to describe this phenomenon, [D. Umehara et al. 2004], [M Katayama et al. 2006] [Christine Hsu et al. 2007]. This probability density function (pdf) is described by the equation,

$$f(x) = \sum_{m=0}^{\infty} \frac{A^m}{m!} e^{(-A)} \left[\frac{1}{\sqrt{2\pi\sigma_m^2}} \right] e^{\left(\frac{-x^2}{2\,\sigma_m^2}\right)} \qquad (1.1)$$

Various impulse levels can be set by varying the parameters A and T in this model [Leslie A. Berry 1981]. This pdf is used in the simulation of this research work, to obtain noise samples in the time domain [Leslie A. Berry 1981].

1.2 Thesis Objectives

In this thesis, an attempt has been made to formulate strategies which can be used to ensure information integrity during the process of data transfer over medium voltage power lines. The thesis begins with a discussion which highlights the importance of PLC technology in a world where resources are becoming increasingly scarce and concern for environmental degradation is constantly increasing. This is followed by a discussion of the state of the art technology in which the research work pertinent to this topic has been briefly described. In the following chapters, a brief overview of Error Control Codes and design procedures used to synthesize BCH codes are presented. Subsequently, the application of Orthogonal Frequency Division Multiplexing (OFDM) and Space Time Coding (STC) to control the effects of channel induced errors is discussed. This is followed by a discussion of the nature of multi-path effects on the

power line channel which requires that the channel be visualized as possessing multiple uncorrelated paths. The use of BCH coded Space Time Code is discussed and a partial hardware realization of this approach is implemented to check its effectiveness. The thesis has been concluded by outlining a few problems that can be tackled by future researchers in this field.

1.3 The main contributions of the dissertation

The main contributions made in this thesis are listed below.

- Design and simulation of a concatenated arrangement involving a Turbo code combined with OFDM using 32 sub carriers and a study of the effectiveness of this arrangement in combating the channel impairments experienced during data transfer on a medium voltage power line.
- Design of a simulation set up to test the effectiveness of BCH coded Space time code for digital data communication over power line where the channel is modeled as being time and frequency variant and the noise is modeled as impulsive.
- Performing Channel State Estimation (CSI) to estimate channel parameters at the receiver. These channel parameters are essential for proper decoding of the Space Time Code. Utilizing the concept of pilot symbol for Channel State Estimation (CSI) for the space time encoding, to assist the real time implementation of the proposed BCH-Space time code for the narrowband power line communication.
- Synthesis of (63, 36) narrow sense, systematic BCH code with 5 bit error correcting capability ($t = 5$). Data was encoded by this code and then encoded a second time using the Alamouti code. The encoder and decoder corresponding to this concatenated code were implemented on a TI (Texas Instrument)'s TMS320C6713 Digital Signal Processor (DSP) [Ralph Chassaing 2002]. The channel model was simulated on a computer. Thus encoded data from the TI DSP processor was presented to the channel model

which introduced the impairments typically associated with the power line channel. The channel output was demodulated and decoded in the decoder running on a second TI processor. Thus, a partial hardware implementation of of the overall scheme was achieved.

After the completion of this work, a comparison of the two approaches was carried out. The comparison is based on the performance of the two schemes which is measured by estimating the bit error rate(BER) at a given value of Signal to Noise ratio (SNR). These results indicate that the two schemes performed equivalently under similar channel (attenuation and noise) conditions and concatenated code comprising of BCH code followed by Alamouti space time code has a scope to be more efficient (by enhancing error correction capacity) and requires lesser bandwidth than that of the Turbo coded-OFDM arrangement.

1.4 Thesis Organization

This thesis includes five chapters, which are briefly summarized below:

The research problem along with a description of the state of art has been introduced in Chapters 1 and 2. The algebraic background required to understand the design of error control codes (also called as channel codes) is provided in Chapter 3. This is followed by a description of the BCH bound and an explanation of the design principles of BCH codes and Turbo codes. Chapter 3 concludes with a description of various digital modulation schemes, an introduction to Orthogonal Frequency Division Modulation (OFDM) and the widely used Alamouti code. Chapter 4 presents a description of power line channel model (including the effects of time and frequency variation). The effect of impulse noise present on power line channels is also considered. Chapter 5 is dedicated to the description of results and their interpretation. Finally a few open research problems (directions for future work) that can be taken up by researchers entering the field are suggested. An appendix is included at the end of the thesis. Appendix A gives a brief technical details about Texas Instruments (TI) Digital Signal Processor (DSP) IC TMS320C6713 experimental kit.

Chapter 2

LITERATURE SURVEY AND REMARK ON PRESENT STATE OF THE ART

After an introduction to the research problem in Chapter 1, a brief description of the state of art is presented in this chapter. An extensive survey of papers published in reputed journals and other documents available in open literature has been carried out. This study has resulted in an understanding of the approach used by other researchers in this field and the limitations of these results. An attempt has been made in this work to incorporate the insight acquired by prior researchers in the field. Based on the foundation provided by this study, state of the art technology has been attempted towards the research problem. A brief review of relevant work and results is presented in the following sections.

2.1 Power line as communication medium

Due to its omnipresence, the electric power distribution grid offers tremendous potential for serving as a medium to facilitate extended fast and reliable communication services. The key advantage of Power line communication (PLC) is that it does not require substantial new investment for the communication infrastructure. PLC has recently gained widespread interest as a viable alternative technology for broadband and narrowband communications.

Power line communication is a wireline technology that is able to use the existing electricity networks for data and voice transmission. It includes Broadband over Power Lines (BPL) with data rates as high as 1 Mbits/s or Narrowband over Power Lines with lower data rate of the order of 100 Kbits/s. The carrier can communicate voice and data by superimposing an analog signal over the standard 50 Hz or 60 Hz alternating current (AC) waveform. Figure 2.1 shows the composite signal of 50 Hz or 60 Hz power signal superimposed with high frequency carrier signal. The high frequency signal suitably modulated with information signal needs to be coupled or injected (from transmitter point) to the power line to form the composite signal shown in Figure 2.1, which then is

propagated over the power line. A coupling arrangement similar to that used at the other end (receiver end) couples the signal to the receiver for information recovery.

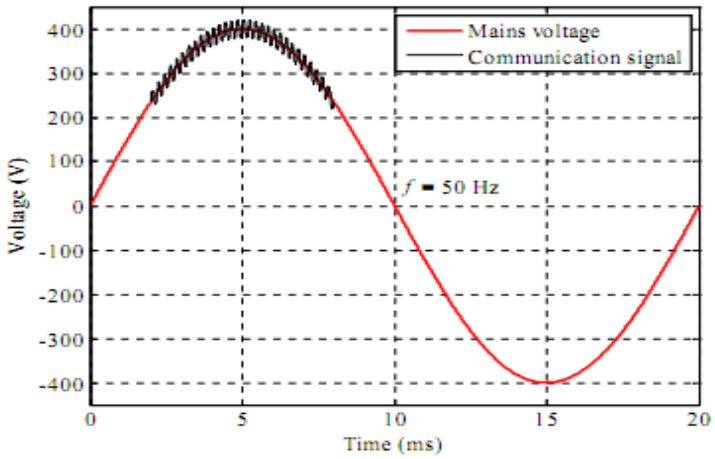

Figure 2.1 Composite signal showing 50 Hz signal superimposed with high frequency carrier signal

A study of literature reveals that two schemes have been widely used to couple data signals to power lines. These are:

- Injecting the information bearing signal to the power line in line–ground configuration.
- Injecting the information bearing signal to the power line in line–line configuration. [A. Cataliotti et al. 2008], [A. Cataliotti et al. 2009].

In the line-ground configuration the signal is injected between the core of one cable and the shield connected to earth. In the line-line configuration, the signal is injected between two phases of a three-phase power system, or between the phase and the neutral conductor of a single-phase power system. In both cases the signal can be injected by capacitive couplers or inductive couplers.

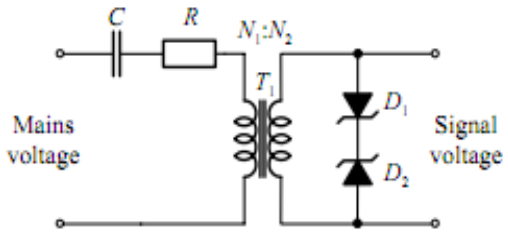

Figure 2.2 Coupling interface used for PLC in a single phase power line (Dostert, 2001).

During the last few decades, power line communication (PLC) has found application both in electricity and indoor distribution networks. However, little attention has been paid to the adoption of this technique to industrial applications [A. Kosonen 2008].

There are several obstacles which have prevented the widespread adoption of this technology. Two serious limitations are:

- Very harsh channel conditions
- Absence of fixed standards.

Since the power grid was originally designed for electrical energy delivery rather than for data transmission, the power line medium does not possess the ideal properties required for a good communication channel. Hence, there is an urgent requirement to evolve and design robust communication techniques that can work effectively in this hostile environment [A. Kosonen 2008]. Channel impairments include heavy attenuation (10 dB/km for medium voltage lines and 100 dB/km length for low voltage lines) [K. H. Zuberi 2003], multi-path propagation, permanent frequency disturbances and impulsive noise. Noise impulses have durations of typically less than 100 μsec [Halid Hrasnica 2004]. A modulation/coding scheme that incorporates frequency- and time diversity can be expected to be robust against both of these disturbances. Another point to be considered is that the high-frequency current flowing in power lines can turn power lines into antennas, which in turn radiate weak radio waves. This is called radiated emission. This can cause interference in the HF band (3-30 MHz) which is widely used for applications such as short-wave broadcasting and amateur radio. Hence, appropriate steps have to be taken to prevent radiation emanating from power lines so that these applications are unaffected.

Another major difficulty for PLC technology is the lack of standardization. There are different standards for different parts of the world, differentiating mainly on the maximum transmitted power and allowable bandwidth limitations.

Despite these limitations, PLC makes a strong case for itself because power line infrastructure is available everywhere. The ability of this system to send high-speed

digital data over the power lines between substations, homes and offices is attracting increasing attention. In seeking to help realize this potential, the Institution of Electrical and Electronics Engineers (IEEE) has developed IEEE P1675, "Standard for Broadband over Power Line Hardware." Testing and verification standards for commonly used hardware, primarily couplers and enclosures for broad band over power line installations and installation methods to enable compliance with applicable codes and standards are available in this document.

2.2 Classification of power line channel

PLC systems have been classified into two groups (Broad band and Narrow band) as briefed in Chapter 1.

- Broadband PLC systems operate in the frequency range of 1 MHz to 30 MHz, and provide data rates of up to 2 Mbps. Current development of broadband PLC technology is directed towards applications in fast Internet access, telephony and home networking.
- On the other hand, narrowband PLC systems operate within the frequency range specified by the European Standard of 3 kHz to 148.5 kHz and the US Standard of 45 kHz to 450 kHz, and provide low data rates up to 100 kbps, with applications in building/home automation, automatic meter reading, real-time pricing and energy management.

2.3 Applications of power line communication

Various fields of application can be envisioned for PLC communication starting with simple inexpensive services embodied into household appliances, where data rates of a few kilobits per second are sufficient.

A second level might be Internet access over the wall socket, where speed is in the lower megabit range [Antonio Cataliotti et al. 2010]. This service can potentially be extended to support high-speed networking that includes fast Internet access, voice over IP (Internet Protocol) and home entertainment (i.e., streaming audio and video at data rates in excess of 10 Mb/s).

Another important field of research is the use of the medium voltage network for communication purpose. This network can be used to convey management and control information for supervision of power plant and distribution facility operations. These tasks call for low data rates in the kilobits per second range.

Thus Power Line Communication (PLC) has also been referred to as power line digital subscriber line (PDSL), power line networking (PLN), or power line telecom (PLT) [Cataliotti et.al. 2010].

Thus when Power Line Communication (PLC) is applied in applications in automation, meter reading, various control applications and in a small number of voice channels, it is classified as Narrowband PLC (less than 100 kbps). Correspondingly, Broadband PLC (greater than 2 Mbps) is applied in Internet access, multiple voice connections, transmission of video signals, high-speed data transmission, in-home networks [Antti Kosonen 2008].

Application of PLC to Medium Voltage networks (1-30 kV) for narrowband is suggested as this type of PLC does not pose any significant interference risk to high frequency (HF) operations. This is because the frequency bands allotted for this application lie less than 500 kHz, a range which is less than that of AM range. Applications intended are remote metering, power quality measurement, fault survey and remote control services. A. Cataliotti et al. [2010] have presented a model for medium voltage power line and have obtained simulation results for a line length ranging between 0.8 to 2 Km with attenuation of less than 25 dB.

2.3.1 Narrowband Power Line Communication (NBPLC), as application for Substation Automation

Many sensor technologies are available to monitor the equipment located within a substation. The challenge lies in transferring the data collected by the sensors cost-effectively and efficiently back to the control house, or regional control center, without compromising security, speed or reliability. This can be conveniently achieved by PLC. A medium voltage substation is required to work in between a high voltage generating station (or a substation) and low voltage consumers as shown in Figure 2.3.

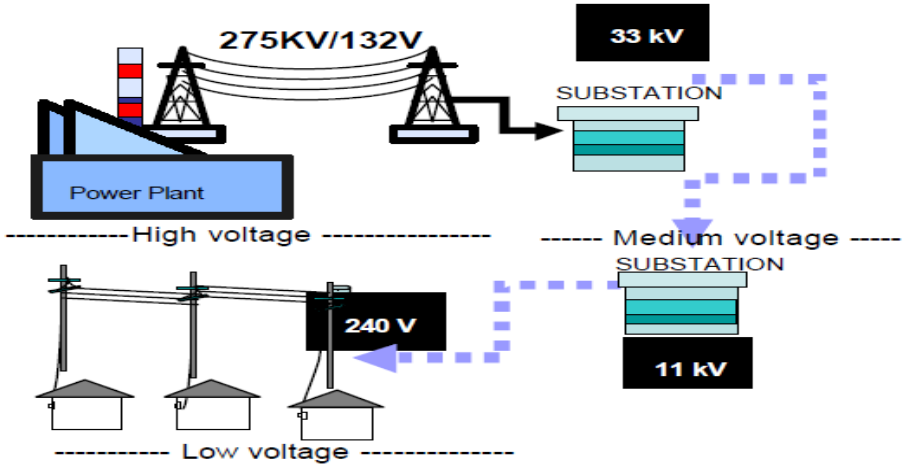

Figure 2.3 Substation with medium voltage, placed between power plant and consumer points. [White paper, Malaysian Communication and Multimedia Commission, 2005].

Automation with PLC could revolutionize the monitoring of critical real-time parameters which can lead to more efficient and safe operation of electrical utilities. With development of suitable signaling protocols, which can increase PLC reliability levels and cost effectiveness, the use of dedicated cabling can be done away with. [Antti Kosonen 2008].

2.4 Attenuation on power line channel

As a result of line impedance variation occurring in the power line circuit due to random load variations, the characteristic impedance of the line is time variant, due to which the attenuation is time variant [Klaus M. Dostert 2003]. Attenuation values strongly depend on individual properties of a link and may be as large as 90dB. Besides the total length of a link, frequency, time and location play major roles. Typical fluctuations with time are around 20 dB [Klaus M. Dostert 2003]. The power line acts as a voltage divider (that is it attenuates the high frequency communication signal), with attenuation increasing with frequency for frequencies above 100 kHz [Antonio Cataliotti 2010].

Researchers have worked to determine the variation of attenuation of carrier signal injected on power line with respect to length of the power line (attenuation per unit distance) and also to find the nature of attenuation variation with respect to frequency

of operation. In the following sections, information about the related work is reviewed.

2.4.1 Attenuation on power line channel with line length

A study comprising of three unipolar MV shielded cables with aluminum core and 185 mm^2 cross-sections with the transmission system being based on a line-ground configuration was conducted for determining the attenuation per unit distance. It was observed that for cable lengths between 1 and 2 km at the frequency of 86 kHz, attenuation assumed values between 15 and 25 dB [Antonio Cataliotti et al. 2010]**.** This variation of attenuation with distance is shown in Figure 2.4.

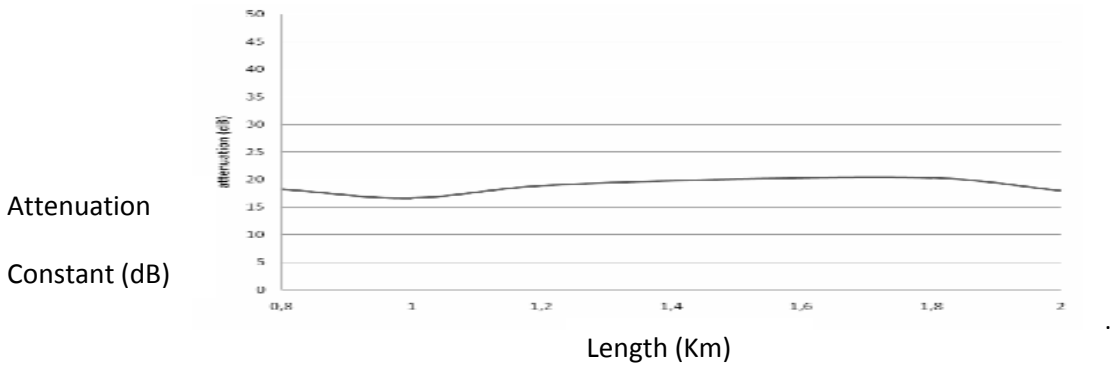

Figure 2.4. Attenuation constant versus length simulated in line to line configuration for f= 86 KHz. (Antonio Cataliotti et.al. 2010).

Several other researchers have worked to determine the attenuation on power line channel by simulation and by actual practical measurements, which are given below for the reference related to signal attenuation on channel along the length of the line.

- K. H. Zuberi [2003] has computed the amount of attenuation on the power line for low voltage and medium voltage lines. He has determined the signal attenuation to be 10 dB/km for medium voltage lines and 100 dB/km for low voltage lines.
- N. Suljanovic[2004] has compared the line attenuation by practical measurements for a 52 km long 400 kV power line with simulation results and finds the attenuation of the line to be with 8 dB to 11 dB, with 200 to 250 KHz.

- Antonio Cataliotti et al. [2010] have considered the application of PLC to Medium Voltage networks (1-30 kV). They have simulated signal propagation on a power line of line length ranging from 0.8Km to 2 Km and have determined that the attenuation is less than 25 dB.

2.4.2 Attenuation on power line channel with frequency

Studies have been conducted to demonstrate the variation of attenuation with respect to frequency. S. Robson et al. [2009] have simulated a substation, to measure the attenuation between different locations. The attenuation between different points in a substation has been measured, using The Electromagnetic Transients Program-Alternative Transient (ATP-EMTP) package. The network diagram employed to represent the substation used in this study is described in Figure 2.5 (a).

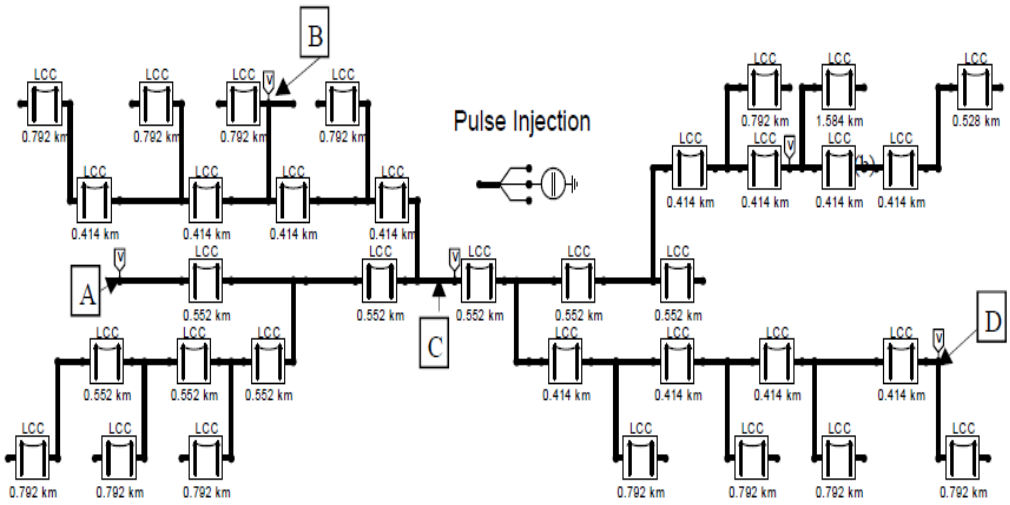

Figure 2.5 Frequency response of a simulated 11 kV overhead rural distribution

The attenuation with respect to frequency between points A and B, A and C and between A and D are shown in Fig. 2.5 (b), (c) and (d) respectively.

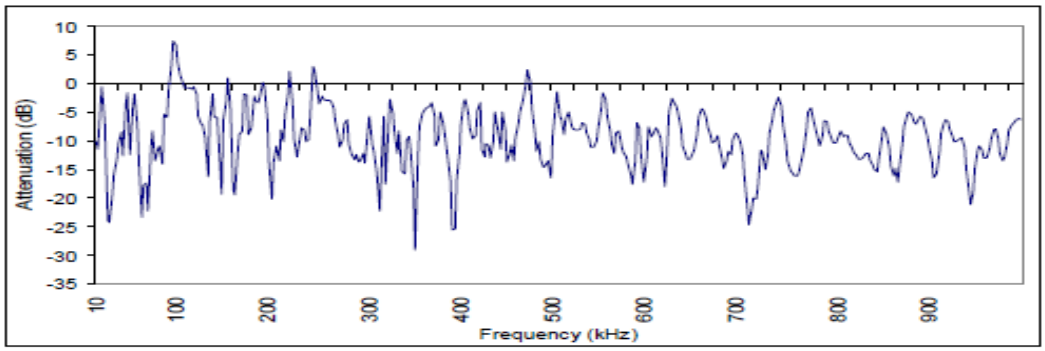

(b) Frequency response, Position A to B [S. Robson et al. 2009]

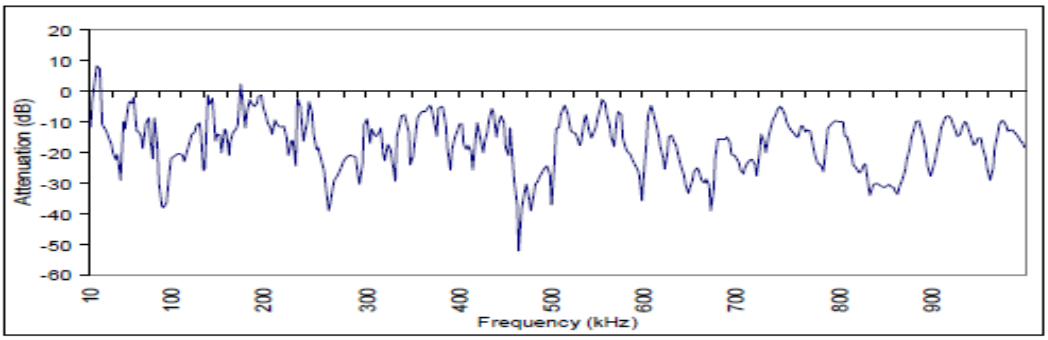

(c) Frequency responses, Position A to C [S. Robson et al. 2009]

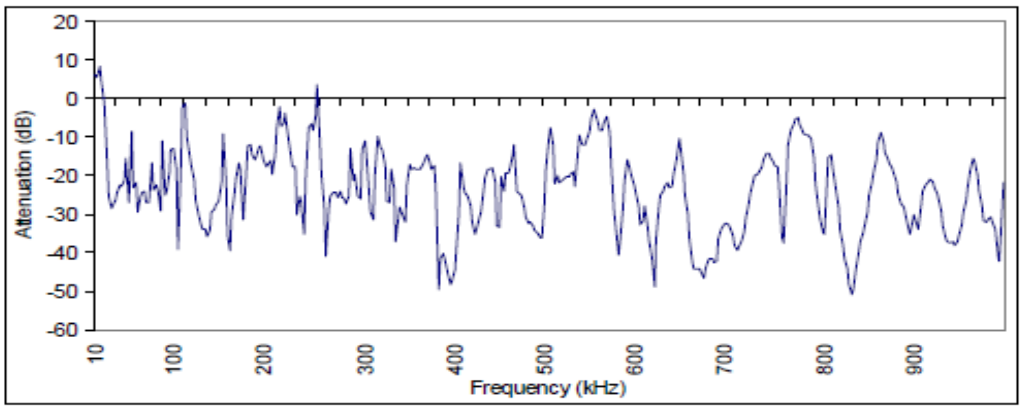

(d) Frequency response, Position A to D [S. Robson et al. 2009]

The plots of Figure 2.5(b) to (d) show that attenuation of signal on power lines varies randomly with variation in frequency of the transmitted signal. This behavior is due to the received signal being a result of superposition of many different reflecting paths on the line, whose path gains and phases are further a function of frequency. It means to say that the frequency response plots shown in Figure. 2.5, aid in depicting power line channel as a frequency variant fading channel, as discussed in section 1.1.6.

Yihe Guo et al. [2009] have investigated the channel characteristics of the MV network for carrier signal propagation in 50 kHz 500 kHz. They have obtained results in which voltage at receiver points 1.76km and 800 m from transmitter in a substation environment, show frequency selective variations.

Lampe L and Vinck AJHan [2011] have studied frequency response for medium voltage power line for narrowband application. Authors obtain the channel transfer function (frequency response) by calculating ABCD parameters as a function of number of loads connected and their distances from transmitter. A varying attenuation less than 40 dBs is observed.

A Dabak et al. [2012] have compared the ABCD-parameter based model for different components in the MV/LV line such as transformers, couplers and MV cables with the measured voltage transfer function. They have obtained the results as channel attenuation varying between 20 to 70 dBs for both measured and simulated model.

Marcel Nassar et al. [2012] have shown the field measurements (i) for industrial low voltage site as in Figure 2.6(a) and (ii) for residential medium voltage to low voltage site as shown in Figure 2.6(b), with frequency selective attenuation in frequency range of 50 kHz to 450 kHz.

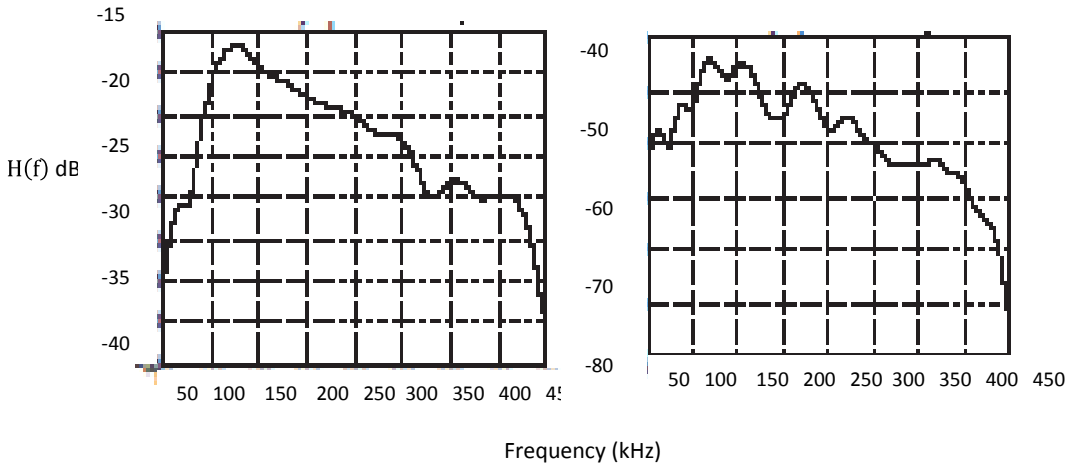

Figure 2.6 Examples of different PLC channels in frequency domain [Marcel Nassar et al. 2012].

2.5 Power line channel model

The discussions made in sections 2.4.1 and 2.4.2, justify the claim that the attenuation on power line channel is a function of frequency, length of the line, and the time of operation (as random load fluctuations may change the attenuation making the channel time variant). The model for the power line which depicts the time variant and frequency variant attenuation for the signal is necessary to be used for studying the modulation and channel coding performance intended to be done in this research work. The model for power line channel incorporating the time and frequency variant channel attenuation is explained in [Halid Hrasnica et al. 2004]. Riccardo Pighi et al. [2007] have used multipath channel model for power line channel.

Figure 2.7 shows the modeling of power line as a multipath channel model. The transfer function of a power line channel is time variant. The transmission medium of the power grid is characterized by a time-varying attenuation and frequency selectivity. Any transmission scheme applied to power lines has to cope with these impairments in addition to the intrinsic dependence of the channel model on the network topology and connected loads, the presence of high-level interference signals due to noisy loads, and the presence of colored noise. Moreover, the channel conditions can change because of connections and disconnections of inductive or capacitive loads. Finally, reflections from impedance mismatch at points where equipments are connected or from non terminated points can result in multipath and various types of noise [Gotz et al. 2004], [Francis Berrysmith et al. 2005].

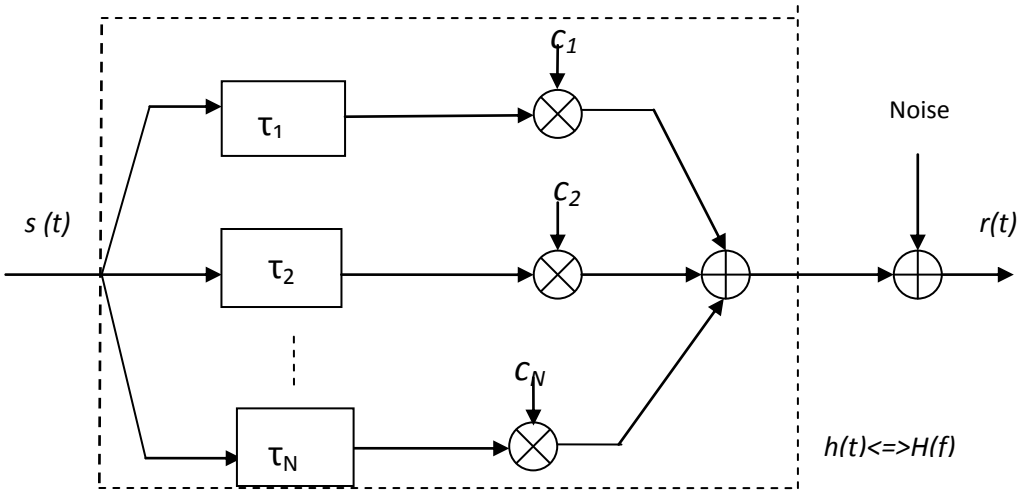

Figure 2.7 Multipath model representing the power line channel

Complying with the multipath or echo model, each transmitted signal reaches the receiver over N different paths. Each path i is defined by a certain delay τ_i and a certain attenuation factor c_i. The PLC channel can be described by means of a discrete-time impulse response $h(t)$ as [Halid Hrasnica et al. 2004],

$$h(t) = \sum_{i=1}^{N} c_i \,.\, \delta(t - \tau_i) \leftrightarrow H(f) = \sum_{i=1}^{N} c_i . e^{-j2\pi f \tau_i} \quad (2.1)$$

The time variant and frequency variant transfer function $H(f)$ in the frequency domain can be written as [Halid Hrasnica et al. 2004],

$$H(f) = \sum_{i=1}^{N} g_i . A(f, l) . e^{-j2\pi f \tau_i} \quad (2.2)$$

In (2.2), g_i represents the gain of the i^{th}reflected path on power line channel.

f - is the frequency of operation. l_i represent the length of each reflected path. N is the total number of reflections that form the received signal. $A(f, l)$ thus represents attenuation caused by the channel with respect to frequency, which is also a function of lengths of reflecting points. Second term in $H(f)$ represents the phase of the reflecting signals as τ_i represent the delays in the reception of delayed impulses in the impulse response of the channel.

2.6 Impulse noise on power line channel

Several noise sources that can be found in low- or medium-voltage power grids. Some of them are [M. Zimmermann and K. Dostert 2002], [Klaus M. Dostert 2003], , [Ezio Biglieri et al. 2003], [Halid Hrasnica et al. 2004]:

Aperiodic asynchronous impulse noise caused by switching transients, which occur all over a power supply network at irregular intervals and periodic asynchronous impulse noise related to switching operations of power supplies are described as:

(i) Colored thermal noise (thermal noise whose power spectral density is not constant and varies with frequency). The power spectral density of this noise model has significantly higher values at low frequencies.

(ii) Periodic synchronous impulse noise mainly caused by switching actions of rectifier diodes within DC power supplies and appliances.

(iii)Narrow-band interference caused by broadcast radio stations [M. Katayama 2006].

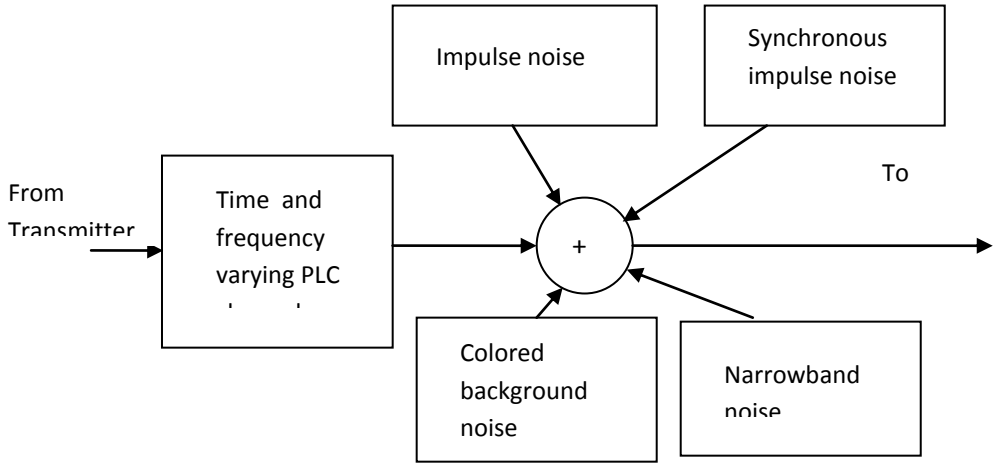

Figure 2.8 Sources of Noise on power line channel

Figure 2.8 shows the various sources of noise that can affect signal propagation on a power line. We see that signal from transmitter gets affected by the channel that is time and frequency variant.

M. Katayama et al. [2006] have described and analyzed several noise sources that can be found in low- or medium-voltage power grids used for narrowband PLC applications.

Umehara et al. [2004] have studied impulsive interference generated on a power line that can cause bit or burst errors during data transmission. They have employed Middleton's Class-A noise model to generate noise samples.

Christine Hsu et al. [2007] in their research work have studied the performance of LDPC code used for correction of data corrupted by noise described using Middleton Class-A model on power line.

The Middleton's Class-A distribution has probability density function (pdf) specified as [Leslie A. Berry 1981],

$$f(x) = \sum_{m=0}^{\infty} \frac{A^m}{m!} e^{(-A)} \left[\frac{1}{\sqrt{2\pi\sigma_m^2}} \right] . e^{\left(\frac{-x^2}{2\sigma_m^2}\right)} \qquad (2.1)$$

Different terms in (2.1) are defined as follows:

(i) σ_m^2 is noise variance with $\sigma_m^2 = \sigma^2 \left[\frac{\left(\frac{m}{A}\right)+T}{1+T}\right]$, with $\sigma^2 = \sigma_G^2 + \sigma_{GI}^2$ is the total noise power, σ_G^2 is Gaussian noise power and σ_{GI}^2 is impulsive noise power.

(ii) Index, $T = \frac{\sigma_G^2}{\sigma_{GI}^2}$ is the Gaussian-to-Impulsive noise power Ratio (GIR).

(iii) Index A is the "Overlap Index" and A indicates the mean value of impulses that occur per unit interval of time. That is, A is taken as the product of average number of emission events impinging on the receiver per second and the mean duration of a typical interfering source emission.

Thus A and T constitute important parameters of Middleton class-A noise.

Index T specifies the ratio of the amplitudes of impulse noise compared to background Gaussian noise. For example, if T is selected as 0.1,

$$T = \frac{\sigma_G^2}{\sigma_{GI}^2} = 0.1 \quad \Rightarrow \quad \sigma_{GI}^2 = \frac{\sigma_G^2}{0.1} = 10.\sigma_G^2$$

This implies that variance of impulse noise is ten times the variance of Gaussian noise. Typical values [Serena M. Zabin 1989] of *A* and *T* for generating samples of impulsive noise that can be used in simulations are:

. $A = 0.1, T = 0.$; $A = 0.1, T = 0.01$

(iv) Values of 'm ' more than 3 do not contribute much to the pdf, it is usual practice to limit the upper value of m as equal to 3.

2.6.1 Impulse noise model

With reference to the literature regarding the impulsive nature of power line channel in section 2.5, it is seen that Middleton's Class-A distribution has been extensively used in PLC literature as the mathematical model best suited to describe impulsive noise encountered in power line environment. Hence it has been used in this thesis to generate impulsive noise samples in simulation studies.

2.7 Need for Carrier power reduction for PLC

In the presence of interference and strong attenuation, distorted received signal in PLC is obviously prone to errors. The signal strength and the modulation used for the high

frequency signal should overcome the channel attenuation. And the signal processing used in the form of forward error correction should ensure the error-free commu nication. But the modulation scheme used for PLC should have low carrier power to satisfy the Electromagnetic Compatibility (EMC) constraints set by regulatory bodies. The restriction on transmitted carrier power or carrier signal strength is put to ensure that the PLC equipment does not cause interference to other RF equipment. The regulations for PLC operation are discussed in the next section.

2.8 PLC regulations

Several standards for Power line communications technology have been in use in different parts of the world. Some of the different standards are briefly described below. The standards differ from each other in the frequency and power level specification.

The frequency band used for narrowband PLC in Europe is from 3-148.5 kHz governed by CENELEC (Committee European de Normalization Electro technique Regulation). In USA it is 10-490 kHz governed by FCC (Federal Communication Commission). In Japan it is 10-450 kHz governed by ARIB and in China it is 3-500 kHz governed by EPRI. Figures 2.9 and 2.10 show the frequency spectrum limitation imposed by the regulatory agencies in the two most important markets: North America and Europe [Luis F. Montoy 2006].

There is only one valid standard in the European Union that concerns signaling on LV (Low Voltage) electrical installations intended for narrowband communication (kbps). The European standard EN 50065-1 (EN, 1991) was first published in 1991 by the European Committee for Electrotechnical Standardization (CENELEC) and it replaced all the other individual national standards in Europe. In Europe, the available frequency intervals for communication systems on low voltage and medium voltage power networks are settled by CENELEC EN 50065-1 (Committee European de Normalization Electro technique CENELEC and regulation EN50065-1) [Antonio Cataliotti et al. 2010]. The standard specifies five different bandwidths from 3 kHz to 148 kHz.

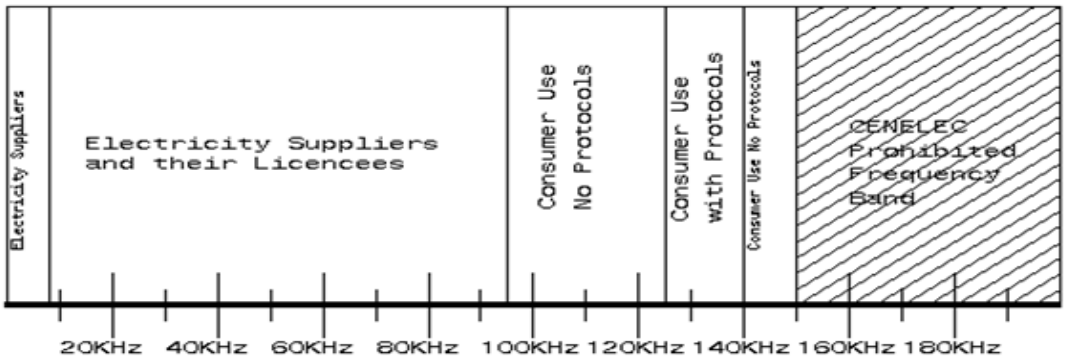

Figure 2.9 CENLEC Frequency Band Allocations for Europe [Luis F. Montoya 2006].

In Northern America and in Japan the regulation is more permissive because it allows one to use frequencies up to 525 kHz, i.e. up to the AM broadcast threshold. [Luis F. Montoya 2006]. General instructions for PLC mentioned for narrowband PLC is that output signal should be < 134 dBµV [Gotz et al. 2004].

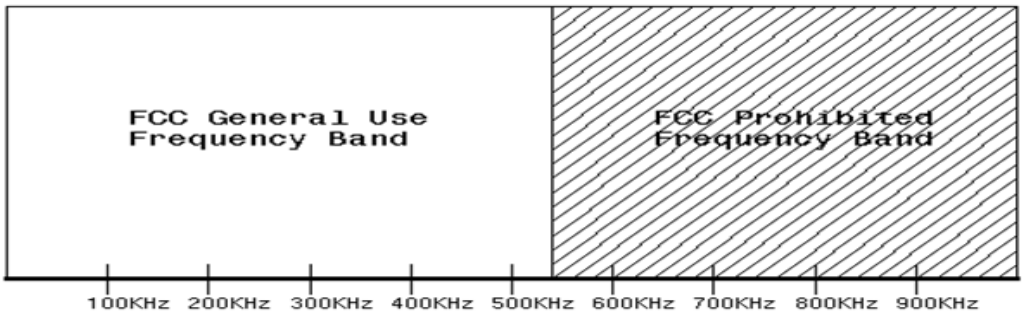

Figure 2.10 FCC Frequency Band Allocations for North America [Luis F. Montoya 2006].

In addition, Germany has a national regulation NB30 that concerns signaling on power lines up to 30 MHz frequencies intended for broadband communication (Mbps). In addition to these regulations, there are specifications, which are intended for manufacturers to support the co-operation of PLC products. The specifications are defined by Open PLC European Research Alliance (OPERA), and HomePlug Powerline Alliance called DS2 and HomePlug, respectively. Furthermore, there is Consumer Electronics Powerline Communication Alliance (CEPCA) that develops and promotes managed coexistence of various PLC technologies.

2.8.1 Observations made from European standard EN 50065-1

The European standard EN 50065-1 specifies the frequency bands allocated to the different applications, limits for the transmitter output voltage in the operating bands and limits for conducted and radiated emissions. In addition, the methods for measurement are defined. The standard does not specify modulation methods or functional features. It reserves the frequency range from 3 kHz to 148.5 kHz (EN, 1991) that is called CENELEC frequency band. These frequencies differ considerably from other regulations for example, those applicable in the United States or in Japan, where a frequency range up to approximately 500 kHz is available [Dostert 2001].

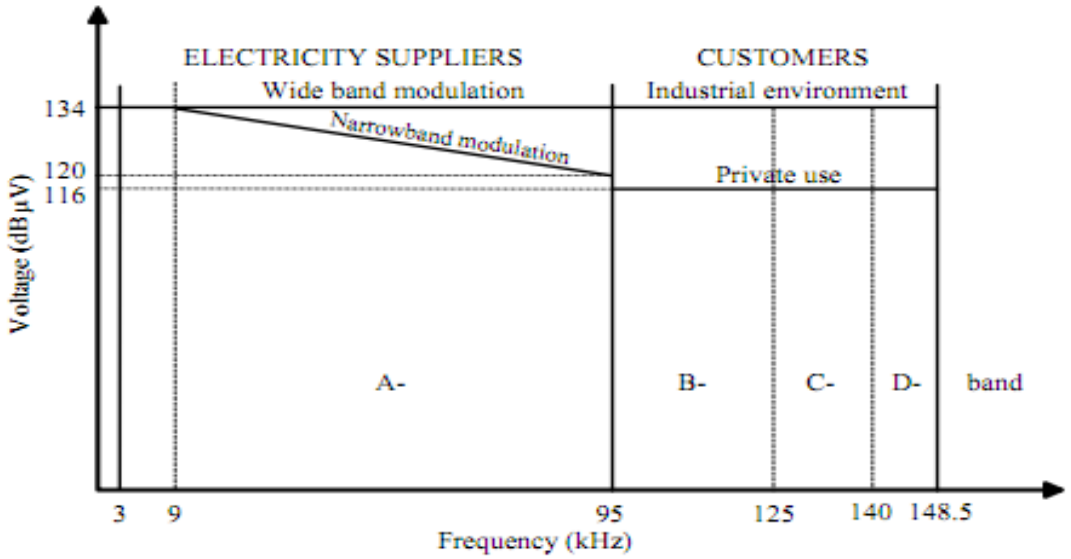

Figure 2.11 Limits for the transmitter output voltage across the standard load in the operating frequency bands according to European CENELEC EN 50065-1 standard for signaling on LV electrical installations (EN, 1991).

In Figure 2.11, the frequency range is divided into two parts, where frequencies below 95 kHz (A band) are reserved for use by electricity suppliers, while the frequencies between 95 and 148.5 kHz (B, C, and D bands) are meant for private use, mainly within buildings. A maximum signal level in general use within B, C, and D bands is 116 dBµV (0.63 V), but in an industrial environment it is allowed to be 134 dBµV (5 V). Similar values within A band may be 134 dBµV @ 9 kHz, and the values are lowered to 120 dBµV (1 V) @ 95 kHz, but with wide band modulation, the maximum level can be 134 dBµV within the whole range.

2.9 Modulation schemes and forward error correction (FEC) coding for PLC technology

Whenever high energy noise impulses hit a data carrier, on the signal processing levels such as modulation, amplification, filtering or demodulation, there is no way to avoid such errors. The intervention must take place in the digital domain by appropriate error control coding (also called as channel coding) techniques to protect the data integrity. Researchers have used different approaches for the combination of digital modulation and channel coding.

Discussion about the modulation and channel coding schemes attempted by researchers, along with the channel model employed for obtaining the results, assumptions made for the simulation/practical results and the resulting performance are discussed in the following points. Inference drawn from the research work taken for reference is mentioned in the immediate paragraph of each point.

2.9.1 Orthogonal Frequency Division Modulation (OFDM)

- Riccardo Pighi [2002] has employed OFDM with Linear block code for power line communication. Author has considered three types of power line channels: good (attenuation less than 20 dB), average (attenuation ranging between 30 to 40 dB) and below average (attenuation ranging between 35 to 60 dB). The BER of 10^{-4} is reached at 14 dB for below average channel and at 12 dB for good channel.

  The assumption made in this study is the perfect knowledge of the channel transfer function at the receiver. In the practical implementation, channel transfer function (also referred to as channel state) will not be known to the receiver. In practice, pilot symbols are used to estimate the channel state.

- Luis F. Montoya [2006] has stated that out of many forms of modulation that could be used over the power line, OFDM is the most suitable because of its immunity to the power line interference. Author mentions that the use of OFDM has resulted in development of technologies which allow high data rates under adverse conditions.

OFDM is suitable for power line because OFDM is very effective in combating inter-symbol-interference when used on frequency selective fading channels. Just as in case of OFDM combating fading (random variations in signal strength) in wireless channel, it is expected to combat fading in power line channel, fading occurring due to random load (and hence channel gain) variations.

- Aminuddin B. et al. [2011] have conducted simulation study to determine performance of OFDM for broadband over power line for frequency range less than 20 MHz. Performance is evaluated by varying path lengths of the multipath channel model used for power line channel and BER of the order of 10^{-4} is found at 14 dB of SNR. But in this simulation study, the effect of channel noise has not been taken into account.

Frequency of operation in the present context of application of narrowband PLC on medium voltage line should be within 450 KHz, unlike broadband. Tests for channel behavior and OFDM performance need to be carried out for frequencies less than 450 KHz. Also noise disturbances need to be considered.

2.9. 2 Turbo coded OFDM

- P. Amirshahi et al. [2006] have employed OFDM with Turbo code for correcting data disturbed with impulsive noise for OFDM signal for broadband transmission over low voltage power-line channels. They have shown a coding gain of nearly 4 to 5 dB in the performance comparison of uncoded and coded OFDM signal.

Coded OFDM on low voltage power line for broadband application is taken in the above study. But coded OFDM on medium voltage power line for narrowband needs to be studied.

2.9.3 BCH codes

- Noura Al-Hinai1 et al. [2009] have studied performance of BCH coded $(n = 63, k = 36, t = 11)$ OFDM signal for impulsive disturbance on power line channel. Multipath model is used for power line channel. Impulse noise from Poisson distribution is added. Performance is evaluated in the form of

quality of received image. Studies on variations of probability of error as a function of SNR need to be provided to evaluate the carrier signal strength.

2.9.4 Space time codes

- Several researchers have attempted to employ Space-Time Codes to enhance reliability of information over PLC. One of the codes that have been used is the code proposed by S. M. Alamouti [1998].

  Alamouti's code is a two transmit antenna space-time block code and which has also been adopted in various global standards of wireless communication. Power line channel can be configured for space time coding scheme and the expected performance improvement can be studied.

- Carlos L. Giovaneli et al. [2003] employed space time coding for 3-phase 415 V power line channel. They have assumed availability of ideal channel state information at the receiver. They claim a performance of 10^{-6} BER for 20 dB SNR.

  Ideal channel state information differs from the practical channel state as channel is time variant. Also, the channel state needs to be predicted by sophisticated channel state estimation schemes, as it is directly not available at the receiver.

- Alamouti scheme is employed for BPLC over low voltage lines. BER of the order of 10^{-5} is observed at about 25 to 30 dB of SNR [L. Stadelmeier et al. 2008].

  Low voltage power lines are employed for in home broadband communication.

- The use of space frequency and space time code has been proposed for indoor power line communication for frequency range less than 20 MHz. This study employs multipath model and Middleton Class-A noise to describe the channel. BER of the order of 10^{-5} is found at 15 db of SNR. Space time coding with 2x1 configurations is used along with OFDM [Bamidele Adebisi et al. 2009].

  Space time codes are employed on low voltage power lines, for indoor broadband communication.

2.10 Scope for further investigation

The discussion on the state of the art presented up to now, presents the power line channel behavior and various digital modulation and channel coding schemes that have been proposed for low/medium voltage narrowband power line communication.

Study of literature indicates that the work done so far in this field has certain limitations. In these references, the channel has been analyzed-

(i) only with attenuation effect (ii) only with impulse noise effect (called as AWAN channel) (ii) ideal channel state is assumed that is: channel gain is assumed equal to one (iii) channel state (transfer function of the channel) is assumed to be known at the receiver (iv) Most of the researchers have concentrated on broadband PLC on low/medium voltage power line (v) Further, the performance of Turbo-OFDM and BCH space time code over a channel perturbed together with attenuation effect and impulse noise effect has not been determined.

An attempt has been made in this thesis work, to address some of these issues by use of suitable modulation to overcome attenuation due to time and frequency variant channel disturbances and by the use of suitable forward error correcting code to overcome channel induced impulse noise disturbances. Channel state is taken as time/frequency variant. Studies on variations on bit error rate as a function of SNR, for different impulsive nature of the power line channel is emphasized and the pertinent graphs have been provided.

Summary: Literature survey of this chapter gives the knowledge of treating the low/medium voltage power line as time and frequency variant channel for narrowband application in the frequency range less than 450 kHz. OFDM, space time coding, Turbo codes, BCH codes form the candidates for the PLC technology.

Chapter 3

CHANNEL CODING AND DIGITAL MODULATION TECHNIQUES: A REVIEW

In this chapter the necessary concepts required to design BCH codes have been elaborated. An understanding of Modern Algebra is essential to acquire a sound understanding of the structure of BCH and Reed Solomon Codes. A brief review of concepts from Modern Algebra required to design and evaluate the performance of BCH codes [Shu Lin and D. J. Costelo 2003] is provided in this chapter. In addition, this chapter gives a brief introduction to the topics of Turbo codes, Orthogonal Frequency Division Multiplexing (OFDM) and Space Time Codes.

Groups, Rings, Fields and vector spaces are algebraic structures which are very useful in the study of Linear Block Codes. A brief discussion stating essential definitions and useful properties is provided in this section [Shu Lin and D. J. Costelo 2003].

3.1 Group

Let G be a set of elements. A binary operation $*$ on G is a rule that assigns to each pair of elements a and b a uniquely defined third element $c = a * b$ in G. When such an operation $*$ is defined on G, we say that G is closed under $*$.

A binary operation $*$ is said to be associative if for any a and b and c in G,

$$a * (b * c) = (a * b) * c$$

Definition of Group

A set G on which a binary operation $*$ is defined is called a group if the following conditions are satisfied.

i. The binary operation $*$ is associative.

ii. G contains an element such that for any a in G,

$$a * e = e * a = a$$

This element e is called an identity element of G.

iii. For any element a in G, there exists another element a^{-1} such that then

$$a * a' = a' * a = e$$

The element e is called an inverse of a.

A group G is said to be commutative if its binary operation $*$ also satisfies the following condition. For any a and b in G,

$$a * b = b * a$$

The following theorems are well known and are stated here without proof.

Theorem 3.1[Shu Lin and D. J. Costelo 2003]: The identity element in a group G is unique.

Theorem 3.2[Shu Lin and D. J. Costelo 2003]: The inverse of a group element is unique.

The number of elements in a group is called the order of the group. In this thesis, we are interested in finite groups. i.e., rather than dealing with groups with infinite elements.

A group of finite order is called a finite group. Finite groups are constructed with modular arithmetic. For example, modulo m addition is expressed as follows:

For any i and j in G, $i * j = r$, where r is the remainder resulting from dividing $i * j$ by m.

3.1.1 Order of a group element

The order of a group element is the minimum number of times the element should operated upon itself using the group operator so that the result is the identity element.

3.1.2 Subgroups

Let G be a group under binary operation $*$. Let S be a nonempty subset of G. Then S is a subgroup of G if the following conditions hold

i. S is closed under the binary operation $*$.

ii. For any element a in S, the inverse of a is also in S.

3.1.3 Cosets

Let S be a subgroup of a group G with binary operation $*$. Let a be an element of G.

Then the set of elements $a * S \triangleq \{a * h: h \in S\}$ is called a left coset of S; the set of elements $S * a \triangleq \{h * a: h \in S\}$ is called a right coset of S.

Properties of cosets of a subgroup S of a group G are:

i. Every element in G appears in one and only one coset of S.
ii. All the distinct cosets of S are disjoint; and
iii. The union of all the distinct cosets of S forms the group G.

3.2 Field

A field is a set of elements in which we can perform addition, subtraction, multiplication and division without leaving the set. Addition and multiplication must satisfy the commutative, associative and distributive laws.

Definition: Let F be a set of elements on which two binary operations, called addition "+" and multiplication "." are defined. The set F together with the two binary operations + and . is a field if the following conditions are satisfied.

i. F is a commutative group under addition +. The identity element with respect to addition is called the *zero element* or the *additive identity* of F and is denoted by 0.
ii. The set of nonzero elements in F is a commutative group under multiplication. The identity element with respect to addition is multiplication is called the unit *element* or the *multiplicative identity* of F and is denoted by 1.
iii. Multiplication is distributive over addition; that is, for any three elements a, b and c in F,

$$a.(b + c) = a.b + a.c$$

The number of elements in a field is called the *order* of the field. A field with finite elements is called a finite field. In a field, additive inverse of an element a is denoted as $-a$ and multiplicative inverse of a is denoted by a^{-1}, provided that $a \neq 0$.

Subtracting a field element b from another field element a is defined as adding the additive inverse, $-b$ of b to a [i.e. $a - b \triangleq a + (-b)$]. If b is a nonzero element, dividing a by b is defined as multiplying a by the multiplicative inverse, b^{-1}, of b [i.e. $a \div b \triangleq a.(b^{-1})$].

3.2.1 Fields with primes

Integers $\{0,1,2, \ldots . p-1\}$ where p is a prime, form a Field F_p. Some small finite fields are, $F_2 = \{0,1\}$, $F_3 = \{0,1,2\}$, $F_5 = \{0,1,2,3,4\}$. Such fields have a prime number of elements and hence are referred to as prime number fields.

3.2.2 Order of the field element

Let β be an element in the field F_p. The smallest integer t such that $\beta^t = 1$ is referred to as the order of the field element β.

3.2.3 Primitive element of a finite field

Let the finite field F_q be represented as, $F_q = \{0, 1, \ldots \ldots . \alpha, \ldots \ldots \beta, \ldots . q-1\}$.

Let α and β be any two elements in F_q, q is a prime or the power of a prime.

The Primitive element of a finite field is defined as that element which has the property that all other elements in the finite field can be expressed as suitable powers of it. Thus, if α is primitive element and if β is another other element in F_q, then we can write,

$\beta = \alpha^i$ where i is an integer. Let us consider the following example:

$F_{11} = \{0, 1, 2, 3, 4, 5, 6, 7, 8, 9, 10\}$ mod 11 addition and mod 11 multiplication, is a field. It can be shown that 2 is a primitive integer in this field. Thus, the other elements of F_{11} can be expressed as powers of this element. This is illustrated below.

$$F_{11} = \{0, 2^1, 2^2, 2^3, 2^4, 2^5, 2^6, 2^7, 2^8, 2^9, 2^{10} = 1\}$$

In the above example, 2 is the generating (primitive) element and $ord(2)$ =10.

3.3 Extension field

The number of elements in a Galois fields is either a prime or a power of a prime.

A Galois field F_q with prime power number of elements is represented as $F_q = F_{p^m}$ where $q = p^m$, p is a prime, m is an integer. A primitive element α in the finite field F_{p^m}, has order p^m - 1. F_{p^m} is referred to as an extension field of the prime order field F_p.

3.3.1 Irreducible polynomial and primitive polynomials

A polynomial $p(x) \epsilon F_p(x)$ is said to be irreducible if $p(x)$ cannot be factored into a product of lower degree polynomials with coefficients in F_p. For example, $x^2 + 1$ is irreducible in $F_3(x)$. An irreducible polynomial $p(x) \epsilon F_p(x)$ of degree m is said to be primitive if the smallest value of n for which $p(x)$ divides a polynomial of the form $x^n - 1$ is $n = p^m - 1$. The following example illustrates this idea.

Example 1: Consider an irreducible polynomial, $x^4 + x + 1 \epsilon F_2(x)$. Here $m=4$.

It can be verified that $x^4 + x + 1$ does not divide $x^5 - 1$, $x^6 - 1$, $x^7 - 1$ etc. The smallest value of n such that $x^4 + x + 1$ divides $x^n - 1$ is $n=15=2^4 - 1$. Hence

$x^4 + x + 1$ is an example of a primitive polynomial.

It should be noted that,

i) Any irreducible polynomial $f(x) \epsilon F_p[x]$ must divide: $x^{p^m - 1} - 1$

ii) Every primitive polynomial is irreducible, but every irreducible polynomial is not primitive.

The following Theorem constitutes the basis for the construction of extension fields as a vector space over a prime order field.

Theorem 3.3 [Shu Lin and D. J. Costelo 2003]: The roots α_j of m^{th} degree primitive polynomial $f(x) \epsilon F_p(x)$ have order $p^m - 1$.

3.3.2 Construction of Extension Fields

To construct the extension field F_{p^m} as an extension of $F_p = \{0, 1, 2, \ldots p-1\}$, we start with a primitive polynomial $p(x) \epsilon F_p(x)$ of degree m. Let α be any one of its roots. It can be easily shown that the non zero elements of the extension field F_{p^m} can be determined as a collection of successive distinct powers of α. Thus,

$F_{p^m} = \{0, \alpha, \alpha^2, \ldots\ldots \ \ldots \ \alpha^{p^m-2}, \alpha^{p^m-1}\}$. The next example illustrates this concept.

Example 2: The finite field F_{2^3} can be expressed as,
$F_{2^3} = \{0,1, \alpha, \alpha^2, \alpha^3, \alpha^4, \alpha^5, \alpha^6, \alpha^7 = 1\}$ where α is a root of the primitive polynomial which is $p(x) = x^3 + x + 1$. It can be verified that $x^3 + x + 1$ is primitive and

$x^3 + x + 1 | x^{2^3-1} - 1$.
The extension field can be represented using power representation and polynomial representation. This is illustrated in Table 3.1 for example 2.

Table 3.1 Power, polynomial and vector representation of elements of F_{2^3}

Power representation	Polynomial representation	Vector representation	Decimal representation
-	0	000	0
α^0	1	100	1
α^1	α	010	2
α^2	α^2	001	4
α^3	$1 \quad \alpha$	110	3
α^4	$\alpha \quad \alpha^2$	011	6
α^5	$1 \quad \alpha \quad \alpha^2$	111	7
α^6	$1 \quad \alpha^2$	101	5

3.3.3 Minimal polynomial and conjugacy classes

Design of algebraic codes focuses on the selection of polynomials over finite fields that have a required set of roots selected from a given finite field F_{q^m}.

It is further required that the polynomials have coefficients in the subfield F_q and that the polynomials have minimal degree. To meet these requirements, the relationship between the subfield from which the coefficients of polynomials are taken and the

roots of the polynomial must be understood. A few preliminary definitions will be stated before exploring this relationship.

Definition: Minimal polynomial.

Let α be an element in the field F_{q^m}. The minimal polynomial of α with respect to F_q is the smallest degree nonzero polynomial $p(x)$ in $F_q[x]$ such that $p(\alpha)$=0.

$\alpha \in F_{q^m}$ and $p(x) \epsilon F_q[x]$ with $p(\alpha)$=0.

Some of the properties of minimal polynomials are presented in the following theorem.

Theorem 3.4 [Shu Lin and D. J. Costelo 2003]**:** For each element α in F_{q^m}, there exists a unique monic polynomial $p(x)$ of minimal degree in $F_q[x]$ such that the following are true.

1. $p(\alpha)$=0.
2. The degree of $p(x)$ is less than or equal to m.
3. $f(x)$=0 implies that $f(x)$ is a multiple of $p(x)$.
4. $p(x)$ is irreducible in $F_q[x]$.

Definition: Conjugates of field elements

Let β be an element in the Galois field F_{q^m}. The conjugates of β, with respect to the sub field F_q are the elements β, β^q , β^{q^2}, B^{q^3} ... . The conjugates of β with respect to F_q form a set called the conjugacy class of C with respect to F_q.

Theorem 3.5[Shu Lin and D. J. Costelo 2003]**:** The conjugacy class of $\alpha \epsilon F_{q^m}$ with respect to F_q contains d elements where $\alpha^{q^d} = \alpha \; and \; d \mid m$.

Conjugacy classes are the key to the factorization of minimal polynomials in $F_{q^m}[x]$.

Theorem 3.6[Shu Lin and D. J. Costelo 2003]**:** Let α be an element in F_{q^m}. Let $p(x)$ be the minimal polynomial of α with respect to F_q. The roots of $p(x)$ are exactly the conjugates of α with respect to F_q.

The sixteen elements of F_{2^4} are segregated according to their conjugacy classes with respect to F_{2^2} in the Table 3.2.

Table 3.2 Conjugacy classes and their minimal polynomials of the elements of F_{2^4} with respect to F_{2^2}

Conjugacy class	Associated minimal polynomial	
0	$M(x) = (x - 0) = x$	X
1	$M_0(x) = (x - 1) = x + 1$	$x + 1$
$\{\alpha, \alpha^4\}$	$M_1(x) = (x + \alpha)(x + \alpha^4)$	$x^2 + x + \alpha^5$
$\{\alpha^2, \alpha^8\}$	$M_2(x) = (x + \alpha^2)(x + \alpha^8)$	$x^2 + x + \alpha^{10}$
$\{\alpha^3, \alpha^{12}\}$	$M_3(x) = (x + \alpha^2)(x + \alpha^8)$	$x^2 + x\alpha^{10} + 1$
$\{\alpha^5\}$	$M_5(x) = (x + \alpha^5)$	$x + \alpha^5$
$\{\alpha^6, \alpha^9\}$	$M_6(x) = (x + \alpha^6)(x + \alpha^9)$	$x^2 + \alpha^5 x + 1$
$\{\alpha^7, \alpha^{13}\}$	$M_7(x) = (x + \alpha^7)(x + \alpha^{13})$	$x^2 + \alpha^5 x + \alpha^5$
$\{\alpha^{10}\}$	$M_{10}(x) = (x + \alpha^{10})$	$x + \alpha^{10}$
$\{\alpha^{11}, \alpha^{14}\}$	$M_{11}(x) = (x + \alpha^{11})(x+\alpha^{14})$	$x^2 + \alpha^{10} x + \alpha^{10}$

3.4 BCH codes (Bose Choudhari Hocquenghem codes)

BCH codes form a large class of multiple random error correcting codes. BCH codes are cyclic codes. BCH codes possess elegant algebraic structure. The first decoding algorithm was devised by Peterson in 1960. Since then many researchers have devised a variety of decoding algorithms for these codes, notable of which are the Berlekamp algorithm and Euclid's algorithm. Binary BCH codes are defined in the following manner [Shu Lin and D. J. Costelo 2003]:

Definition: For any integer $m \geq 3 \; and \; t < 2^{m-1}$, there exists a binary BCH code with following parameters-

Block length or code length $n < 2^m - 1$

Number of parity digits $n - k \leq mt$

Minimum distance $d_{min} \geq 2t + 1$

where t is the error correcting capability of the code.

This code is capable of correcting any combination of t or fewer errors in a block of length $n < 2^m - 1$. Hence we call it as t error correcting BCH code.

3.4.1 Generator polynomial approach to design BCH codes

When constructing an arbitrary cyclic code there is no guarantee as to the resulting minimum distance. Given an arbitrary generator polynomial $g(x)$, we must conduct a computer search of all corresponding nonzero code words to determine the minimum weight codeword and thus the minimum distance of the code. BCH codes, on the other hand, take advantage of a useful result that ensures a minimum '**design distance'**, given a particular constraint on the generator polynomial. This result is known as 'BCH bound'.

BCH bound thus gives the instructions to form the design steps, by putting constraints on the generator polynomial.

3.4.2 BCH bound [Shu Lin and D. J. Costelo 2003]

Let c be a q ary (n, k) cyclic code with generator polynomial $g(x)$. Let m be the multiplicative order of q modulo n, i.e. $q^m = 1 \bmod n$. F_{q^m} is thus the smallest extension field of F_q that contains a primitive n^{th} root of unity. Select $g(x)$ to be a minimal degree polynomial in $F_q(x)$ such that,

$g(\alpha^b) = g(\alpha^{b+1}) = g(\alpha^{b+2}) = \cdots g(\alpha^{b+\delta-2)} = 0$, for some integers $b > 0$ and $\delta \geq 1$.
$g(x)$ thus has δ-1 consecutive powers of α as zeros (as most of the time, b=1).

3.4.3 BCH code design procedure

To construct t error correcting BCH code of length n,

1. Find a primitive n^{th} root of unity α in a field F_{q^m}, where m is minimal.
2. Select $\delta - 1 = 2t$ consecutive powers of α, starting with α^b, for some non negative integer b.
3. Let $g(x)$ be the least common multiple of the minimal polynomials for the selected powers of α with respect to F_q (Each of the minimal polynomial should appear only once in the product).

3.4.4 Systematic encoding procedure

1. Represent the message sequence **m** by its equivalent polynomial representation $m(x)$. Multiply this polynomial by x^{n-k}, which is equivalent to shifting $m(x)$ to the right by $(n-k)$ positions.

2. Divide $x^{n-k}.m(x)$ by the generator polynomial to find the remainder $r(x)$.

3. Add the remainder to the shifted message polynomial that is,
   $c(x) = x^{n-k}.m(x) + r(x)$. $c(x)$ gives the code word in systematic form.

3.5 Decoding of BCH codes

Decoding is considerably more complicated and requires three steps after a data vector is received. Given a BCH code that can correct t errors, the steps are:

1) Computation of a syndrome vector whose $2t$ components belong to F_{2^m}.

2) Converting this to an error location polynomial of degree t or less over F_{2^m}

3) Finding the roots of this polynomial which correspond to bit error locations in the received vector.

Peterson first outlined the method [W. W. Peterson 1960] which was considerably refined by Berlekamp and others. A brief outline of the Berlekamp algorithm is presented in this section.

In this section, Berlekamp Massey (BM) algorithm for decoding BCH codes is explained [Shu Lin and D. J. Costelo 2003], [Clifford Kraft 1990].

Let $c(x) = c_0 + c_1x + c_2x^2 + c_3x^3 + c_{n-1}x^{n-1}$ denote the code vector,

$e(x) = e_0 + e_1x + e_2x^2 + e_3x^3 + e_{n-1}x^{n-1}$ denote the error pattern and

$r(x) = r_0 + r_1x + r_2x^2 + r_3x^3 + r_{n-1}x^{n-1}$ denote the received vector at the destination end. The first step in decoding is to calculate the syndrome set.

Syndromes are obtained by substituting $\alpha, \alpha^2, \alpha^3, \ldots \alpha^{2t}$ (t denotes the error correcting capability of the code) into the polynomial representation of the received polynomial $r(x)$.

This is represented as, $S_j = r(\alpha^j) = \sum_{i=0}^{n-1} r_i\, \alpha^{ij},\ 0 \le j \le 2t.$

We have, $S_1 = r(\alpha)$, $S_2 = r(\alpha^2)$ .....$S_{2t} = r(\alpha^{2t})$

Using the syndrome components as data, the Berlekamp algorithm iteratively computes the error locator polynomial. The roots of the error locator polynomial yield

the error locations. These are determined by the Chein search procedure. An example illustrating the steps involved in the Berlekamp algorithm when applied to a t=3 error correcting length n=15 BCH code is illustrated in Table 3.3. $\sigma^6(\mathrm{x}) = \sigma(\mathrm{x})$ obtained in the last step denotes the error locator polynomial whose roots are extracted to determine the error locations. Since this is a binary code, once the error locations are determined, the correct symbols at these locations can be obtained by flipping the bits at these positions.

Following the steps listed above, he table is completed as shown in Table 3.3.

Table 3.3 BCH decoding using Berlekamp Massey algorithm.

μ	$\sigma^{\mu}(x)$	d_{μ}	l_{μ}	$\mu - l_{\mu}$
-1	$\sigma^{-1}(x) = 1$	1	0	-1
0	$\sigma^{0}(x) = 1$	α^{12}	0	0
1	$\alpha^{1}(x) = 1 + \alpha^{12}x$	α^{7}	1	0($\rho = -1$)
2	$\alpha^{2}(x) = 1 + \alpha^{3}x$	1	1	1 ($\rho = 0$)
3	$\alpha^{3}(x) = 1 + \alpha^{3}x + \alpha^{3}x^{2}$	α^{7}	2	1 ($\rho = 0$)
4	$\alpha^{4}(x) = 1 + \alpha^{4}x + \alpha^{12}x^{2}$	α^{10}	2	2 ($\rho = 2$)
5	$\alpha^{5}(x) = 1 + \alpha^{7}x + \alpha^{4}x^{2} + \alpha^{6}x^{3}$	0	3	2 ($\rho = 3$)
6	$\alpha^{6}(x) = 1 + \alpha^{7}x + \alpha^{4}x^{2} + \alpha^{6}x^{3}$			

$\sigma(x)$=$1 + \alpha^{7}x + \alpha^{4}x^{2} + \alpha^{6}x^{3}$ is the error locator polynomial. The reciprocals of the roots of this polynomial denote error locations.

Chien search and error correction: To determine the roots of $\sigma(x)$, a simple trial-and-error procedure called Chien search is performed. All nonzero elements β of $GF(2^m)$ are generated and the condition $\sigma(\beta^{-1})$ = 0 is tested.

This procedure yields the error location numbers $\beta_1 = \alpha^{12}, \beta_2 = \alpha^{6}, \beta_3 = \alpha^{3}$

Therefore, $e(x) = x^3 + x^6 + x^{12}$

Now, $v(x) = r(x) + e(x)$

$v = x^3 + x^6 + x^{12} + x^3 + x^6 + x^{12}$

$= \{0, 0, 0, 0, 0, 0, 0, 0, 0, 0, 0, 0, 0, 0, 0\}$ is the decoded code vector. In this case, the number of errors introduced by the channel is equal to the error correcting

capability `$t$' of the code. Hence, correct decoding has occurred. If the number of errors introduced by the channel exceeds `t' erroneous decoding can occur.

3.6 Design of BCH code for $n = 63, k = 36, t = 5$

BCH code of $n=63, k=36$ with $t=5$ has been employed in this research work. Design of this code is presented in this section.

The finite field with 64 elements $F_{64} = F_{2^6}$ can be expressed as,

$$F_{2^6} = \left\{ \begin{matrix} 0,1,\alpha,\alpha^2,\alpha^3,\alpha^4,\alpha^5\alpha^6,\alpha^7\alpha^8,\alpha^9\alpha^{10},\alpha^{11}\alpha^{12},\alpha^{13}\alpha^{14},\alpha^{15}\alpha^{16},\alpha^{17}\alpha^{18},\alpha^{19}\alpha^{20}, \\ \alpha^{21},\alpha^{22}\alpha^{23}\alpha^{24}\alpha^{25},\alpha^{26},\alpha^{27},\alpha^{28},\alpha^{29},\alpha^{30},\alpha^{31},\alpha^{32},\alpha^{33},\alpha^{34},\alpha^{35},\alpha^{36},\alpha^{37},\alpha^{38},\alpha^{39}, \\ \alpha^{40},\alpha^{41},\alpha^{42},\alpha^{43},\alpha^{44},\alpha^{45},\alpha^{46},\alpha^{47},\alpha^{48},\alpha^{49},\alpha^{50},\alpha^{51},\alpha^{52},\alpha^{53},\alpha^{54},\alpha^{55},\alpha^{60},\alpha^{61},\alpha^{62} \end{matrix} \right\}$$

where α is the primitive 63rd root of unity (i.e. $\alpha^{63} = 1$).

Let primitive polynomial be, $p(x) = 1 + x + x^6$ so that, $\alpha^6 = 1 + \alpha$

Using $\alpha^6 = 1 + \alpha$, all the elements of the field F_{2^6} are found. The first few are listed for reference as shown in Table 3.4.

Table 3.4 Galois field elements of the field F_{2^6}

0	0						000000
1	1						100000
α		α					010000
α^2			α^2				001000
α^3				α^3			000100
α^4					α^4		000010
α^5						α^5	000001
α^6	1 +	α					110000
α^7		$\alpha +$	α^2				011000
. .							

The elements can be segregated into conjugacy classes and the corresponding minimal polynomials can be calculated. The conjugacy classes showing cyclotomic cosets for F_{2^6} are listed in Tables 3.5.

Table 3.5 Conjugacy class and cyclotomic cosets for F_{2^6}

$C0 = \{0\}$	$\{\alpha^0\}$
$C1 = \{1, 2, 4, 8, 16, 32\}$	$\{\alpha^1, \alpha^2, \alpha^4, \alpha^8, \alpha^{16}, \alpha^{32}\}$
$C3 = \{3, 6, 12, 24, 48, 33\}$	$\{\alpha^3, \alpha^6, \alpha^{12}, \alpha^{24}, \alpha^{33}, \alpha^{48}\}$
$C5 = \{5, 10, 20, 40, 17, 34\}$	$\{\alpha^5, \alpha^{10}, \alpha^{20}, \alpha^{17}, \alpha^{34}, \alpha^{40}\}$
$C7 = \{7, 14, 28, 35, 56, 49\}$	$\{\alpha^7, \alpha^{14}, \alpha^{28}, \alpha^{35}, \alpha^{49}, \alpha^{56}\}$
$C9 = \{9, 18, 36\}$	$\{\alpha^9, \alpha^{18}, \alpha^{36}\}$
$C11 = \{11, 22, 44, 25, 50, 37\}$	$\{\alpha^{11}, \alpha^{22}, \alpha^{25}, \alpha^{37}, \alpha^{44}, \alpha^{50}\}$
$C13 = \{13, 19, 26, 52, 41, 38\}$	$\{\alpha^{13}, \alpha^{19}, \alpha^{26}, \alpha^{38}, \alpha^{41}, \alpha^{52}\}$
$C15 = \{15, 30, 39, 51, 57, 60\}$	$\{\alpha^{15}, \alpha^{30}, \alpha^{39}, \alpha^{51}, \alpha^{57}, \alpha^{60}\}$
$C21 = \{21, 42\}$	$\{\alpha^{21}, \alpha^{42}\}$
$C23 = \{23, 29, 43, 46, 53, 58\}$	$\{\alpha^{23}, \alpha^{29}, \alpha^{43}, \alpha^{46}, \alpha^{53}, \alpha^{58}\}$
$C27 = \{27, 45, 54\}$	$\{\alpha^{27}, \alpha^{45}, \alpha^{54}\}$
$C31 = \{31, 47, 55, 59, 61, 62\}$	$\{\alpha^{31}, \alpha^{47}, \alpha^{55}, \alpha^{59}, \alpha^{61}, \alpha^{62}\}$

For the first conjugacy class, elements are found as-

$\alpha,\ (\alpha)^{2^1} = \alpha^2, (\alpha)^{2^2} = \alpha^4, (\alpha)^{2^3} = \alpha^8, (\alpha)^{2^4} = \alpha^{16},\ (\alpha)^{2^5} = \alpha^{32},\ (\alpha)^{2^6} = \alpha^{64} = \alpha,$

Therefore, C1= {1, 2, 4, 8, 16, 32}.

Similarly other classes are found as shown in Table 3.5.

For the design of BCH code with t=5, we now have the parameters as:

$n = 63, m = 6, t = 50.$ Since $n - k = m.t = 30$, $k = 63 - 30 = 36.$

Another parameter for narrow sense BCH code is, $b = 1.$

For the generator polynomial $g(x)$ to be a minimal degree polynomial in $F_2[x]$,

$$g(\alpha^b) = g(\alpha^{b+1}) = g(\alpha^{b+2}) = ..g(\alpha^{b+\delta-2}) = 0$$

For $b = 1,$ we need to find minimal polynomials for $g(\alpha^1)$ to $g(\alpha^{2t}) = g(\alpha^{10})$.

Using the coset table obtained as in Table 3.5, all the minimal polynomials are listed as in Table 3.6.

Table 3.6 Minimal polynomials for F_{2^6}

$M_0(x) = (x+1)$
$M_1(x) = (x+\alpha)(x+\alpha^2)(x+\alpha^4)(x+\alpha^8)(x+\alpha^{16})(x+\alpha^{32}) = 1+x+x^6$
$M_3(x) = (x+\alpha^3)(x+\alpha^6)(x+\alpha^{12})(x+\alpha^{24})(x+\alpha^{33}) = 1+x+x^2+x^4+x^6$
$M_5(x) = (x+\alpha^5)(x+\alpha^{10})(x+\alpha^{20})(x+\alpha^{17})(x+\alpha^{34})(x+\alpha^{40}) = 1+x+x^2+x^5+x^6$
$M_7(x) = (x+\alpha^7)(x+\alpha^{14})(x+\alpha^{28})(x+\alpha^{35})(x+\alpha^{49})(x+\alpha^{56}) = 1+x^3+x^6$
$M_9(x) = (x+\alpha^9)(x+\alpha^{18})(x+\alpha^{36}) = 1+x^2+x^3$
$M_{11}(x) = (x+\alpha^{11})(x+\alpha^{22})(x+\alpha^{25})(x+\alpha^{37})(x+\alpha^{44})(x+\alpha^{50}) = 1+x^2+x^3+x^5+x^6$
$M_{13}(x) = (x+\alpha^{13})(x+\alpha^{19})(x+\alpha^{26})(x+\alpha^{41})(x+\alpha^{38})(x+\alpha^{52}) = 1+x+x^3+x^4+x^6$
$M_{15}(x) = (x+\alpha^{15})(x+\alpha^{30})(x+\alpha^{39})(x+\alpha^{51})(x+\alpha^{57})(x+\alpha^{60}) = 1+x^2+x^4+x^5+x^6$
$M_{21}(x) = (x+\alpha^{21})(x+\alpha^{42}) = 1+x+x^2$
$M_{23}(x) = (x+\alpha^{23})(x+\alpha^{29})(x+\alpha^{43})(x+\alpha^{46})(x+\alpha^{53})(x+\alpha^{58}) = 1+x+x^4+x^5+x^6$
$M_{27}(x) = (x+\alpha^{27})(x+\alpha^{45})(x+\alpha^{54}) = 1+x+x^3$
$M_{23}(x) = (x+\alpha^{31})(x+\alpha^{47})(x+\alpha^{55})(x+\alpha^{59})(x+\alpha^{61})(x+\alpha^{62}) = 1+x^5+x^6$

Using the Table 3.6, we find that polynomials for $g(\alpha^1)$ to $g(\alpha^{10})$ are required to be: $M_1(x), M_3(x)M_5(x)M_7(x)$ and $M_9(x)$.

Generator polynomial is now given as the product of minimal polynomials as:

$$g(x) = LCM\{M_1(x), M_3(x), M_5(x), M_7(x), M_9(x)\}$$

Using the expressions for field elements as in Table 3.4, simplified expressions for $M_1(x)$ to $M_9(x)$ are found (shown in Table 3.5).

$g(x)$ is then given as,

$$g(x) = LCM\{(1+x+x^6), (1+x+x^2+x^4+x^6), \left(1+x+x^2+x^5+x^6\right),$$
$$\left(1+x^3+x^6\right), (1+x^3+x^6)\}$$

And we get, $g(x) = x^2+x^4+x^8+x^{15}+x^{17}+x^{18}+x^{27}$

The generator polynomial is now used for systematic encoding of the message polynomial as per the steps given in 3.4.4.

Decoding is performed using BM algorithm as per the steps explained in 3.5.

In sections 3.1 to 3.6, background information needed to appreciate the algebraic structure of Block codes (specifically BCH codes) has been briefly presented. This has been followed by an explanation of the design procedure used to synthesize, encode and decode BCH codes. The synthesis of (63, 36) BCH code that has been employed in this research work is illustrated. In the next section, design principles of Turbo codes will be briefly presented.

3.7 DESIGN OF TURBO CODE

The use of a concatenated arrangement consisting of a Turbo code for forward error correction and Orthogonal Frequency Division Multiplexing (OFDM) as digital modulation scheme have been suggested by several researchers [Halid Hrasnica 2004], [M. Katayama et al.], [Francis Berrysmith], for narrowband power line communication.

The power line channel suffers from several impairments, the most significant of which are, time variant impedance mismatch and impulse noise. It has been established that Turbo code is effective in correcting errors arising from impulsive disturbances in channels perturbed by Gaussian noise [Berrou et al. 1993]. It is natural to expect that a Turbo code and OFDM arrangement would be able to perform well over the power line channel that is perturbed by time variant impedance mismatch and impulse noise. Following this approach, an attempt was made to study the performance of a concatenated arrangement comprising of a Turbo code and 32-carrier OFDM modulator. The design of Turbo code encoder/decoder, design of OFDM modulator/demodulator and performance of this concatenated arrangement over a channel perturbed by additive white Gaussian noise (AWGN) and impulse noise has been presented in this chapter.

The Turbo code employed in this thesis is a four state Parallel Concatenated Convolutional Code (PCCC). An encoder and decoder for this code has been successfully designed and tested in simulation platform.

3.7.1 Introduction to Turbo codes

The field of 'channel coding' started with Claude Shannon's 1948 landmark paper [C. E. Shannon 1948]. The invention of Turbo codes in the early 1990's and their first public presentation in May 1993, by Berrou, Alain Glavieux and Thitimajashima, titled "Near Shannon Limit Error-Correcting coding and Decoding: Turbo Codes", at the IEEE International Conference on Communications (ICC) at Geneva [Berrou et. al. 1993], highlighted the importance of this approach for securing information against channel induced errors [Alain Glavieux 2007].

3.7.2 Concatenation of codes

The power of FEC increases with code word length n, and approaches Shannon's limit only for very large values of n. In addition, decoding complexity increases very rapidly with code word length. Thus, it would be desirable to build a long, complex code out of much shorter component codes which can be decoded much more easily. Concatenation provides a very straight forward means of achieving this. Turbo codes can be concatenated in two ways: either in parallel concatenated turbo codes or in serial concatenated turbo codes [Shu Lin, D. J. Costelo 2003].

3.8 Turbo encoder [Shu Lin, D. J. Costelo 2003]

The block diagram of Turbo encoder is as shown in Figure. 3.1. The encoder consists of two identical rate R=1/2 Recursive Systematic Convolutional (RSC) encoder in parallel.

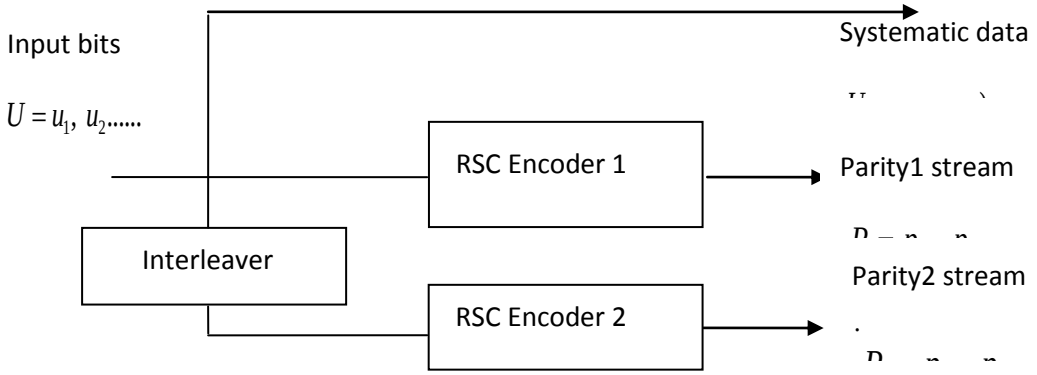

Figure 3.1 Turbo Encoder Block Diagram

The input data is transmitted to the upper RSC Encoder 1 in normal order while it is interleaved before being fed to the lower RSC Encoder 2. The output of the encoder consists of the systematic information and the parity information from the upper RSC Encoder 1 (Parity1 Data) and the parity information from the lower RSC Encoder 2 (Parity2 Data). The overall code rate of the parallel concatenated code is therefore, R = 1/3.

3.8.1 Recursive Systematic Convolutional (RSC) Encoder

RSC encoder differs from convolutional or non-recursive in (NSC) terms of the feedback. In an RSC encoder there is a feedback from output back to the input. The recursive systematic convolutional (RSC) encoder is obtained from the nonrecursive nonsystematic (conventional) convolutional encoder by feeding back one of its encoded outputs to its input. Figure 3.2 shows the RSC encoder.

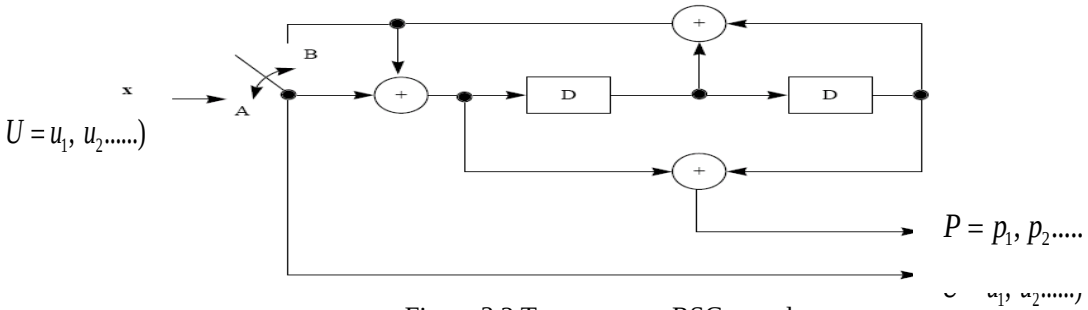

Figure 3.2 Two memory RSC encoder.

The RSC encoder consists of shift registers and modulo two adders. The contents of the shift register at any time define the state of the encoder and modulo two adders perform exclusive OR operation. In the two memory RSC encoder shown in the Figure 3.2, output consists of systematic data bits and RSC encoded data bits. The switch is turned on to position A, for encoding the input sequence and is turned on to position B, for terminating the trellis. Figure 3.3 shows the state diagram of the RSC component encoder. The encoder employs a shift register of length 2 (m=2). Hence, it has four states. These are indicated in Figure 3.3.

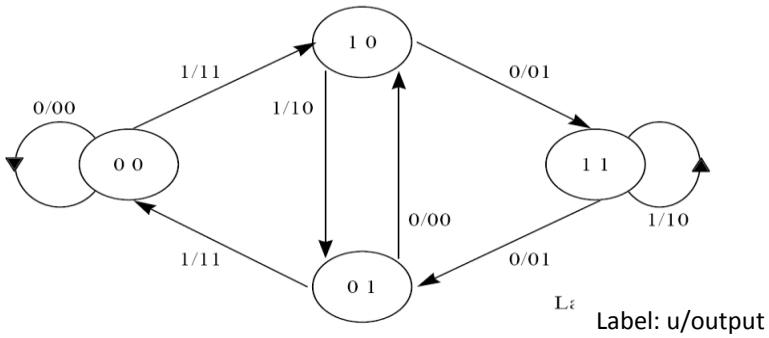

Figure 3.3 State diagram for two memory RSC encoder.

3.8.2 Trellis Termination

After the input bits have been encoded, the trellis is forced into the all-zeros state by the proper selection of tail bits. This is called trellis termination. Tail bits are padded at the end of the encoding of information bits in a particular frame. The tail bits of a RSC encoder depend on the state of the encoder. It is necessary to calculate each encoder's tail bits separately and transmit them, since the states of the two encoders would be different after the data bits have been encoded [Alain Glavieux 2007].

3.9 BCJR ALGORITHM [Shu Lin, D J Costelo 2003], [Alain G. 2007].

In 1974 Bahl, Cocke, Jelinek and Raviv (BCJR) introduced Maximum Aposteriori Probability (MAP) decoder called as BCJR algorithm, which can be applied to any linear code, block code or convolutional code. The algorithm calculates the aposteriori L values (likelihood values) called the APP L values, of each information bit.

3.9.1 Working of BCJR decoding Algorithm

The BCJR algorithm works on a trellis representing the finite-state machine which describes the channel and the complexity of the algorithm is proportional to the number of trellis states. Likelihood ratio for the decision is given as-

$$\mathrm{L}(u_l) \equiv \ln\left[\frac{P(u_l=+1|r)}{P(u_l=-1|r)}\right] \qquad (3.1)$$

The decoder output is given by $\widehat{u_l} = +1, if\ L(u_l) > 0\ and - 1\ if\ L(u_l) < 0.$

The Aposteriori probability (APP) values in (3.1) are modified by making use of trellis structure of the code[Alain Glavieux 2007], [Shu Lin, D J Costello 2003] and (3.1) is rewritten as-

$$\mathrm{L}(u_l) \equiv \ln\left[\frac{\sum_{(s',s)\epsilon\,\Sigma_l} P(s_l = s', s_{l+1} = s|r)}{\sum_{(s',s)\epsilon\,\Sigma_l} -P(s_l = s', s_{l+1} = s|r)}\right] \tag{3.2}$$

where s' is the previous state, s is the present state and r is the received vector.

$$p(s', s|r) = e^{\beta^*_{l+1}(s)+\lambda^*_l(s',s)+\alpha^*_l(s')} \tag{3.3}$$

where, $\alpha^*_l(s')$ is ***forward metric*** with initial condition,

$$\alpha_0(s) = 1 \quad \text{for } s = 0$$
$$= 0 \quad \text{for } s \neq 0$$

$\beta^*_{l+1}(s)$ is ***backward metric*** with initial condition,

$$\beta_k(s) = 1 \;\; for\; s = 0$$
$$= 0 \;\; for\; s \neq 0$$

$\gamma^*_l(s', s)$ is the ***branch metric*** calculated differently for message and tail bits.

(3.1) is rewritten by considering α, β and γ as

$$L(u_l) = \ln\{\Sigma_{(s_l,s)\epsilon\Sigma_l^+} e^{\beta^*_{l+1}(s)+\gamma^*_l(s',s)+\alpha^* l(s')}\} - \ln\{\Sigma_{(s_l,s)\epsilon\Sigma_l^-} e^{\beta^*_{l+1}(s)+\gamma^*_l(s',s)+\alpha^* l(s')}\} \tag{3.4}$$

max* function is used for a two variable or three variable function can be defined by following equation, $\max(x, y, z) \equiv \ln(e^x + e^y + e^z) = max^*[max^*(x, y), z]$

Finally by using the above equations we calculate APP L-values as a function of max^* as [Alain Glavieux 2007]

$$L(u_l) = max^*_{(s_l,s)\epsilon\Sigma_l^+}[\beta^*_{l+1}(s) + \gamma^*_l(s', s) + \alpha^*_l(s')] -$$
$$max^*_{(s_l,s)\epsilon\Sigma_l^-}[\beta^*_{l+1}(s) + \gamma^*_l(s', s) + \alpha^*_l(s')] \tag{3.5}$$

3.9.2 LOG MAP Algorithm [Shu Lin, D J Costelo 2003], [Alain G. 2007]

BCJR decoding algorithm given by (3.9) is LOG MAP algorithm given by following steps:

- Initialize forward and backward recursions $\alpha_0(s)$ and β^*_N(s)
- Initialize forward and backward recursions $\alpha_0(s)$ and β^*_N(s)
- Compute branch metrics $\gamma^*_l(s', s)$

- Carry out forward recursion $\alpha_{l+1}^{*}(s)$ based on $\alpha_{l}^{*}(s)$
- Carry out backward recursion $\beta_{l-1}^{*}(s)$ based on $\beta_{l}^{*}(s)$.
- Compute APP L-value
- Compute the hard decision values.

The most difficult calculations in the above algorithm is the evaluation of the exponential term needed in computation of max^{*} operation. These calculations can be simplified as in (3.10) where the maximum of two values [Alain Glavieux 2007] is found using max-log-map algorithm which uses-

$$\max(x, y, z) \equiv \ln(e^{x} + e^{y} + e^{z}) = max^{*}[max^{*}(x, y), z]$$
$$max^{*}(x, y) = \ln(e^{x} + e^{y}) \cong max(x, y).$$

3.10 TURBO DECODER [Shu Lin, D J Costelo 2003], [Alain G. 2007].

The Turbo decoder consists of two elementary decoders in a serial concatenation scheme [Shu Lin, D J Costelo 2003], [Alain Glavieux, 2007]. Since soft decoding performs better than hard decoding, the first decoder provides a weighted soft decision in the form of Aposteriori probabilities (APPs) to the second decoder. The decoding proceeds in an iterative fashion. The block diagram of a turbo decoder is as Figure 3.4.

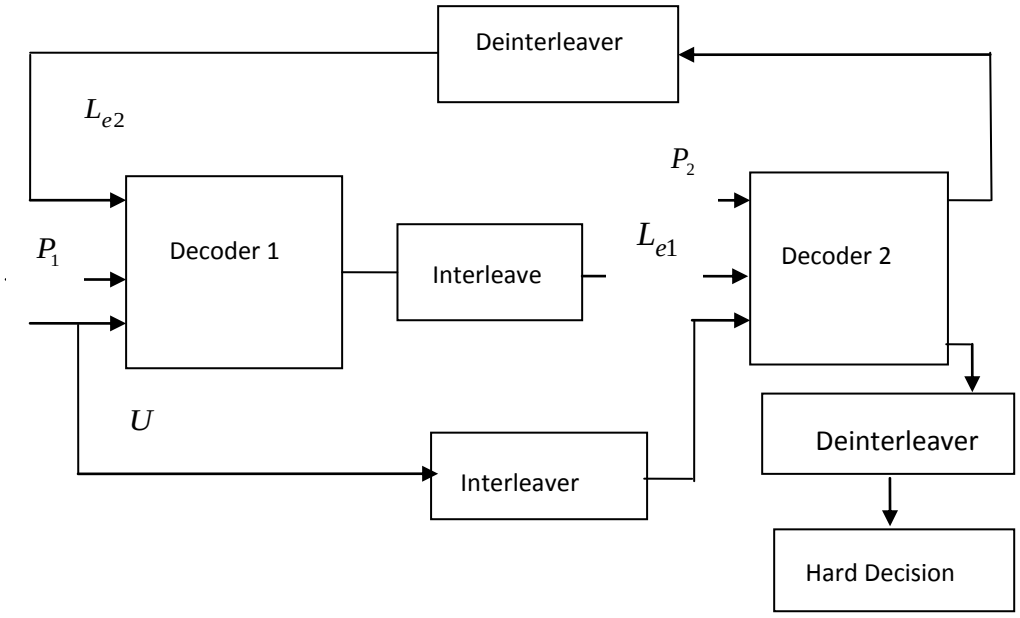

Figure 3.4 Block diagram of turbo decoder

The inputs to the first decoder are the observed systematic bits(U), the parity from the second decoder (P_1) and the soft information from the second decoder fed back to the first decoder (after the first iteration is complete). This is called the extrinsic or the a priori information (L_{e2}). This information is not available for the first decoder during the first iteration and is therefore initialized to zero.

The inputs to the second decoder are the interleaved versions of systematic bit stream (U) the observed parity bit stream (P_2) from the second RSC and the interleaved versions of extrinsic information (L_{e1}) from the first decoder.

The main task of the iterative decoding procedure, in each component decoder is an algorithm that computes the *a posteriori* probability (APP) of the information symbols which is the reliability value for each information symbol. The sequence of reliability values generated by a decoder is passed to the other one. In this way, each decoder takes advantage of the suggestions of the other one. The soft information is exchanged between the two decoders until the desired performance level is achieved. This is referred to as iterative decoding which is performed here using BCJR algorithm.

3.10.1 Parameters required in iterative decoding

Branch metric computation – γ unit

In the algorithm for turbo decoding the first computational block is the branch metric computation. The branch metrics are computed based on the knowledge of input and output associated with the branch during the transition from one state to another. There are four states and each state has two branches, which gives a total of eight branch metrics. The computation of branch metric is done using following equation,

$$\gamma_l(s', s) = \{u_l * L_a(u_l)\}/2 + L_C\ /2(u_l r_{ul} + p_l\, r_{pl})$$

$$= u_l/2[\, L_a(u_l) + L_C r_{ul}] + p_l/2 L_C r_{pl} \qquad (3.6)$$

$$L_C = 4 * (E_S/N_0)$$

where u_l ($U = u_1, u_2$ ...) is the systematic bits of information at the time instant l, L_C is the channel reliability factor which corresponds to the maximum signal to noise ratio (E_S/N_0), $L_a(L_{e1} or\ L_{e2})$ is the information that is fed back from one decoder to

the other decoder (a priori), p_l is the encoded parity bits of the encoder, r_{ul} is the received systematic bit, r_{pl} is the received parity bit. The branch metrics for all branches in the trellis are computed and stored.

Forward metric computation – α unit

The *forward metric* α is the next computation in the algorithm, which represents the probability of a state at time$l$, given the probabilities of states at previous time instance. α is calculated using (3.7).

$$\alpha_{l+1} = \max\left[\gamma_1(s', s) + \alpha_l(s')\right] \qquad (3.7)$$

α is computed at each node at a time instance l, in the forward direction traversing through the trellis. This metric is termed as forward metric because the computation order is from 0, 1, 2,... The α unit recursively computes the metric using γ values computed in the above step.

Backward metric unit- β Unit

The backward state probability being in each state of the trellis at each time l, given the knowledge of all the future received symbols, is recursively calculated and stored. The backward metric β is computed using (3.8) in the backward direction, going from the end to the beginning of the trellis at time instance l-1, given the probabilities at time instance l.

$$\beta_1(s) = \max\left[\gamma_l(s^1, s) + \beta_l(s')\right] \qquad (3.8)$$

The computation is the same as for α, but starting at the end of the trellis and going in the reverse direction.

Log likelihood ratio llr unit

Log likelihood ratio *llr* is the output of the turbo decoder. This output *llr* for each symbol at time l is calculated as-

$$llr[l-1] = \ln\frac{\sum_{u_l=1}\alpha[l-1]\beta[l]\,\gamma_{S',S}\,[l]}{\sum_{u_l=0}\alpha[l-1]\beta[l]\,\gamma_{S',S}\,[l]} \qquad (3.9)$$

The values γ, α unit output and the β values obtained from the above steps are used to compute the *llr values*. The main operations are comparison, addition and subtraction. Finally, these values are de-interleaved at the second decoder output, after the required number of iterations to make the hard decision, in order to retrieve the information that is transmitted.

Extrinsic unit

Compute the extrinsic information that is to be fed to the next decoder in the iteration sequence. This is the *llr* minus the input probability estimate. Extrinsic information computation uses the *llr* outputs, the systematic bits and the apriori information to compute the extrinsic value. This is the value that is fed back to the other decoder as the apriori information. This sequence of computations is repeated for each iteration by each of the two decoders. After all iterations are complete, the decoded information bits can be retrieved by simply looking at the sign bit of the *llr*: if it is positive the bit is a one, if it is negative the bit is a zero. This is because the *llr* is defined to be the logarithm of the ratio of the probability that the bit is a one to the probability that the bit is a zero. Extrinsic information is denoted by $L_e(u_1)$.

3.10.2 Trellis Diagram

In order to compute the above parameters the decoder makes use of stored information about the states and their transitions to next states with outputs defined for particular input represented either by code tree or trellis diagram. Trellis diagram is a tree like structure with re-emerging branches. Trellis is represented by number of states. A two-bit memory encoder forms a four state trellis structure shown in Figure 3.5. The four possible states of the encoder are depicted as four rows of horizontal dots. There is one column of four dots for the initial state of the encoder and one for each time instant during the message. The solid lines connecting dots in the diagram represent state transitions when the input bit is a one. The dotted lines represent state transitions when the input bit is a zero.

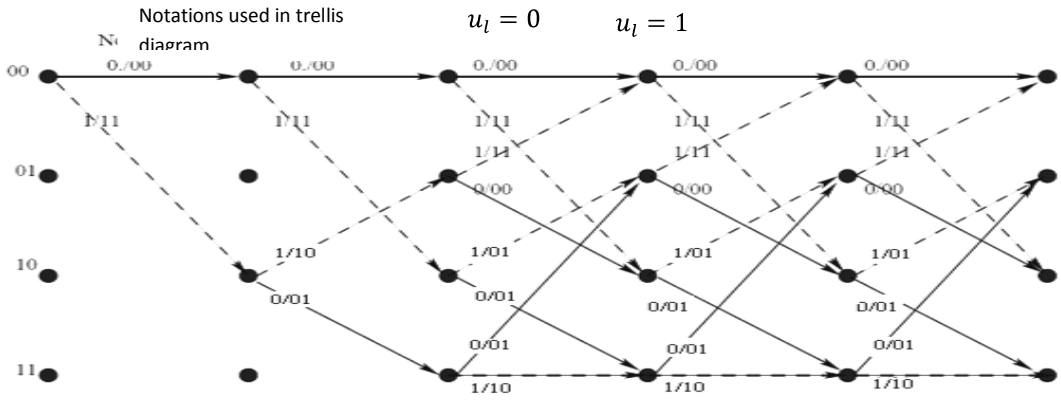

Figure 3.5 Trellis diagram for two bit memory RSC encoder

Since the initial condition of the encoder is State 00_2, the trellis starts out at State 00_2 and end up at the same state. At time instant $t = 0$, state 00 bifurcates into two branches. At time $t = 1$, there are two states each generating two branches, in all, four states are formed at time $t = 2$. At $t = 3$ all the eight branches are generated by four states. This is continued for all the message and tail bits.

3.10.3 INTERLEAVERS

Interleaving is a process of rearranging the ordering of a data sequence which is a practical technique to enhance the error correcting capability of coding. The inverse of this process is called deinterleaving which restores the received sequence to its original order. In the design of turbo code used in this research work, interleaving is done using a block interleaver, before the information data is encoded by the second component encoder.

In sections 3.7 to 3.10, algorithms to design encoder and decoder for four state Turbo code are explained. Turbo code designed in simulation platform is tested to work successfully.

Performances of Turbo code combined with Orthogonal Frequency Division Modulation (OFDM) are presented in section 5.2. The discussion on OFDM is followed in the next section.

3.11 Orthogonal Frequency Division Modulation (OFDM)

A combination of Turbo Convolutional code for forward error correction and OFDM as digital modulation scheme have been suggested in [Halid Hrasnica 2004], [Massaki Katayama et al. 2006], [Francis Berrysmith 2005], for narrowband power line communication. In this section, the basic principles of OFDM (Orthogonal Frequency Division Modulation) and the steps involved in the design of combination of Turbo coded OFDM arrangement have been is explained.

OFDM can be seen as either a modulation technique or a frequency multiplexing technique. OFDM is a digital multi-carrier modulation scheme, which uses a large

number of closely-spaced orthogonal sub-carriers. Each sub-carrier is modulated with different symbols with suitable conventional modulation scheme and then all the sub carriers are frequency-multiplexed, using orthogonal frequencies.

3.11.1 Merits of OFDM

In single carrier system, duration of a symbol becomes smaller if symbols need to be transmitted at a faster rate. This translates into a single carrier system being more susceptible to inter symbol interference which reduces the capability of the system to sustain higher throughputs. OFDM minimizes the inter-symbol interference by having longer symbol periods. This is because parallel transmission reduces the data rate that each individual carrier must convey which in turn lengthens the symbol. This is illustrated in Figure 3.6.

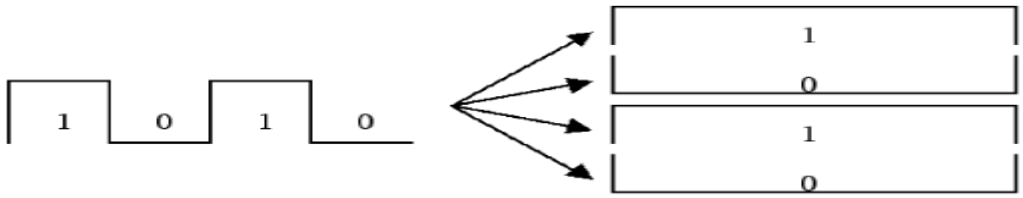

Figure 3.6 Symbol period comparisons

In addition, OFDM utilizes several parallel sub-carriers simultaneously; it is able to recover from errors more efficiently. This is because, not all of the information carried on different frequencies can be impacted from interference sources.

Sub-carriers in an OFDM system are precisely orthogonal to one another. Thus, they are able to overlap without interfering. As a result, OFDM systems are able to maximize spectral efficiency without causing adjacent channel interference.

3.11.2 Significance of OFDM

OFDM did not find mainstream application for many years because the generation of a large number of sub carriers in the conventional manner requires arrays of sinusoidal generators and coherent demodulators required in parallel. Such a system can become unreasonably expensive and complex. The receiver needs precise

phase information about all the carriers used to perform correct demodulation. Achieving and maintaining this synchronization can be very difficult in practice.

The application of the discrete Fourier transform (DFT) to parallel data transmission system as part of the modulation and demodulation process eliminates the banks of sub carrier oscillators and the need of coherent demodulators. The processing power of modern digital signal processors has increased to a point where realization of OFDM using DFT has become feasible and economical.

3.12 Fading channel [Proakis J. 1995]

To understand the fading and intersymbol interference (ISI) caused by multipath propagation consider the figure shown in Figure 3.7, for data transmission in a wireless channel. Because the signal reflects from large objects such as mountains or buildings, the receiver sees more than one copy of the signal. In communication terminology, this is called **multipath**.

The reflected signals arrive at the receiver with random phase offsets, because each reflection generally follows a different path to reach the receiver. The result is random signal variation (fading) as the reflections destructively (and constructively) superimpose on one another. This has the effect of effectively cancelling part of the signal energy for brief periods of time.

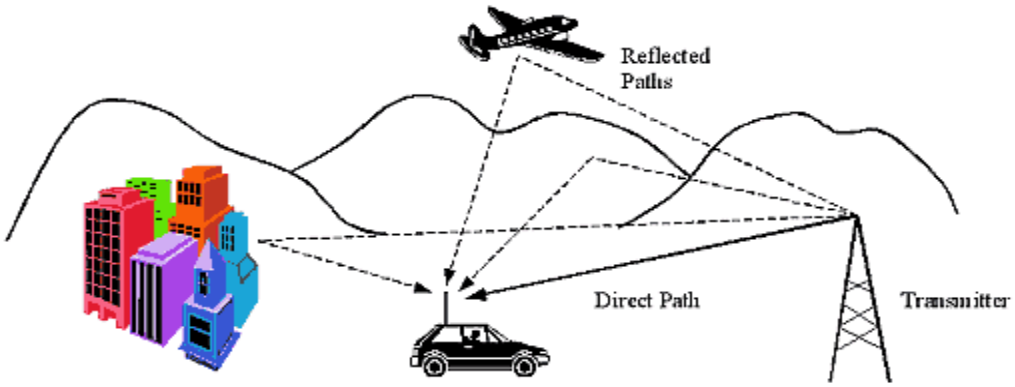

Figure 3.7 Multipath demonstration [Eric Lawrey 1997]

The random variation in the signal strength is referred to as fading which is inherent nature of the multipath channel. The terms **'Multi-path channel'** and **'fading channel'** are interchangeably used to describe a channel experiencing random

signal strength fluctuation. As a result of `multi-path effect', delayed copies of the signal interfere with the direct signal and this results in Inter Symbol Interference (ISI).

Note that in contrast to fading channel of a mobile or wireless channel where multiple reflections occur due to the presence of scatterers and obstacles in the medium, multiple reflections experienced on a power line channel are due to the different loads connected to the same power lines which are randomly switched ON and OFF. Important technical definitions related to fading channel are hereby provided.

Figures 3.8, 3.9 and 3.10 provide more information about various fading manifestations. Figure 3.8 shows the broad classification of a fading channel as large scale fading and small scale fading. Figure 3.9 shows the variation of signal strength due to large scale fading and small scale fading. The further classifications of small scale fading are explained in section 3.12.1.

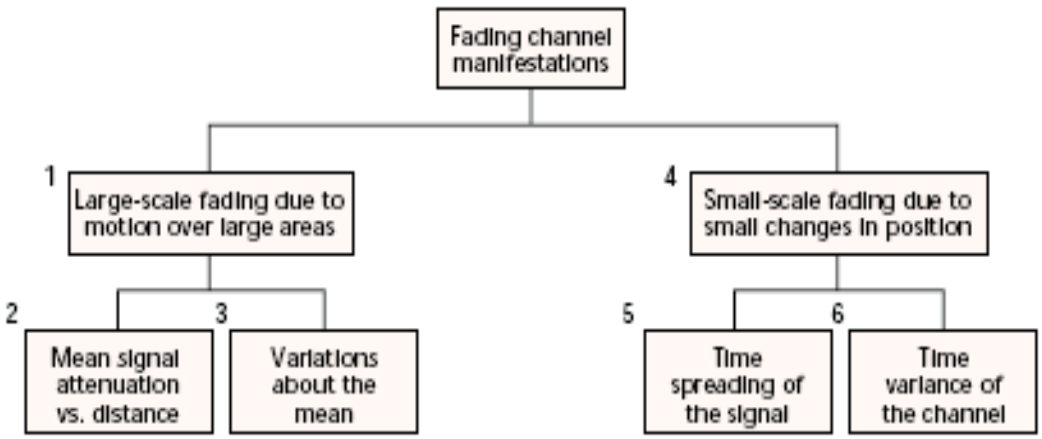

Figure 3.8 Fading channel manifestations [Bernard Sklar 1997].

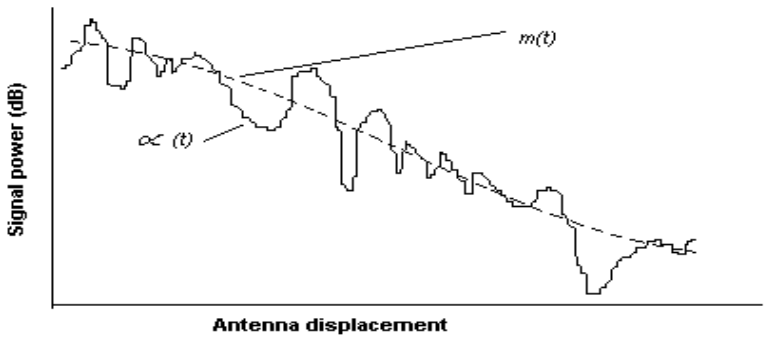

Figure 3.9 Small scale fading superimposed on large scale fading [Bernard Sklar 1997].

In order to model the received signal, it is assumed that different signal components arriving at a receiver location with different delays are uncorrelated. In Figure 3.10, a multipath intensity profile (Received signal power plotted as a function of time) is sketched [Bernard Sklar 1997]. The two important terms of fading channel, time delay (or time spread) and coherence bandwidth are explained using Figure 3.10.

3.12.1 Time delay and coherence bandwidth

For a transmitted impulse the average received power varies as a function of time delay τ. The term **time delay** refers to the **excess delay**. It represents the signal's propagation delay that exceeds the delay of the first signal arrival at the receiver. For a single transmitted impulse, the time T_m between the first and last received component represents the maximum excess delay, after which the multipath signal power falls below some threshold level relative to the strongest component.

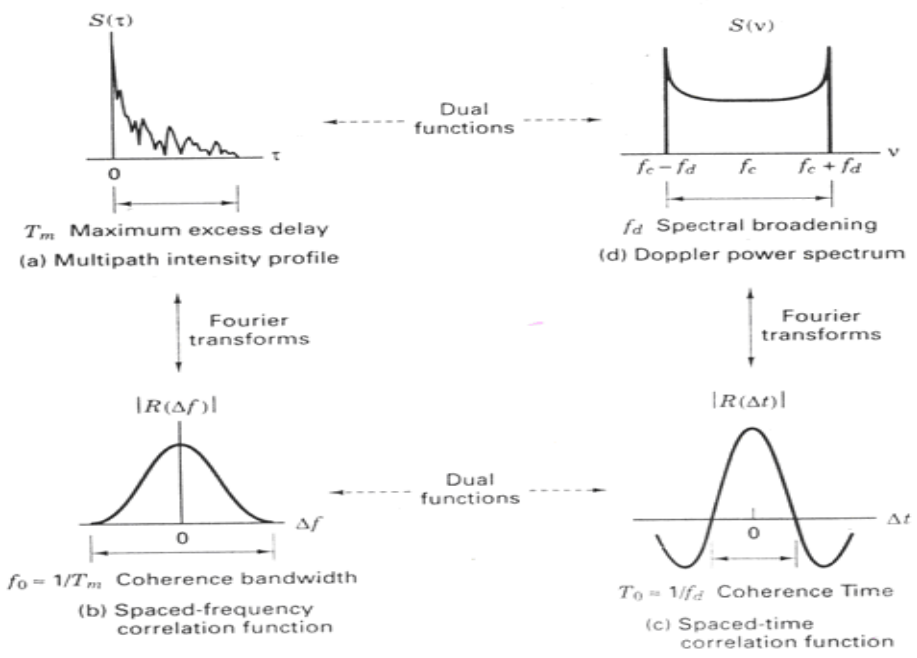

Figure 3.10 Relationship among channel correlation functions and power density functions [Bernard Sklar 1997].

Coherence bandwidth of fading channel is defined by viewing the time dispersion phenomenon in frequency domain. It is denoted as f_o and is defined as $f_o = \frac{1}{T_m}$. Time dispersion represents distortion to the signal and is manifested by the spreading in time

of the modulation symbols. Coherence bandwidth represents the range of frequencies over which spectral components exhibit correlated fading. Time dispersion leads to inter-symbol interference, or ISI, where the energy from one symbol spills over into another symbol, and as a result, the bit error rate (BER) is increased.

In many instances, the fading due to multi-path will be frequency selective, randomly affecting only a portion of the overall channel bandwidth at any given time. Frequency selective fading occurs when the channel introduces time dispersion and when the delay spread exceeds the symbol period.

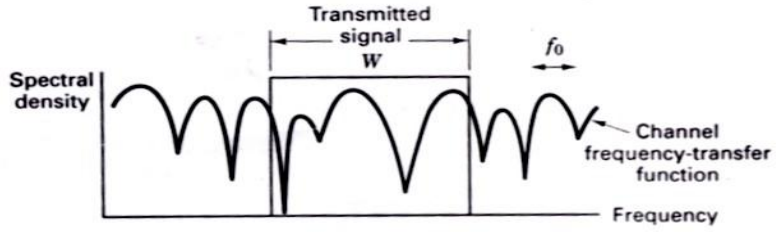

(a) Typical frequency-selective fading case $f_0 < W$.

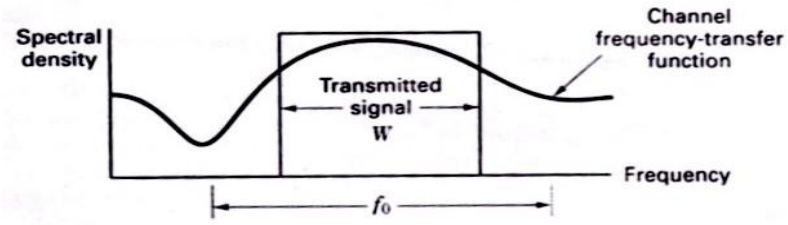

(b) Typical flat fading case $f_0 > W$

Figure 3.11 Relationships between channel frequency transfer function and a transmitted signal with bandwidth W [Bernard Sklar 1997].

In other words, a channel is referred to as **frequency-selective if $f_0 < W$**, where the symbol rate $1/T_s$, is nominally taken to be equal to the signaling rate or signal bandwidth W. Frequency-selective fading distortion occurs whenever a signal's spectral components are not all affected equally by the channel. Some of the signal's spectral components falling outside the coherence bandwidth will be affected differently

(independently), compared with those components contained within the coherence bandwidth. This is shown in Figure 3.11 (a).

When there is no dispersion and the delay spread is less than the symbol period, the fading will be flat, thereby affecting all frequencies in the signal equally. A channel is referred to as **Frequency-nonselective or flat-fading if** $f_0 > W$. Hence, all of the signal's spectral components will be affected by the channel in a similar manner. This is illustrated in Figure 3.11(b).

Flat fading does not introduce channel-induced ISI distortion, but performance degradation can still be expected due to the loss in SNR whenever the signal is fading. In order to avoid channel-induced ISI distortion, the channel is required to exhibit flat fading. This occurs, provided that $f_0 >$ W. Hence, the channel coherence bandwidth f_0 sets an upper limit on the transmission rate that can be used without incorporating an equalizer in the receiver.

3.12.2 Doppler spread and coherence time

Doppler spread describes the random changes in the channel introduced as a result of a user's mobility and the relative motion of objects in the channel. Doppler effect has the effect of shifting or spreading the frequency components of a signal. The **coherence time** of the channel is the inverse of the **Doppler spread** [Bernard Sklar 1997] and is a measure of the speed (rate) at which the channel characteristics change. This in effect determines the rate at which fading occurs. When the rate of change of the channel parameters is higher than the modulated symbol rate, **fast fading** occurs. **Slow fading** on the other hand, occurs when the channel changes are slower than the symbol rate.

3.13 Principles of operation of OFDM

In the discussions made in above paragraphs, if $f_0 > W$, then distortion due to ISI is minimized in a multipath channel. OFDM can be used for signal transmission in frequency selective fading channel while avoiding the use of an equalizer. This is achieved by lengthening (increasing) the symbol duration. The approach is to partition

a high symbol rate sequence into N symbol groups, so that each group contains a sequence with a lower symbol rate (by a factor$(1/N)$) than the original sequence. The signal band is made up of N orthogonal carrier waves, and each one is modulated by a different symbol group. The goal is to reduce the symbol rate (or signal bandwidth W) on each carrier such that it is less than the channels coherence bandwidth f_o.

For example, if a 100-tone system were used, a single data stream with a rate of 1 megabit per second (Mbps) would be converted into 100 streams of 10 kilobits per second (kbps). By creating slower parallel data streams, the bandwidth of the modulation symbol is effectively decreased by a factor of 100, or equivalently, the duration of the modulation symbol is increased by a factor of 100. The increase in symbol duration as explained, reflects in minimizing ISI.

3.13.1 Structure of OFDM

OFDM is a technique that divides the spectrum into a number of equally spaced tones. A tone can be thought of as a frequency. The "orthogonal" part of the OFDM name indicates that there is a precise mathematical relationship between the frequencies of the carriers in the system.

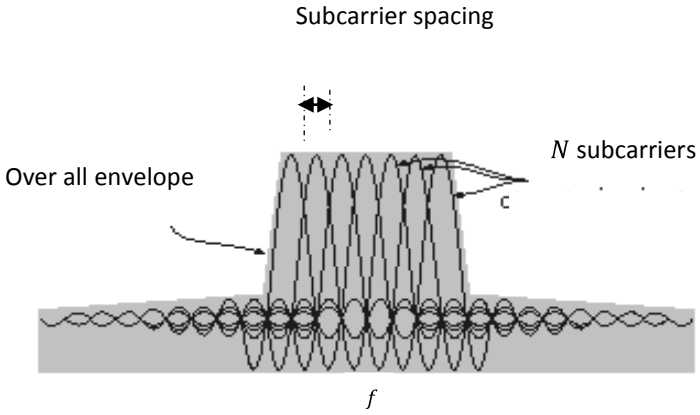

Figure3.12 **OFDM Spectrum showing N subcarriers and subcarrier spacing [Dusan Metic 1999]**

The orthogonality of the tones means that each tone has an integer number of cycles over a symbol period. Due to this, the spectrum of each tone has a null at the centre frequency of each of the other tone in the system as shown in Figure 3.12.

3.13.2 Mathematical description of OFDM [Dusan Matic 1999]

Mathematically, each carrier can be described as a complex wave:

$$s_c(t)=A_c(t)e^{j[\omega_c t+\varphi_n(t)]} \quad (3.10)$$

The real signal is the real part of $s_c(t)$, $A_c(t)$ and $f_c(t)$, the amplitude and frequency of the carrier can vary on a symbol by symbol basis, but the values of the parameters are constant over the symbol duration period T_S.

OFDM consists of many carriers. Thus the complex signals $s_s(t)$ is represented by:

$$s_s(t) = \frac{1}{N}\sum_{n=0}^{N-1} A_n(t)e^{j[2\pi f_n t+\varphi_n(t)]} \quad (3.11)$$

where, $\omega_n = \omega_0 + n\Delta\omega$

This is of course a continuous signal. If we consider the waveforms of each component of the signal over one symbol period, then the variables $A_n(t)$ and $\varphi_n(t)$ take on fixed values, which depend on the frequency of that particular carrier, and so can be rewritten:

$$\varphi_n(t) \Rightarrow \varphi_n \text{ and } A_n(t) \Rightarrow A_n$$

If the signal is sampled using a sampling frequency of $1/T$, then by substituting $t = kT$ the resulting signal (3.11) is,

$$s_s(kT) = \frac{1}{N}\sum_{n=0}^{N-1} A_n e^{j[(\omega_0+n\Delta\omega)kT+\varphi_n]} \quad (3.12)$$

If we now simplify (3.12), without a loss of generality by letting ω_0=0, then the signal becomes:

$$s_s(kT) = \frac{1}{N}\sum_{n=0}^{N-1} A_n e^{j(n\Delta\omega)kT}.e^{j\varphi_n} \quad (3.13)$$

Now (3.13) can be compared with the general form of the (N point) inverse Fourier transform:

$$g(kT) = \frac{1}{N}\sum_{n=0}^{N-1} G\left(\frac{n}{NT}\right)e^{j2\pi nklN} \quad (3.14)$$

In (3.14), the function $A_n e^{j\varphi_n}$ is no more than a definition of the signal in the sampled frequency domain, and $s(kT)$ is the time domain representation. (3.13) and (3.14) are equivalent if:

$$\Delta\omega = 2\pi f \text{ and } \Delta f = \frac{1}{NT} \quad (3.15)$$

This shows that OFDM signal can be defined by using Fourier transform procedures.

3.13.3 Block Diagram of OFDM

Discussions on mathematical description of an OFDM signal show that OFDM signal is equivalent to Inverse Discrete Fourier transform (DFT) signal and hence OFDM signal can be generated by using the same. The Fast Fourier transform (FFT) is merely a rapid mathematical method for computer applications of DFT.

As shown in Figure 3.13 [Eric Lawrey, 1997], at the transmitter, an OFDM system takes a data stream and splits it into N parallel data streams, each at a rate 1/N of the original rate. Each stream is then mapped to a tone at a unique frequency and combined together using the Inverse Fast Fourier transform (IFFT) to yield the time-domain waveform to be transmitted. At the receiver, the reverse operation to the transmitter is performed. i. e. The FFT of each symbol is taken to find the original transmitted signal [Eric Lawrey, 1997].

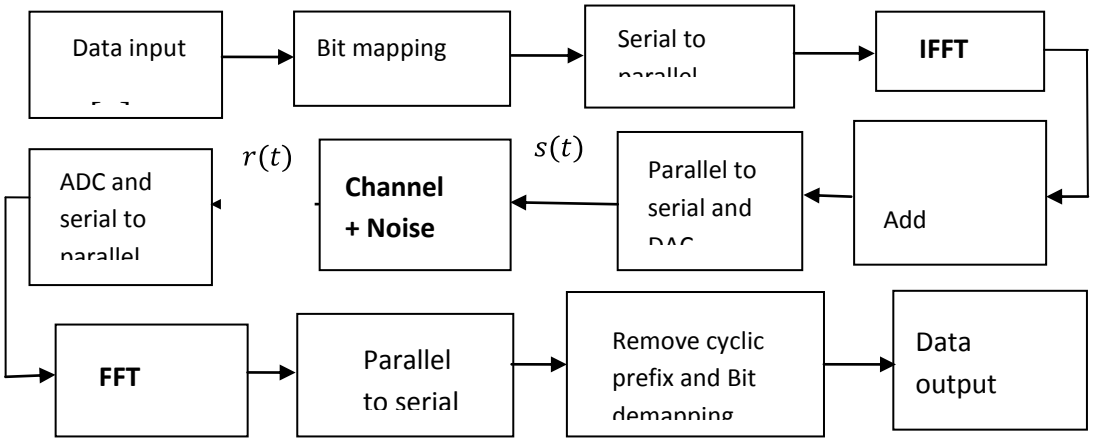

Figure 3.13 Block diagram of OFDM

The input $s[n]$ is a serial stream of binary digits. The input serial data stream is formatted into the word size required for transmission, which is termed as bit mapping (constellation), (e.g. 2 bits/symbol for QPSK) and then shifted into N parallel streams. Note that the constellations may be different, so some streams may carry a higher bit-rate than others. An inverse FFT is computed on each set of symbols

(N parallel streams), giving a set of complex time-domain samples. The real and imaginary components of these samples are then converted to the analogue domain using digital-to-analogue converters (DACs); the analogue signals are then used to modulate cosine and sine waves at the carrier frequency f_c, respectively. These signals are then summed to give the transmission signal $s(t)$. The received signal $r(t)$ is sampled and digitized using analog-to-digital converters (ADCs), and a forward FFT is used to convert back to the frequency domain. This returns N parallel streams, each of which is converted to a binary stream using an appropriate symbol detector. These streams are then re-combined into a serial stream $\widehat{s[n]}$, which is an estimate of the original binary stream at the transmitter.

3.13.4 Cyclic prefix

The term ***cyclic prefix*** refers to the prefixing of a symbol with a repetition of the end. Cyclic prefix acts as a buffer region where delayed information from the previous symbols can get stored. The receiver has to exclude samples from the cyclic prefix which get corrupted by the previous symbol when choosing the samples for an OFDM symbol. The effect of ISI on an OFDM signal can be further improved by the addition of cycliccopy as a guard period to the start of each symbol.

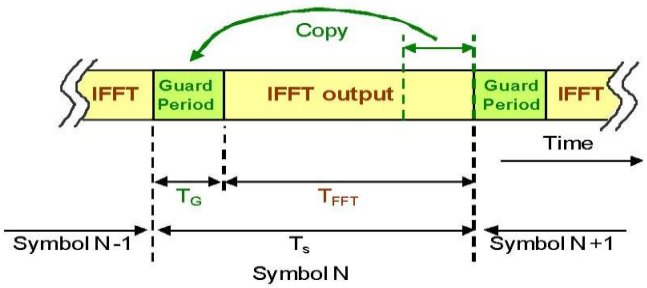

Figure.3.14 shows the insertion of a guard period [Christian H. et al. 2001]

Figure 3.14 shows the insertion of a guard period. The total length of the symbol is $T_S = T_G + T_{FFT}$, where T_S is the total length of the symbol in samples, T_G is the length of the guard period in samples and T_{FFT} is the size of the IFFT used to generate the OFDM signal.

In conclusion, OFDM has emerged as a widely used technique in wireless communications. The use of OFDM transforms a high data rate wide band signal into

several low data rate narrow band signals and decreases the complexity of equalization required at the receiver. In view of this promise, a number of researchers have tried to use this technique to improve the integrity of information carried over power lines.

3.14 Space time code

Space Time codes have been designed to take advantage of the fact that a multi-path channel provides a rich scattering environment. It is known that receivers separated by a distance exceeding half wavelength experience uncorrelated signal fading. This effect is referred to as space diversity. Space Time Codes (STC) exploit space diversity along with time diversity to achieve reliable communication on channels perturbed by multi-path effects and signal fading [Proakis J. 1995] [Bernard Sklar 1997]. The Alamouti Space Time Code has been widely used by a number of researchers in diverse applications [S.M. Alamouti 1998]. A brief introduction to this pioneering Space Time Code has been presented.

Alamouti's space time coding schemes comprises of $M = 2$ transmit antennas and $N = 1\ or\ 2$ receive antennas. These schemes are described as 2x1 Alamouti and 2x2 Alamouti respectively. In this report, 2x1 space time diversity scheme has been employed and the details are explained in the following section. Figure 3.15 gives the schematic of space time coding using 2x1 Alamouti scheme. (2 transmit antennas, 1 receive antenna).

3.14.1 Two Transmit One Receive (2x1) scheme of space time coding

Table 4.1 gives the transmit scheme for communication system shown in Figure 3.15. Let s_0 and s_1 represent symbols transmitted in two time slots as per Table 3.7. r denotes the received signal, h_0 and h_1 are transfer functions of channel 1 and channel 2 respectively. These are also referred to as channel parameters or as channel states.

$$h_0 = \propto_0 e^{j\theta_0}$$
$$h_1 = \propto_1 e^{j\theta_1}$$

Table 3.7 Alamouti's space time coding scheme at transmitter [S.M. Alamouti 1998].

	Antenna 0	Antenna 1
time *t*	s_0	s_1
time *t+T*	$-s_1^*$	s_0^*

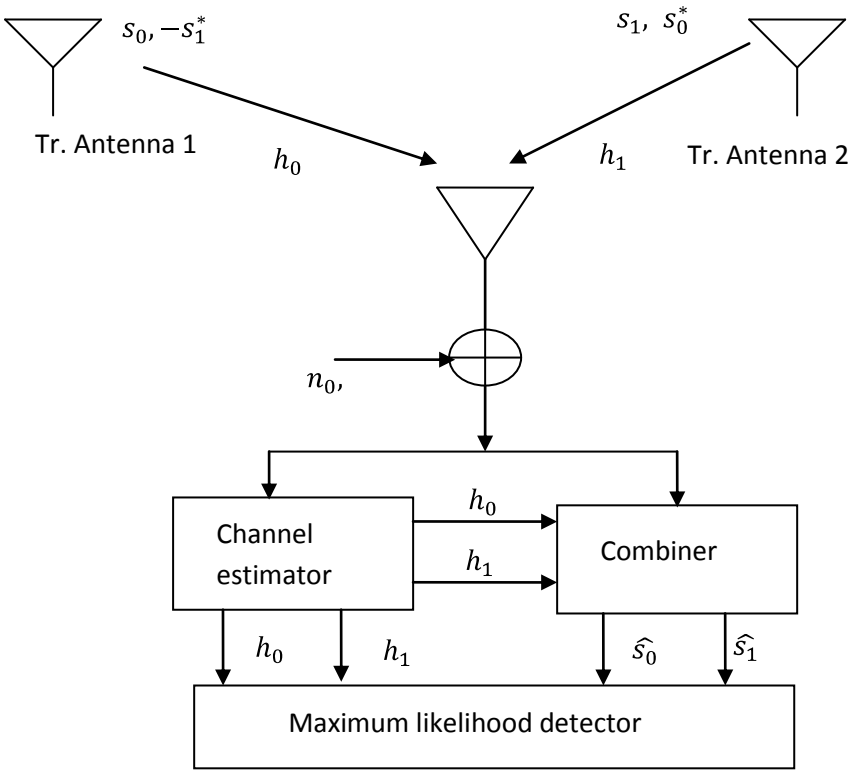

Figure 3.15 Two transmit, one receive diversity scheme [S.M. Alamouti 1998].

Figure 3.16 represents the simplified form of Figure 3.15.

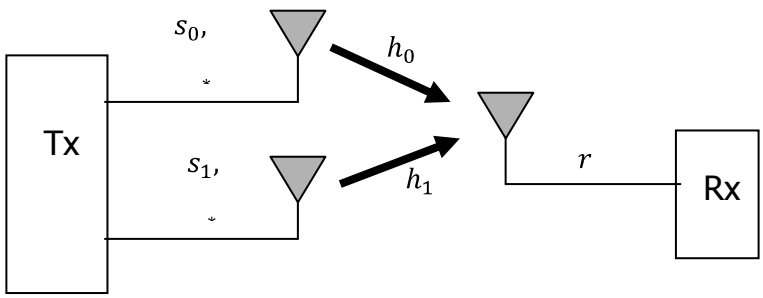

Figure 3.16 Alamouti's 2x1 space time coding

The received signal at the receiver due to the two transmit paths is given as-

$$r_0 = r(t) = h_0 s_0 + h_1 s_1 + n_0 \qquad \text{at time } t_0 \tag{3.16}$$

$$r_1 = r(t+T) = h_0(-s_1^*) + h_1 s_0^* + n_1 \quad \text{at time } t_1 \tag{3.17}$$

n_0 and $n_1$complex random variables representing receiver noise and interference.

$\widehat{s_0}$ and $\widehat{s_1}$ are estimates of symbols s_0 and s_1 at time slots t_0 and t_1 at the receiver, which are determined by (3.18) and (3.19).

3.14.2 Recovery of data at receiver

$$\widehat{s_0} = h_0^* r_0 + h_1^* r_1^* \tag{3.18}$$

$$\widehat{s_1} = h_1^* r_0 - h_0 r_1^* \tag{3.19}$$

The detailed mathematical support to derive receiving scheme is given in [S.M. Alamouti 1998]. Signal detection at the receiver requires the knowledge of the channel states (Channel State Information).

3.14.3 Channel state estimation

It is seen that recovery at the receiver requires the knowledge of channel states for performing symbol detection at the receiver. Knowledge of channel states is also referred to as Channel State Information (CSI). Many different approaches have been used for deriving CSI, in order to faithfully recover space time encoded data at the receiver. Accurate CSI is essential for faithful recovery of space time encoded data at the receiver.

Channel estimation in this report is performed by adding known dummy pilot symbols along with data symbols. Channel state during dummy symbol duration is estimated by dividing the received data with known symbols. This information is then employed for signal detection during actual data (information) symbol duration.

3.15 Power Line as multipath fading channel

The equivalent of two transmitting antennas in the Alamouti's space time coding scheme can be realized in power line channel, as power line channel provides uncorrelated paths for signal propagation. This property makes possible the use of space time coding scheme for a power line channel. In recent years, Rehan [Rehan

Hashmat et al. 2010] and Lopez et al. [Carlos Lopez et al. 2011] have shown the existence of uncorrelated paths on power lines.

L. Stadelmeier et al. have employed Alamouti scheme for Broadband PLC over low voltage lines and have observed BER of the order of 10^{-5} at about 30 dB of SNR in simulation studies[L Stadelmeier et. al. 2008].

Another concept of space frequency and space time code is used by B. Adebisi et al. [Bamidele Adebisi et al. 2009] for indoor power line communication at carrier frequencies less than 20 MHz. The multi-path model is used to represent the channel perturbations and Middleton Class-A model is used to represent channel noise. BER's of the order of 10^{-5} at 15 db SNR have been obtained in simulation studies. The Alamouti 2x1 Space time code is used along with OFDM.

These developments wherein the power line has been modeled as a multipath channel comprising of uncorrelated paths has encouraged researchers to think of adopting space time codes for protecting information integrity on power line channels. In this thesis, the performance of a concatenated arrangement consisting of a BCH code followed by the 2x1 Alamouti space time code on a medium voltage power line channel has been studied. In the following section, configuring of power line as equivalent to transmit and receive antennas for implementing space time coding has been explained.

3.15.1 Configuring Single phase power line for space time code

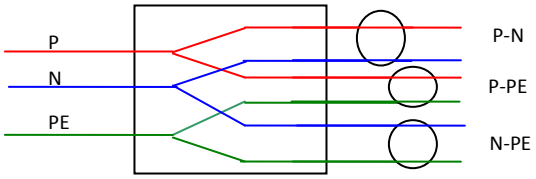

Figure 3.17 Splitter used for MIMO paths in a single phase power line.
P-Phase, N-neutral, PE-Protective Earth [Rehan Hashmat et al. 2010]

Power line channel can be treated as a multipath channel [Rehan Hashmat et. al. 2010]. The medium voltage power line consists of P (Phase), N (Neutral) and PE (Protective Earth) wires as shown in Figure 3.17. This arrangement is viewed as providing three possible paths with P-N, P-PE and N-PE, for differential signal transmission and reception.

3.15.2 Configuring three phase power line channel for space time code

A three phase power line is shown to provide three paths (or more). Signal propagation on these paths can be assumed to be statistically independent [Carlos López Giovaneli, Bahram Honary and Patrick G. Farrell 2011]. The three phases P1 (phase 1), P2 (phase 2), P3 (phase 3) can provide paths say P1-P2, P 2-P3 and P1-P3, as shown in Figure 3.18.

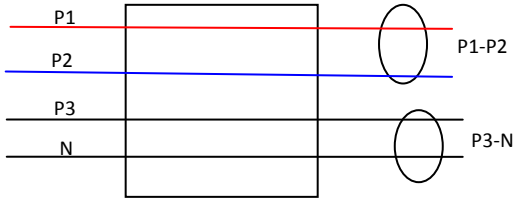

Figure 3.18 MIMO paths in a three phase powerline.
P1-Phase 1, P2-Phase 2, P3-Phase 3, N-Neutral [Rehan Hashmat et al. 2010]

3.16 Digital Modulation

In digital modulation, an information-bearing discrete-time symbol sequence (digital signal) is converted or impressed onto a continuous-time carrier waveform

A general carrier wave may be written:

$$c(t) = A_c \cos 2\pi f_c\, t$$

In Phase-Shift Keying (PSK), the phase of the carrier is changed in response to information and all else is kept fixed. In Binary PSK bit 1 is transmitted by a carrier of one particular phase and bit 0 by another phase by keeping amplitude and frequency constant.

$c(t) = A_c \cos 2\pi f_c\, t$ for bit "1"

$c(t) = A_c \cos(2\pi f_{c1} t + \pi)$ for bit "0"

PSK is used in the proposed work for modulating the digital data to an analog carrier signal to be coupled to the line. The digital data is coded by Alamouti's code and then PSK modulated for transmission.

Summary: This chapter has been devoted to the presentation of fundamental concepts needed to appreciate the work presented in this thesis. Since the purpose of the present research work is to verify data integrity on medium voltage power lines using different channel coding and modulation schemes, the essential theoretical concepts of the design of error correcting codes (Turbo codes and binary BCH codes) used in this thesis are explained. After a discussion of fundamentals of Galois field theory, a brief discussion of Turbo codes has been presented. OFDM is used along with Turbo code as one of the channel coding/modulation scheme, taken for study in the present work. Also Alamouti 2x1 scheme (normally applied to wireless channel), is applied to power line channel, chosen for improving data integrity, a study taken in this research work. Therefore a discussion of relevant ideas from OFDM and Space Time Codes forms the later part of this chapter. In the next chapter, the modeling of power line as a medium affected by multi-path propagation and impulsive noise will be presented.

Chapter 4

MODELING POWER LINE COMMUNICATION CHANNEL

To investigate the performance of a communication system that can work well in a medium voltage power line environment (channel), it first becomes essential to know the characteristics of attenuation and noise associated with the channel. After accurate modeling of transfer function and noise, the channel can be simulated and a study of the performance of the communication system operating on this channel can be carried out. Hence, this chapter is devoted to a study of the various models that have been proposed for understanding the behavior of the power line and associated noise.

Several researchers [A. Cataliotti et al. 2009], [M Zimmermann 2002], [Gotz et al. 2004] have worked on the problem of deriving suitable mathematical models for describing the data transmission behavior of power line channels. Models proposed by these researchers have aided the understanding and modeling of the behavior of the power line channel.

Researchers [Halid Hrasnica 2004], [M Katayama et al. 2006] have discussed the origin and behavior of several noise sources that can be found in low or medium-voltage power grids for narrowband PLC. They have mentioned that impulse noise generated in accordance with Middleton's Class-A model adequately represents the impairments on the power line caused by random impedance variations on the line brought about by appliances being switched on and off. Many researchers [D. Umehara et al. 2004], [Christine Hsu et al. 2007] have used Middleton's Class-A noise model for studying and analyzing impulsive interference on power lines.

In sections 4.1 and 4.2, the models for transfer function and noise used in this research work are described. Simulation results pertaining to channel attenuation are presented in section 4.3 and section 4.5 is devoted to deriving sample functions of noise

process governed by Middleton's Class-A distribution. The frequency response of the MV channel is plotted for different channel conditions and noise samples are generated for different channel disturbances. These models are used to test the communication systems proposed in this thesis.

It is proposed to model the power line as a multiple input multiple output (MIMO) channel. This allows the use of Alamouti space time coding scheme and concatenated BCH code to protect data against channel induced errors which is the focus of this research work. The power line channel simulated using the models explained in this chapter have been used to verify that successful data communication can be achieved using the BCH coded Alamouti space time coding scheme. These results are discussed in section 4.7.

4.1 Channel transfer function

The power line medium has unfavorable channel characteristics with considerable noise and high attenuation. This is because this infrastructure has been primarily designed for energy distribution and not for data transmission.

The impedance of power line channels exhibits strong variation with frequency and on network arrangement [Klaus M. Dostert 2003], [S. Robson et al. 2009]. Reflections are generated at the cable branches through the impedance discontinuities. Impedance is mainly influenced by the characteristic impedance of the cables, the topology of the considered part of network and the nature of the connected electrical loads. Statistical analysis of measurements has shown that nearly over the whole spectrum the mean value of the impedance is between 100 and 150 ohms. However, below 2 MHz, this mean value tends to drop towards lower values between 30 and 100 ohms. Owing to this variance of impedance, transmission losses are a common phenomena in PLC networks [A. Cataliotti 2008].

Different approaches have been proposed to describe the channel model of the power line medium. The optimum approach consists of considering the PLC medium as a multipath channel [M Zimmermann 2002], [Gotz et al. 2004], because of the multipath nature of power line that arises from the presence of several branches and

impedance mismatches which cause many signal reflections. This approach has the advantage that it provides a good match between measurements and the theoretical model and has been widely investigated. In this approach, it is necessary to take into consideration the very high number of paths associated with all the possible reflections from the unmatched terminations along the line.

Another approach has also been proposed, in which the transfer functions of equivalent circuits of the circuits/networks in the propagating path are derived and then the overall transfer function between transmitting and receiving point is derived as the resultant of cascaded two-port networks (2PN) of individual ones [T. Banwell and S. Galli 2001]. 2PN representation of the power line link is represented by means of transmission matrices also called ABCD matrices [Francis Berrysmith 2005].

From the multipath model suggested by Zimmerman [M. Zimmermann and K. Dostert 2002] and other literature studies of late, [Marcel Nassar et al. 2012] it has been determined that the power line channel can be viewed as a multipath channel for both broadband PLC and narrowband PLC.

In the following sections, the transfer function of power line channel offered by the multipath channel, the parameters that govern the transfer function and the simulation plots are discussed.

A simple approach to rough estimation of the transfer function of power line channels was presented by C. Hensen et al. [1999]. The attenuation increasing with higher frequencies can be interpolated by a straight line, so a simple equation can be found to calculate the amplitude of the channel transfer function. As this approach does not consider multipath propagation and the resulting notches (random reduction in signal level) of the channel transfer function, more detailed models had to be developed. Multipath propagation (echo model) has been found to be suitable for describing the transmission behavior of power line channels. Many researchers including [M. Zimmermann 2002], [Luis F. Montoya 2006], [A. Cataliotti et al. 2008], [A. Cataliotti et al. 2009] have proposed channel models based on this approach.

Echo model describes the channel impulse response as a superposition of N Dirac pulses representing the superposition of signals from N different paths. Each of these impulses is multiplied by a complex attenuation factor and delayed by a time factor. This model allows realistic reproduction of random signal fluctuations and the corresponding variation of the channel transfer function and is therefore well suited to describe power line channels [Gotz et al. 2004], [Francis Berrysmith 2005].

The propagation of signals over power line introduces an attenuation, which increases with the length of the line and the frequency. This attenuation is a function of the power line characteristic impedance Z_L and the propagation constant γ. These two parameters can be defined by line constants which comprise of the resistance R per unit length, the conductance G per unit length, the inductance L per unit length and the capacitance C per unit length, which are generally frequency dependent. Z_L and γ are formulated as [Halid Hrasnica et al. 2004]:

$$Z_L = \sqrt{\frac{R(f)+j2\pi L(f)}{G(f)+j2\pi C(f)}} \tag{4.1}$$

and

$$\gamma(f) = \sqrt{\big(R(f) + j2\pi f.L(f)\big).\big(G(f) + j2\pi f.C(f)\big)} \tag{4.2}$$

$$\gamma(f) = \alpha(f) + j\beta(f) \tag{4.3}$$

By considering a matched transmission line, which is equivalent to regarding only the propagation of the wave from source to destination, the transfer function of a line with length 'l' can be formulated as follows:

$$H(f) = e^{-\gamma(f).l} = e^{-\alpha(f).l}.e^{-j\beta(f).l}$$

$$\alpha(f) = Re\{\gamma\} = \frac{1}{2Z_L}\sqrt{\frac{\pi\mu_0}{Kr^2}}f + \frac{Z_L}{2} \tag{4.4}$$

μ_0, K and r represent permeability constant, conductivity and radius of the cable. Equation (4.4) can be given as-

$$\alpha(f) = Re\{\gamma\} = k_1.\sqrt{f} + k_2.f \tag{4.5}$$

with substitutions, $k_1 = \frac{1}{2Z_l}\sqrt{\frac{\pi\mu_0}{kr^2}}f$ and $k_2 = \frac{Z_L}{2}$

By comparing results obtained from this equation (4.5) with values obtained using field measurements, [Halid Hrasnica et al. 2004] has arrived at an approximation that is specified in (4.6).

$$\alpha(f) = a_0 + a_1 . f^k \qquad (4.6)$$

where a_0, a_1 are attenuation parameters and k is exponent of the attenuation factor [Halid Hrasnica et. al. 2004], [Francis Berrysmith 2005].

The propagation loss calculated above represents the loss of the signal per unit length. The attenuation over a medium is a function of its length $'l'$. By a suitable selection of the attenuation parameters a_0, a_1 and k the power line attenuation, representing the amplitude of the channel transfer function, can be defined as-

$$A(f, l) = e^{-\alpha(f).l} = e^{-(a_0 + a_1 . f^k).l} \qquad (4.7)$$

Equation (4.7) describes the relation of attenuation of a signal on a power line. As the transfer function of the power line is a function of attenuation function and phase function, this attenuation function is utilized in the construction of transfer function of power line as explained in section 4.2.

4.2 Modeling of the PLC Channel using multipath model

In addition to the frequency dependent attenuation that characterizes the power line channel, deep narrowband notches occur in the transfer function, which may be spread over the whole frequency range. These notches are caused by multiple reflections at impedance discontinuities. This behavior can be described by an "echo model" of the channel as illustrated in Figure 4.1.

Complying with the echo model, each transmitted signal reaches the receiver over N different paths. Each path i is defined by a certain delay τ_i and a certain attenuation factor c_i. The PLC channel can be described by means of a discrete-time impulse response $h(t)$ as,

$$h(t) = \sum_{i=1}^{N} c_i . \delta(t - \tau_i) \Leftrightarrow H(f) = \sum_{i=1}^{N} C_i . e^{-j2\pi f \tau_i} \qquad (4.8)$$

Factoring in the formula of the channel attenuation, the transfer function in the frequency domain can be written as,

$$H(f) = \sum_{i=1}^{N} g_i . A(f, l_i) . e^{-j2\pi f \tau_i} \qquad (4.9)$$

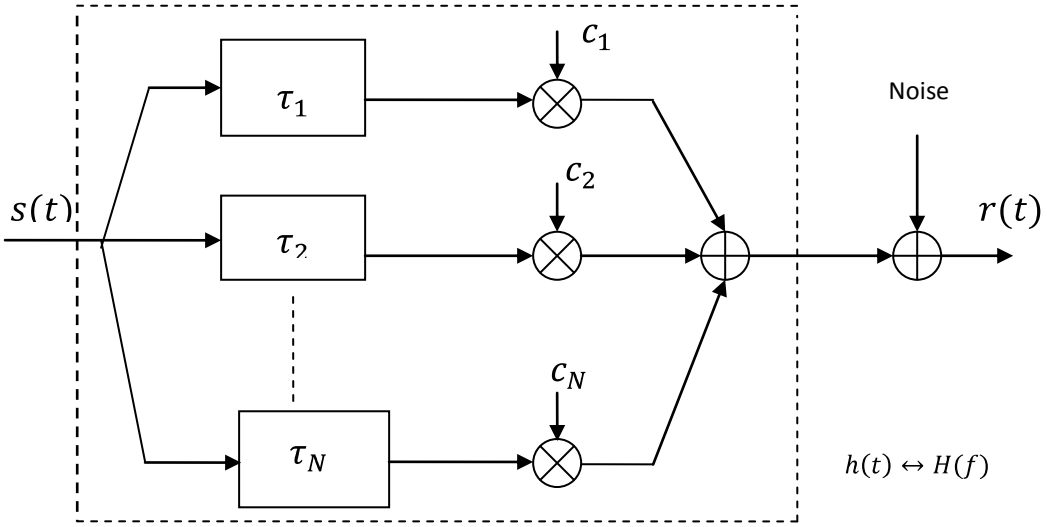

Figure 4.1 Echo model representing the multipath PLC channel model.

where g_i is a weighting factor for pat i h, representing the gain of each path. The variable $\tau_i (\tau_i = v_p/d_i)$, representing the delay introduced by the path i, is calculated by dividing d_i the length of path i, by the phase velocity.

By replacing the medium attenuation $A(f, l)$ the final equation of the PLC channel model is obtained, encompassing the parameters of its three characteristics, namely, the attenuation, impedance fluctuations and multipath effects. This equation is mainly composed of a weighting term, an attenuation term and a delay term [Halid Hrasnica et al. 2004].

$$H(f) = \sum_{i=1}^{N} \underbrace{g_i}_{\text{Weighting}} . \underbrace{e^{-(a_0 + a_1 . f^k) . l_i}}_{\text{Attenuation term}} . \underbrace{e^{-f2\pi f \tau_i}}_{\text{Delay}} \qquad (4.10)$$

The term g_i in (4.10) represents the gain of each path (weighting term), exponent of second term in (4.10) represents the attenuation of $H(f)$ with respect to frequency and the exponent of third term in (4.10) represents the delay (phase changes) in the received multipaths. It should be noted further that the attenuation and delay are functions of distance of multipath created as a function of time. Thus (4.10) represents the time variant and frequency variant channel transfer function.

Values taken on by g_i, $d_i$and τ_i are sample values of independent variables. Values of a_0, a_1 and k are the power line cable properties [Halid Hrasnica et al. 2004]. $\tau_i = d_i/v_p$ where v_p represents the velocity of signal propagation given as, $v_p = \frac{c_0}{\sqrt{\varepsilon_r}}$. ε_r is dielectric constant of the insulating material used in power cable.

A discussion on the study undertaken by research community [K. H. Zuberi 2003], [N. Suljanovic 2004], [Yihe Guo et al. 2009], [S. Robson et al. 2009], [Antonio Cataliotti et al. 2010], [Lampe L and Vinck AJHan 2011], [Marcel Nassar et al. 2012], [A Dabak et al. 2012], on channel attenuation as a function of line length and frequency is given in sections 2.4.1 and 2.4.2. In continuation, more insight into the frequency selective nature of power line channel is obtained by referring to the following observations:

- Frequency response $H(f)$ and corresponding impulse response plots of the power line for the frequency range of 3 MHz to 20 MHz, (both simulated and measured) have been discussed in [Matthias Gotz et al. 2004]. They have also provided a description of frequency response for broadband PLC. This helps in the visulaization of the channel frequency response in higher frequency (MHz range).

- Frequency response $H(f)$ and corresponding impulse response plots of the power line for the frequency range of 0 to 30 MHz have also been discussed in [Francis Berrysmith 2005]. These figures have been reproduced for reference in Figure 4.2.

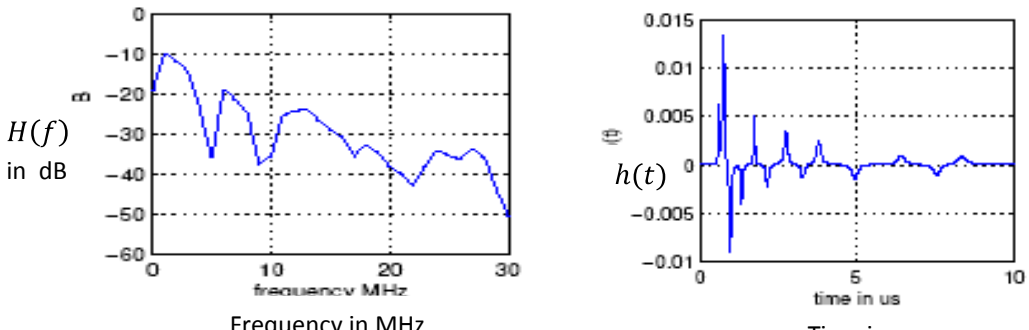

Figure 4.2 Attenuation response and impulse response for simulated channel [Francis Berrysmith 2005].

- Attenuation ($H(f)$) plot in dB (both measured and simulated) for a medium voltage to low voltage transformer-coupler arrangement in the range 3kHz to 500kHz has been determined by [A. Dabak et al. 2012]. This information has been reproduced in Figure 4.3. From Figure 4.3 it can be seen that attenuation shows random fluctuations with frequency and increases with frequency.

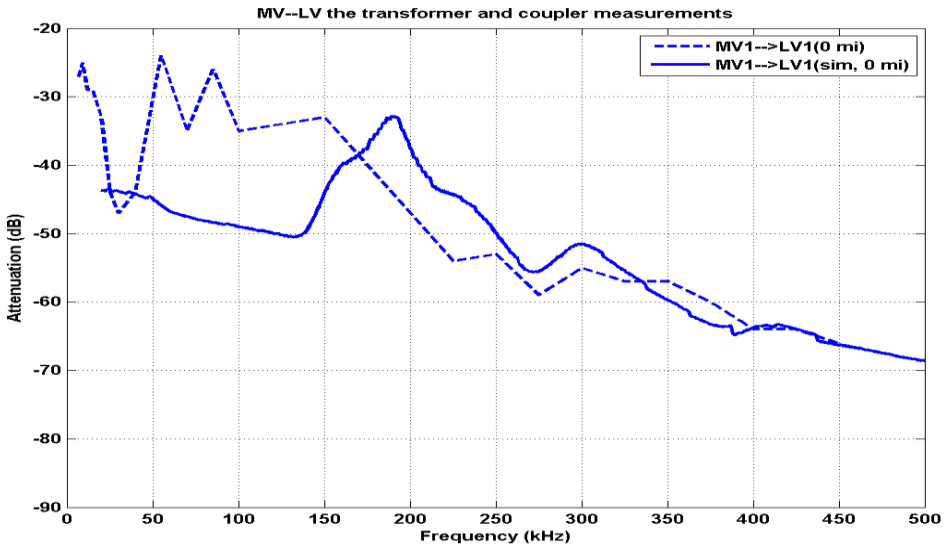

Figure 4.3 Magnitude of Transfer function of power line in dB vs. Frequency for a MV/LV Transformer-coupler by [A. Dabak et al. 2012]

- Channel attenuation for MV channels (1 to 30 kV) was measured by Il Han Kim et al. [Il Han Kim, Anand Dabak, David Rieken, Gordon Gregg 2012], in the frequency range from 50–450 kHz. Two distances 0.25 mile and 1.3 mile between two MV stations were used for this test. Tests also were conducted to check the effect of a capacitor bank inserted between the transmitter and receiver. From the results given by these researchers, it has been realized that attenuation for 0.25 mile distance was between 50 to 60 db while for 1.3 mile distance, the attenuation was between 60 to 85 dB. Further, the presence of a capacitor bank as a load point placed in between the transmitter and receiver, introduced a loss of about 20 dB in the signal in both cases.

These observations give insight into the magnitude of attenuation that can be present on the MV power line. The channel transfer function simulated in this thesis takes into account that channel attenuation is frequency variant (and time variant) function with the attenuation magnitude taking values up to 100 dB.

- Similarly, Figure 2.5 in chapter 2 shows the channel attenuation with frequency when more loads are connected on the transmission line between transmitter and receiver. This study has been conducted by Robson [S. Robson et al. 2009] in a simulated substation, the frequency response of which is described in section 2.4.2.

  The results observed by Robson [S. Robson et al. 2009] show more variations in the attenuation ranging from 0dB to 60dB than that observed by [Il Han Kim et al. 2012]. This behavior of channel attenuation can be explained by observing that the path of signal propagation used by the former had more number of loads being connected in the test, where as Han Kim et al. used only a capacitor unit as a disturbing load.

The study of relevant literature on field tests and simulation tests on the behavior of MV power line channel attenuation as discussed in the above paragraphs, are helpful in simulating a power line channel for study purpose in this thesis, which will have similar type of attenuation variations as compared to a realistic channel. In the next sections, simulation results on power line channel attenuation which are carried out as a first step of research work are given.

4.3 Simulation studies on Power Line channel model

- It is necessary to mention here that the focus of the thesis is the study of a few Channel coding and Modulation schemes to improve information integrity of power line channels carrying data. The study relates to channel coding for power line communication using medium voltage (1kV to 30 kV) power lines keeping in view the environment of medium voltage substation. In order to test the channel coding schemes, a model of power line that will account for time and frequency variant attenuation/channel coefficients exhibited by the channel is used and the attenuation parameters are appropriately chosen. The AM (Amplitude Modulation) broadcast range sets a limit on the frequency range of narrowband power line communication for substation automation. The frequencies employed should be less than the lower end of the AM broadcast range i.e. less than 500 kHz. Therefore to simulate the transfer function of the power line for narrowband PLC, frequency response needs to be evaluated between 3 kHz to 450 kHz. In addition, keeping in view the nature

of interfering mechanisms, multi-path channel model is used. The channel attenuation plots with respect to frequency have been presented in this section.

The variation of channel attenuation $|H(f)|$, with respect to frequency depends upon (refer Figure 4.2 and Figure 4.3), the selection of number of reflecting paths, lengths of reflecting paths , attenuation coefficient of each path and the structure of the cable that decides the parameters a_0, a_1 and k.

In order to obtain a test channel to be used in this thesis, using suitable values for N, g_i, d_i and a_0, a_1 and k, the magnitude of frequency response $|H(f)|$, in dBs for power line, is computed using (4.10). Sample graphs of $|H(f)|$, vs. frequency are simulated are shown in Figure 4.4 to Figure 4.7.

Table 4.1 Values of attenuation parameters for Figure 4.4

N	3	Number of interfering paths (N=3) is chosen as 3. This implies that there are three disturbing loads between transmitter and receiver
a_0	0	a_0 is usually taken as 0
a_1	0.33×10^{-12}	a_1 value is chosen to offer sufficient attenuation that may suit to a realistic channel situation
k	0.8	k decides the slope of decay of attenuation with frequency
d_i	[100 200 300]	It is assumed that transmitter and receiver will be at distance of 300m. N=3 indicates that there will be three paths that form the received signal, originating from load points connected at distances 100m, 200m and 300m
g_i	g_i =[0.0951 -0.3146 -0.2909]	path gains also decide the attenuation: chosen to provide the suitable attenuation as shown in Figure 4.5

Table 4.1 gives the values of typical channel parameters that provide the channel attenuation shown in Figure 4.4. Relative permittivity $\varepsilon_r = 3.2$ is used assuming that the power cable has polyvinyl chloride insulation (PVC) [D. Mansson and R. Thottappilli 2008]. Four different attenuation scenarios are explained as follows-

(1) For Figure 4.4, a typical channel condition is assumed as per the values given in Table 4.1.

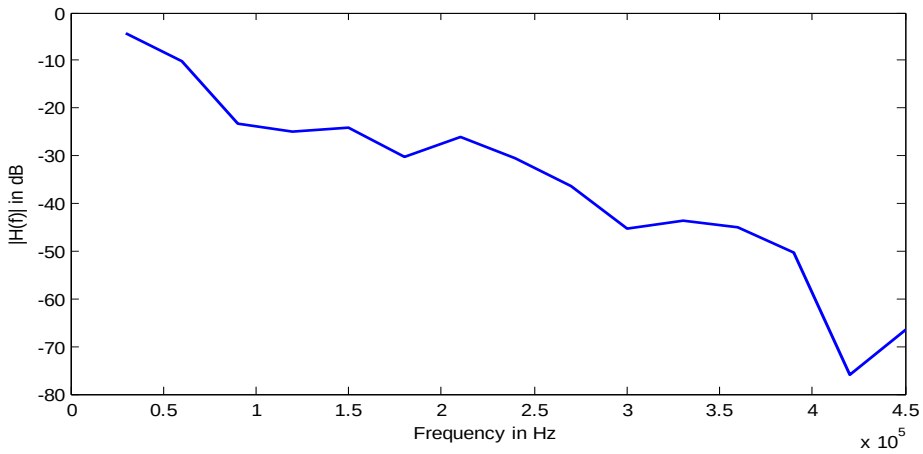

Figure 4.4 Channel attenuation of power line in dB vs. Frequency

(2) The effect of a change in the value of N: In Figure 4.4, N is used as 3. Here N is used to represent the number of disturbing loads in the signal propagation path. Now with other all parameter values remaining same as in Table 4.1, but with N =10, the attenuation plot is shown in Figure 4.5.

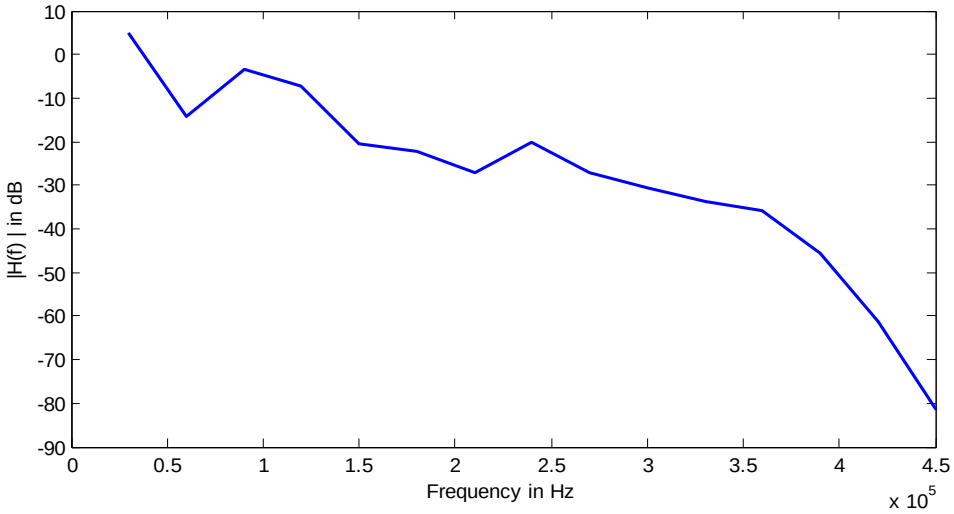

Figure 4.5 Channel attenuation $|H(f)|$ of power line in dB vs. frequency.

(3) The effect of a change in the value of $k(k = 0.9)$with other parameters remaining same, the plot shown in Figure 4.6 is obtained.

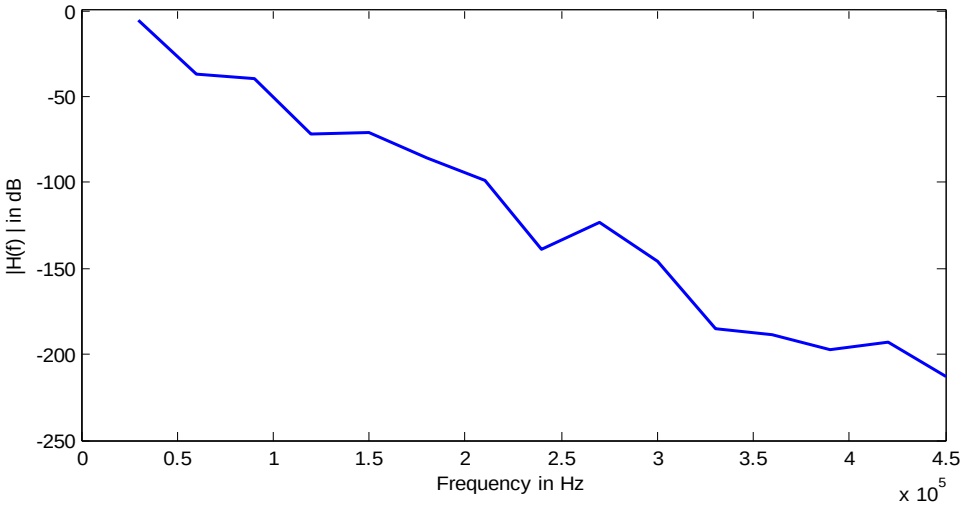

Figure 4.6 Channel attenuation $|H(f)|$ of power line in dB vs. frequency.

(4) The Effect of of d_i (d_i = [10 15 20 25 30 35 40 45 50 55]) is demonstrated by the following plot. Other parameter values remain unchanged.

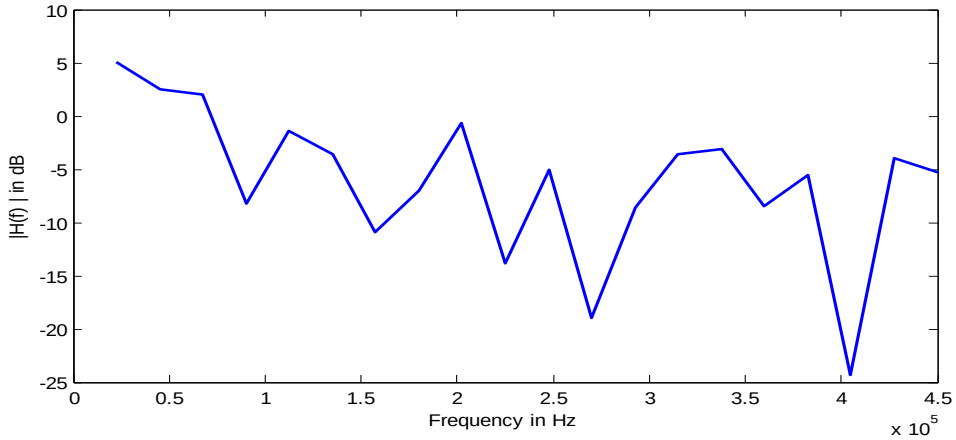

Figure 4.7 Channel attenuation $|H(f)|$ of power line in dB vs. frequency.

With reference to Figures 4.4 to 4.7, following observations are made:

(i) channel attenuation increases with number of discrete multi-paths N.

(ii) channel attenuation increases with attenuation factor k

(iii) channel attenuation decreases when distances d_i between reflecting points are decreased.

It is necessary to visualize the channel impairments in time domain as channel is time variant. As the channel is time varying, it becomes necessary to understand the nature of this variation and compute the typical values of attenuation encountered. In Figures 4.8, 4.9 and 4.10, the magnitude of the transfer function, $|H(f)|$ (in dBs) is plotted as a function of time. That is in these figures, x-axis is marked with numbers representing information symbols sent on the channel and y axis is marked with attenuation. It is observed that different attenuation values are observed for different symbol values. Each symbol conveyed over the channel is affected by a different attenuation value. Thus, the simulated channel model for attenuation can now be referred to as a time varying channel (as symbols change with respect to time and hence the channel attenuation with each symbol). We assume the frequency of operation to be constant and compute $|H(f)|$ as a function of sample number (equivalent to time variation). Since for every symbol, the channel environment in terms of path gains (g_i) and path delays ($\tau_i = d_i / v_p$) changes, even if operating carrier frequency is kept constant, the reflections governed by frequency as well as g_i and τ_i, along with fixed values of a_0, a_1 and k will cause a frequency variant attenuation at each time of symbol. In Figure 4.8, the attenuation $|H(f)|$ in dBs with different symbols for a particular carrier frequency (f_c=200 kHz) of operation is shown.

Thus a simulation model for power line channel, whose frequency response approximately fits the behavior of a realistic channel shown in section 2.4.2, is obtained.

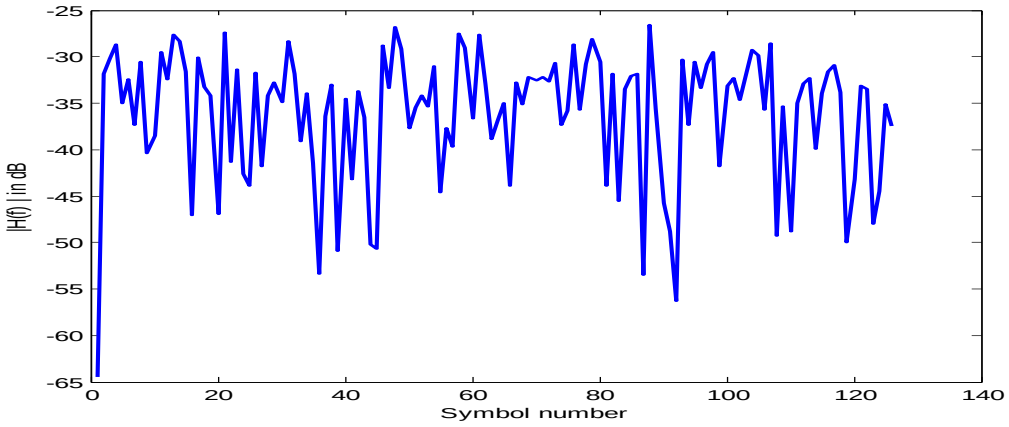

Figure 4.8 Channel attenuation $|H(f)|$ varying randomly with symbols.

Since in the study of performance evaluation of different channel coding schemes for power line channel, there is a need to use 63 bits as one frame, as BCH codes possessing lengths n = 127 and n = 63 are used. Therefore, assuming that carrier as 200 kHz, and the sampling frequency as 400 kHz, a symbol will take a duration of 2.5µsec. For 63 symbols, the frame duration will be 0.1575 msec. Assuming that power line channel environment will not change for one frame duration, channel attenuation is simulated to be constant or same for one frame, as shown in Figure 4.9 and Figure 4.10.

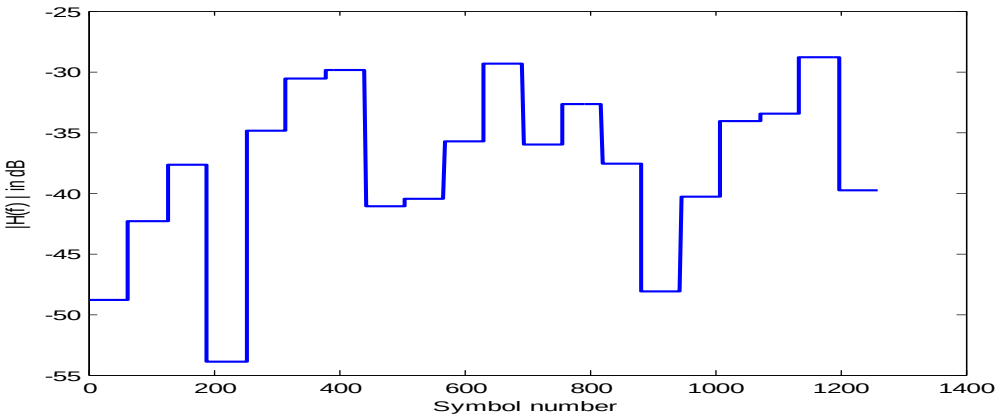

Figure 4.9 Channel attenuation $|H(f)|$ constant for one frame of 63 bits.

In Figure 4.9, the attenuation $|H(f)|$ in dBs with different symbols for a particular carrier frequency (f_c =200kHz) of operation is shown. $|H(f)|$ is assumed as being constant for one frame of bits. Each frame is assumed to consist of 63 bits (Ten frames are shown).

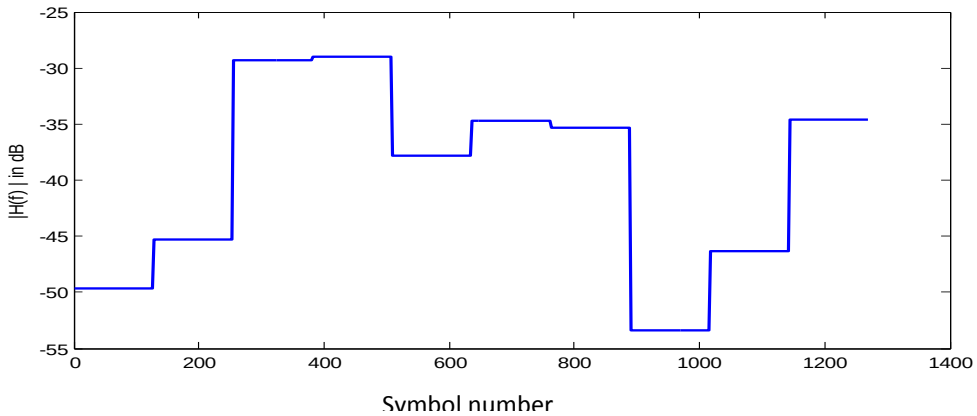

Figure 4.10 Chanel attenuation $|H(f)|$ constant for one frame (127 bits).

In Figure 4.10, the attenuation $|H(f)|$ in dBs with different symbols for a particular carrier frequency (f_c =200kHz) of operation is shown. $|H(f)|$ is assumed as being constant for one frame of bits. Each frame is assumed to consist of 127 bits (Ten frames are shown).

In the discussion so far, emphasis has been on the description of channel attenuation variation as a function of time, frequency and number of reflections from various connected loads. However, a complete understanding requires a specification of noise induced on the channel as well. Noise models appropriate for narrow band power line channels are described in Section 4.4.

4.4 Noise on power line

In contrast to most other well designed communication channels, the noise on the power line cannot be accurately modeled by Additive White Gaussian Noise (AWGN) model, whose power spectral density can be assumed to be constant over the whole transmission spectrum. The interference scenario is complicated, as not only colored broadband noise, but also narrowband interference and different types of impulsive disturbance can occur. The length of the impulses and the number of the occurred peaks can vary considerably depending on the environment.

If impulse durations exceed the communication symbol length, correct symbols cannot be received. Besides the distortion of the information signal owing to cable losses and

multipath propagation, noise superposed on the signal energy make correct reception of information more difficult. The amplitude and duration of the disturbances can be significant and thus seriously affect communications. A proper choice of the combination of modulation and error correction code which can help users to recover from errors induced by this phenomenon thus becomes important in the MODEM technology of power line communication used in substation automation.

A number of investigations and measurements have been performed in order to determine a detailed description of the noise characteristics in a PLC environment. A detailed study of noise sources that are found in low or medium voltage power grids for narrowband PLC can be found in [Halid Hrasnica 2004] and [M Katayama et al. 2006]. The noise waveform observed in low or medium voltage power grids for narrowband PLC, noise is seen as superposition of impulsive noise types, distinguished by their origin, time duration, spectrum occupancy and intensity as illustrated in Figure 4.11.

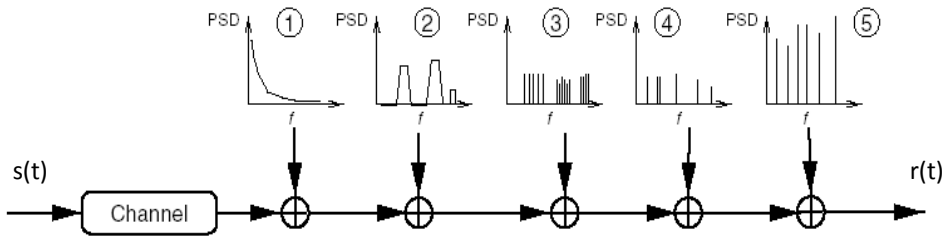

Figure 4.11 Additive noise types in PLC environments [Halid Hrasnica 2004].

In Figure 4.11, s(*t*) is the information signal (or symbol) and r(*t*) is the received signal (or symbol). The figure shows that s(*t*) will get affected by channel environment in two ways: channel attenuation symbolically shown by a block called "channel" and different types of noise get superimposed on the signal attenuated by the channel. For each class of noise, the approximate representation of power spectral density (PSD) is shown.

4.4.1 Different types of impulse noise

The interference scenario as shown in Figure 4.11 is roughly separated into five classes, which are briefly explained as follows [Halid Hrasnica 2004]:

(i) Colored background noise (Type-1), whose power spectral density (PSD) is relatively lower and decreases with frequency. This type of noise is mainly caused by a superposition of numerous noise sources of lower intensity. Contrary to the white noise, which is a random noise having a continuous and uniform spectral density that is substantially independent of the frequency over the specified frequency range; the colored background noise shows strong dependency on the considered frequency.

(ii) Narrowband noise (Type-2), most of the time has a sinusoidal form, with modulated amplitudes. This type occupies several sub bands, which are relatively small and continuous over the frequency spectrum. This noise is mainly caused by the ingress of signals from broadcast stations over medium and shortwave broadcast bands. Their amplitude generally varies over the daytime, becoming higher by night when the reflection properties of the atmosphere become stronger.

(iii) Periodic impulsive noise, asynchronous to the main frequency (Type-3), with a form of impulses usually has a repetition rate between 50 and 200 kHz and results in the spectrum with discrete lines with frequency spacing according to the repetition rate. This type of noise is mostly caused by switching power supplies. A power supply is a buffer circuit that is placed between an incompatible source and load in order to make them compatible. Because of its high repetition rate, this noise occupies frequencies that are too close to each other, and builds therefore frequency bundles that are usually approximated by narrow bands.

(iv) Periodic impulsive noise, synchronous to the main frequency (Type-4), is impulsive with a repetition rate of 50 or 100 Hz and is synchronous with the main power line frequency. Such impulses have a short duration, in the order of microseconds, and have a power spectral density that decreases with the frequency. This type of noise is generally caused by power supply operating synchronously with the main frequency, such as the power converters connected to the mains supply.

(v) Asynchronous impulsive noise (Type-5), whose impulses are mainly caused by switching transients in the networks. These impulses have durations of some microseconds up to a few milliseconds with an arbitrary interarrival time. Their power spectral density can reach values of more than 50 dB above the level of the background noise, making them the principal cause of error occurrences in the digital communication over PLC networks.

The study and measurements conducted by Hrasnica [Halid Hrasnica 2004] have shown that generally, noise types 1, 2 and 3 remain usually stationary over relatively longer periods. Therefore, all these three can be summarized in one noise class that is seen as colored PLC background noise class and is called “Generalized background noise”, whose frequency occupation and mathematical model are discussed by Hrasnica [Halid Hrasnica 2004]. The noise types 4 and 5 are, on the contrary, varying in a time span of milliseconds and microseconds and can be gathered in one noise class called “impulsive noise”, which is also described in PLC literature as “impulse noise”. Because of its relatively higher amplitude, impulse noise is considered the main cause of burst error occurrence in data transmitted over the high frequencies of PLC medium.

4.4.2 Impulsive Noise

The impulsive noise class is composed of the periodic impulses that are synchronous with the main frequency and the asynchronous impulsive noise. The measurements [Halid Hrasnica 2004] show that this class is largely dominated by the last noise type (Type-5). For this reason, the modeling of this class is based on the investigations and the measurements of Type-5. Hrasnica has shown that these impulses are modeled as a pulse train with pulse width t_w, pulse amplitude A, inter-arrival time t_a and a generalized pulse function $p(t/t_w)$ with unit amplitude and impulse width t_w [Halid Hrasnica 2004].

Practical measurements of noise waveforms for different types of appliances on low voltage power line are given in [Francis Berrysmith 2005]. The same are given here for reference in Figure 4.12 (a), (b) and (c).

Measurements of the noise level in the 20-450 kHz band were performed by L. Selander, T. I. Mortensen and G. Lindell [L. Selander et al.1998]. These measurements show that the noise power spectral density is roughly -110 dB (W/Hz) at 25 kHz, is non-white, and decays with increasing frequency.

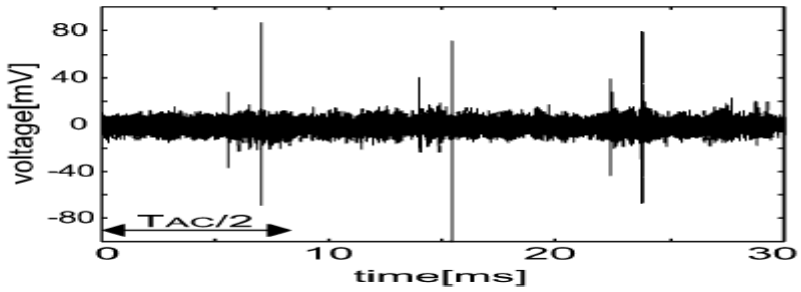

(a) Noise waveform by a CRT color TV

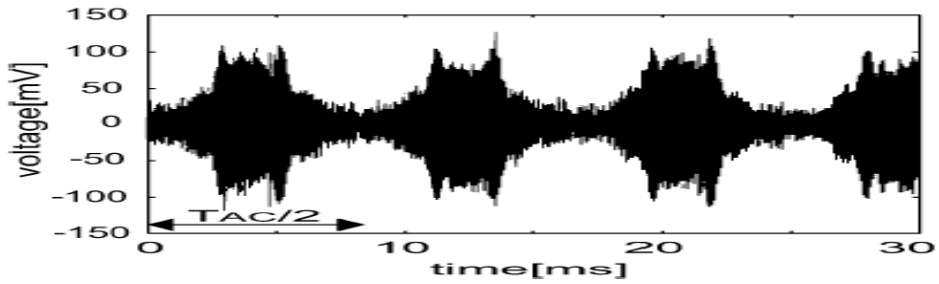

(b) Noise waveform by an inverter driven fluorescent lamp (30 W)

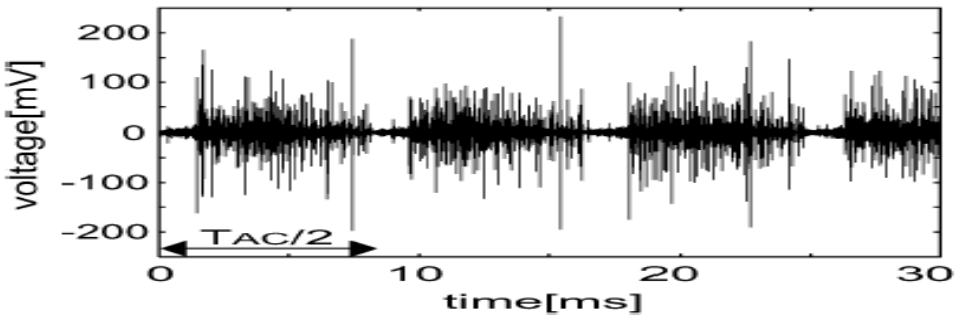

(c) Noise waveform by a vacuum cleaner with brush motor (600 W)

Figure 4.12 Noise waveforms for different types of appliances [Francis Berrysmith, 2005].

Of late, there is increasing awareness about the use of MV power line as a communication medium. In recent literature, [Marcel Nassar and Anand Dabak et al. (2012)], have referred to the type of noise shown in Figure 4.12 (a), (b) and (c), as cyclostationary noise. The noise is periodic with half the period of power line frequency and is a mixture of Gaussian noise. Cyclostationary noise has also been discussed by Ohno et al. [Osamu Ohno

and Masaaki Katayama et al. 1998]. It has been claimed by Nasser et.al [Marcel Nassar and Anand Dabak et al. 2012] and other members of the research community [Osamu Ohno and Masaaki Katayama et al. 1998], that for narrowband power line application, cyclostationary noise is another noise mechanism. A brief description of this type of noise along with an explanation of the nature of impulse noise is provided in section 4.5.

4. 5 Impulse noise model

In continuation of the introduction to the nature of noise on power line as given in section 4.4 and the discussion in research community amongst those who have studied this problem, more points of discussion on impulsive noise on power line are given below for further reference.

- In [M Katayama, H. Okada 2006], several noise sources that can be found in low or medium voltage power grids for narrowband PLC, are explained.
- In [D. Umehara et al. 2004], impulsive interference generated on a power line that cause bit or burst errors in data transmission is modeled by Middleton's Class-A noise model.
- In [Christine Hsu et al. 2007], performance of LDPC code for data corrupted with Middleton Class-A noise is studied.

From the discussions in the literature mentioned in above paragraphs, we have concluded that Middleton's Class-A noise can be used to model impulse noise disturbances on power line channel. In this thesis work, the performance analysis of channel coding and modulation has been studied with channel noise modeled by Middleton's Class-A noise. The pdf (probability density function) of Middleton's Class-A Noise is a heavily tailed distribution which is given by (4.11) [Leslie A. Berry 1981].

$$f(x) = \sum_{m=0}^{\infty} \frac{A^m}{m!} e^{(-A)} \left[\frac{1}{\sqrt{2\pi\sigma_m^2}} \right] . e^{\left(\frac{-x^2}{2\sigma_m^2} \right)} \qquad (4.11)$$

Equation (4.11) is the pdf for Middleton Class-A noise model. It is a weighted sum of Gaussian distributions where different terms in (4.11) are explained in section 2.6.

Cyclostationary noise is described as a mixture of various forms of Gaussian noise. The total noise variance given as [Osamu Ohno and Masaaki Katayama et al. 1998],

$$\sigma^2(t) = \sum_{k=0}^{k-1} A_k \left| \sin(2\pi f_{ac} t + \varphi_k) \right|^{n_k} \quad (4.12)$$

where f_{ac} is the frequency of the A.C. voltage, A_k and φ_k are amplitude and phase of various components, n_k is parameter which quantifies the degree of impulsiveness. A different way of simulating cyclostationary noise is given by Nassar et al. [Marcel Nassar and Anand Dabak et al. 2012], by dividing the half period of power signal into three different regions and fitting stationary and impulsive noise in the three regions.

Middleton Class-A noise model is used as impulse noise model for the analysis of channel coding schemes in this thesis work. Noise samples are generated using noise pdf given in (4.11). Different impulse behavior is listed as explained in section 4.6.

4 .6 Simulation of impulse noise

In this section, the modeling of Impulse noise with the help of the Middleton Class-A model will be discussed. It has been emphasized in the previous sections that the dominant noise mechanism in PLC systems is Impulsive noise. Hence, it is necessary to represent this phenomenon with a mathematically tractable and accurate mathematical model. To create impulsive environment for the signal to be passed on power lines in the simulation study, it is necessary to generate impulse noise samples. To begin with, the impulse noise pdf is realized using (4.11). This information is then employed to generate noise samples. Graphs of pdf of Middleton Class-A model simulated in this thesis work using (4.11), are shown in Figure 4.13, Figure 4.14 and Figure 4.15. These are found to match with the plots of pdf presented in [Leslie A. Berry 1981].

Figures 4.13 to 4.15 depict the pdfs of impulse noise for different values of A and T, indicating different channel state disturbances and at different Signal to Noise Ratio (SNR) values.

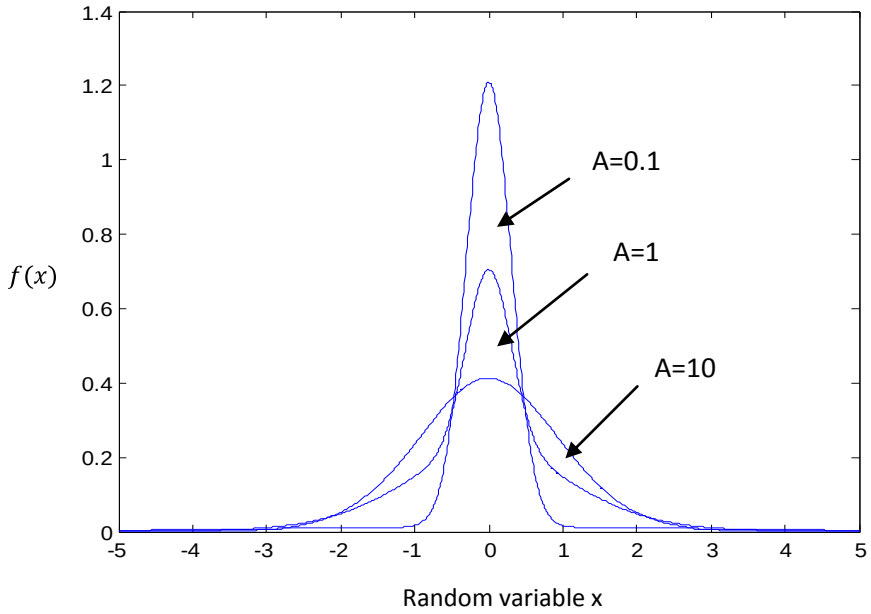

Figure 4.13 pdf for Simulated Class-A noise $(T = 0.1, A = 0.1, 1, 10)$.

As seen from the pdf plot shown in Figure 4.13, it is clear that as the parameter A called as noise index increases, noise pdf approaches Gaussian pdf.

The noise pdf shown in Figure 4.13 is for the noise parameter T=0.1. T is the Gaussian to Impulse noise power ratio called as GIR. Here T=0.1 indicates that impulse noise power is 10 times that of Gaussian noise power. Other case of pdfs for T=0.01 and T=0.001 are given in Figure 4.14 and Figure 4.15.

It is observed that for the same value of A=0.1 noise pdf takes different values for different values of T. In the case of T=0.1, the pdf takes the peak value as 1.2 where as for the case T=0.01, pdf for A=0.1 takes larger value as 3.5. This is justified because as T decreases to 0.01, the impulse noise power is increased to 100 times the Gaussian noise power and for the combination of lesser value of A=0.1 with T=0.01, there will be more of impulsive nature in the noise samples.

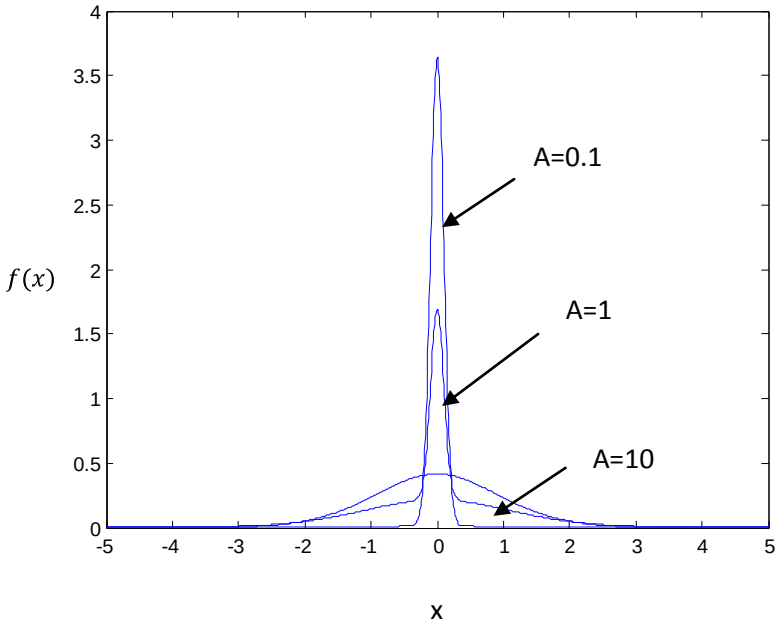

Figure 4.14 pdf for simulated Class-A noise$(T = 0.01, A = 0.1, 1, 10)$.

Similar type of observation made by comparing the pdfs for Figure 4.13 and Figure 4.14, can be made with the pdfs for Figure 4.14 and Figure 4.15.

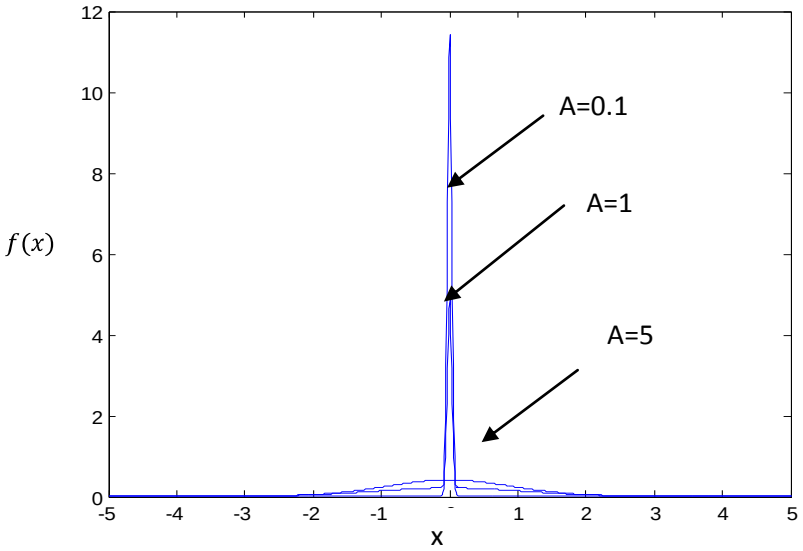

Figure 4.15 pdf for simulated Class A noise $(T = 0.001, A = 0.1, 1,5)$..

The nature of noise for different values of relevant parameters A and T is elaborated on in Table 4.2.

Table 4.2 Different combinations of impulse noise parameters

Case number	A	T	Significance of case
1	0.1	0.1	Impulsive with moderate impulsive amplitude (10 times Gaussian), frequency of impulsiveness very close
2	0.1	0.01	Impulsive with higher impulsive amplitude (100 times Gaussian), frequency of impulsiveness very close
3	0.1	0.001	Impulsive, high impulsive amplitude (1000 times Gaussian), frequency of impulsiveness very close
4	0.01	0.1	Impulsive, moderate impulsive amplitude (10 times Gaussian) frequency of impulsiveness decreases (less than that for *A*=0.1, *T*=0.1)
5	0.01	0.01	Impulsive, high impulsive amplitude (100 times Gaussian), frequency of impulsiveness decreases (less than that for *A*=0.1, *T*=0.01)
6	0.01	0.001	Impulsive, very high impulsive amplitude (10 00 times Gaussian) frequency of impulsiveness decreases (less than that for *A*=0.1, *T*=0.001)

Since the above cases mentioned in Table 4.2, depict approximately real channel noise scenarios, these parameter values are used in the generation of noise sample values to represent various conditions that can be experienced in the channel. Noise samples generated for some of the cases are shown in Figure 4.16 to Figure 4.19 (signifying different degrees of impulsiveness) and for different Signal to Noise Ratio (SNR).

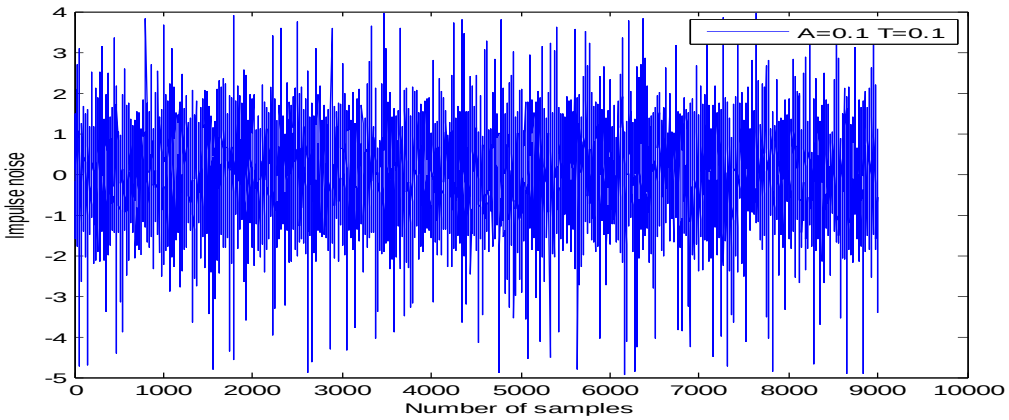

Figure 4.16 Simulated Class-A noise waveform at SNR = 1dB for *A*=0.1, *T*=0.1(case 1).

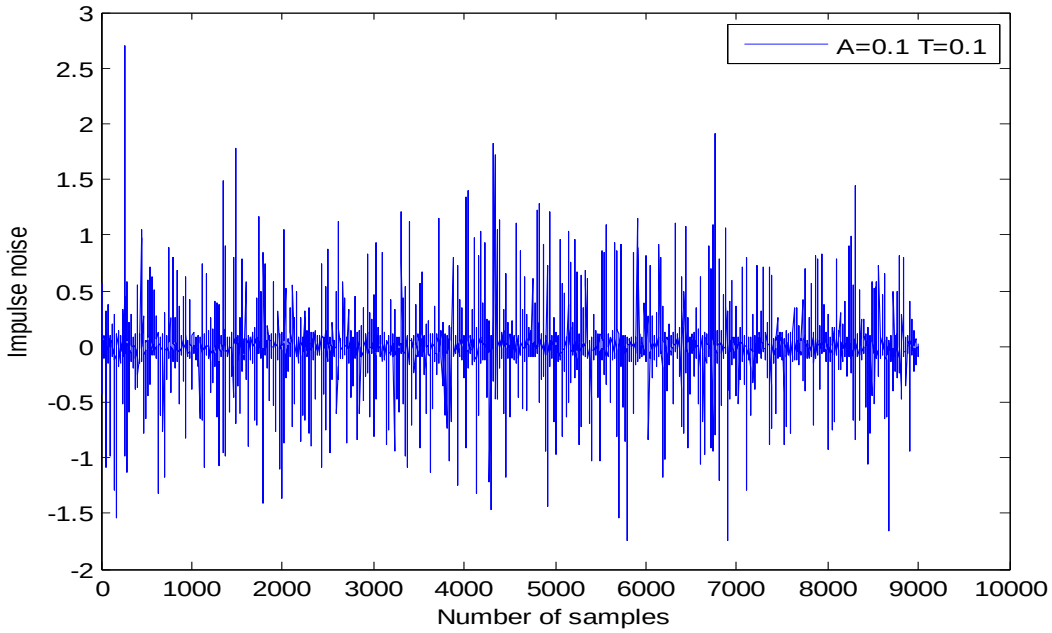

Figure 4.17 Simulated Class A noise waveform at SNR = 15dB for *A*=0.1, *T*=0.1(case 1).

Figure 4.16 shows the noise samples for the *A*=0.1, *T*=0.1(case 1), for signal to noise ratio (SNR) of 1 dB. Noise samples for the same values of *A* and *T*, but for SNR at 15 dB are shown in Figure 4.17. It is seen from the comparing of the two that only the magnitudes of noise samples have decreased as SNR is increased, but the impulsive nature has been preserved. It is also observed that the nature of noise samples shown in Figure 4.16 and Figure 4.17, match the description of case 1 given in Table 4.2.

Figure 4.18 shows the noise samples for the A=0.01, T=0.1(case 4), for signal to noise ratio (SNR) of 1 dB. Noise samples for the same values of *A* and *T*, but for SNR at 15 dB, are shown in Figure 4.19. It is seen from comparing the two that only the magnitudes of noise samples have decreased as SNR is increased, but the impulsive nature has been the same. This is because the values of *A* and *T* have remained unchanged. Also observe that the nature of noise samples shown in Figure 4.18 and Figure 4.19, match to the description of the case 4 given in Table 4.2.

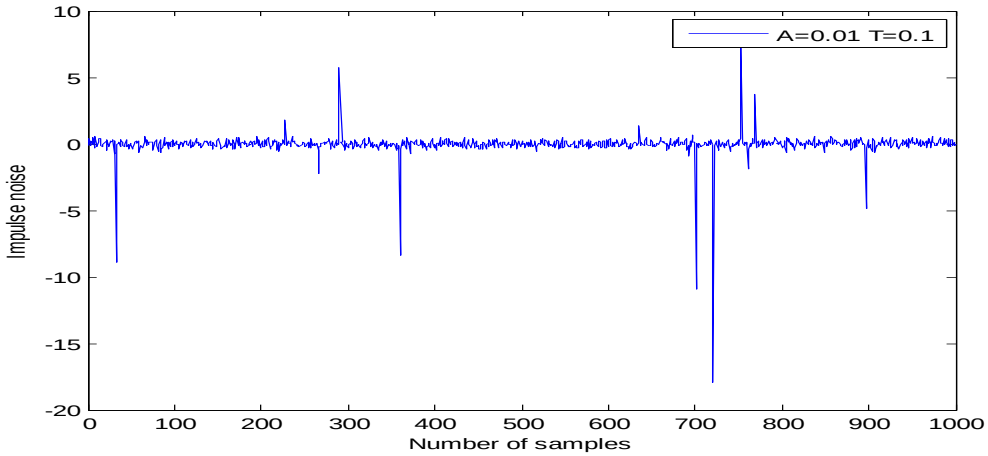

Figure 4.18 Simulated Class-A noise waveform at SNR = 1dB for *A*=0.01, *T*=0.1(case 4).

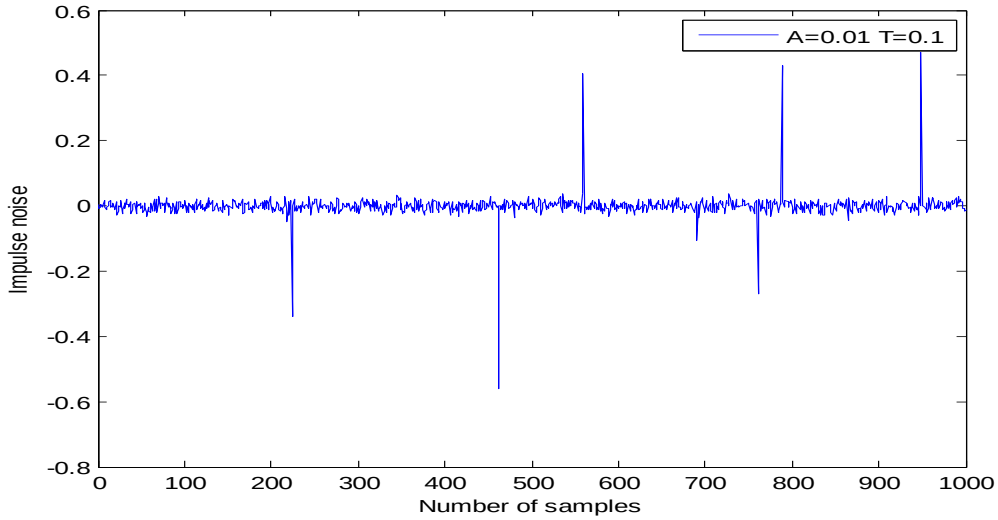

Figure 4.19 Simulated Class-A noise waveform at SNR = 15dB for *A*=0.01, *T*=0.1(case 4).

From the graphs of simulated class-A noise pdf and the noise samples derived out of it, following observations are made-

(i) The number of impulses shows a decreasing trend with a decrease in the value of A. This is apparent from a comparison of Figures 4.16 and 4.18.

(ii) The magnitude of the peak values of impulse increases with a decrease in value of *T*.

(iii) For same values of say $\mathrm{A} = 0.1, \mathrm{T} = 0.1$ amplitude of noise sample exhibits a decrease with increase in SNR. This is illustrated in Figure 4.16 and in Figure 4.17.

(iv) From the graphs, it is observed that for large values of "A", the noise tends to be Gaussian.

These observations are in accordance with the mathematical definition of Class-A noise.

Having finalized the model for power line that can be used to test the performance of a channel coding and modulation scheme, in section 4.6, results of tests conducted to verify the performance of Alamouti 2x1 space time coding scheme when applied to the simulated power line are presented in the following section.

4.7 Simulation results for BCH (*n*=127, *k*=22, *t*=21) coded Alamouti 2x1 Space time code for power line channel

In this section, results out of a study conducted to verify the ability of space diversity to reduce the effect of channel induced errors on a power line channel are explained. Alamouti 2x1 space time coding scheme was simulated in Matlab to check the signal recovery when the two simulated uncorrelated transmitting paths behave differently. BCH code with n=127, k=22 and t=21 is used for channel encoding. For the simplicity of understanding the results, the level of attenuations provided by the two channels in the power line are classified as follows.

Table 4.3 Classification of attenuation levels

0 dB < $\|H(f)\|$ < -5 dB	Very Low
-5 dB < $\|H(f)\|$ < -15 dB	Low
-10 dB < $\|H(f)\|$ < -45 dB	Medium
-30 dB < $\|H(f)\|$ < -80 dB	High
-40 dB < $\|H(f)\|$ < -130 dB	Very High

Simulations have been performed to determine the levels of data integrity as channel attenuation on the two channels takes on various possible values as classified in Table 4.3. Parameters of impulse noise are also varied as per Table 4.2 and results are tabulated Table 4.4, 4.5 and 4.6. A plot of the bit error rate (BER) vs. signal to noise ratio (SNR), obtained by designing channel 1 to provide very high attenuation and channel 2 to provide medium attenuation is provided in Figure 4.20. Number of interfering paths (N) is chosen to be 5, with distances of loads (reflectors), d_i in meters are chosen to be [1 3 5 8 10]. Frequency of operation is 200 kHz which is

fixed at a value less than 450 kHz. Impulse noise parameters *A* and *T* are fixed for case 1 [A=0.1, T=0.1] as given in Table 4.2. Data size is 5x10^6 bits. The channel state information (CSI) necessary for space time decoding, is made available to the decoder by use of a simple pilot symbol addition. With these specifications, the BER vs. SNR plot is shown in Figure 4.20.

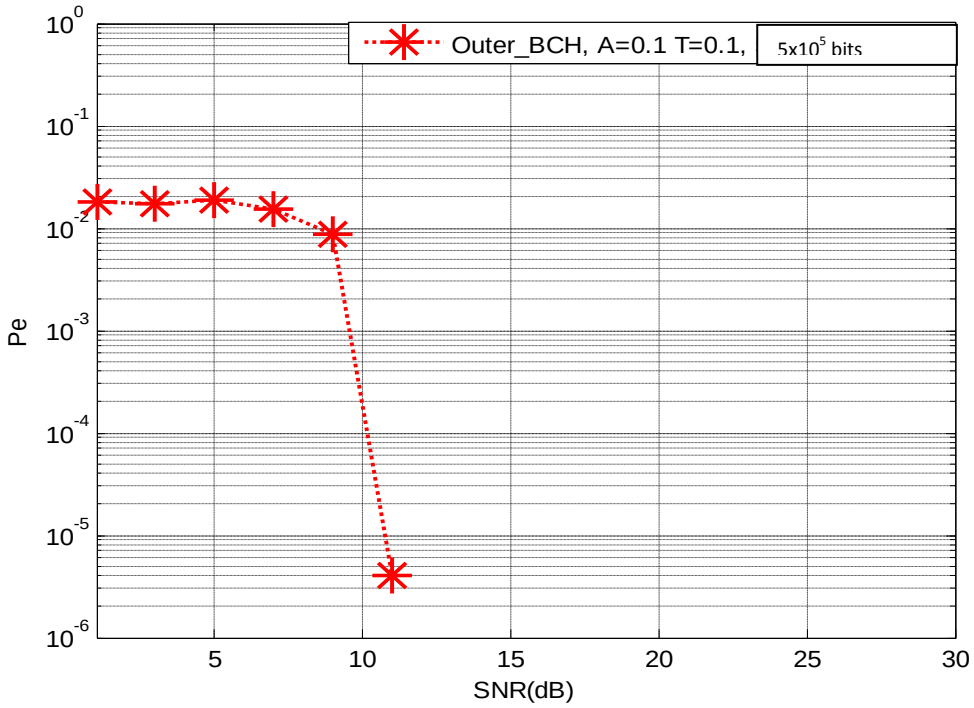

Figure 4.20 BER vs. SNR plot for BCH coded 2x1 Alamouti scheme for power line with 5x10^5 bits, channel 1-very high attenuation, channel 2- medium attenuation, impulse noise case 1.

From the BER plot shown in Figure 4.20, it is seen that when signal in one path-1 has suffered very high attenuation, reasonable BER performance of the order of 10^{-5} at a SNR of approximately 12 dB is still possible. This is possible because the space time decoding scheme utilizes received information from both the paths-1 and 2. Here, path-2 has medium attenuation. This result provides verification of the fact that diversity provided by two uncorrelated paths can be employed to improve the reliability of information transfer over harsh communication channels.

Performance of the MV narrow band power line channel has been tested for various channel conditions that can prevail on the two independent channels. The results are tabulated in Table 4.4 and Table 4.5.

In the results given in Table 4.4, path-1 takes low, medium, high and very high attenuation and path-2 has medium attenuation. The condition is reversed in the results shown in Table 4.5, path-1 has low and medium attenuation while path-2 takes on low, medium, high and very high attenuation values. BER vs. SNR plots are obtained and to obtain each result, data size used is $5x10^6$ bits. From the BER plots, the value of SNR at which BER< 10^{-4}, is noted and marked in Table 4.4 and Table 4.5.

Table 4.4 Performance of error correction with channel 2 experiencing moderate attenuation and channel 1 experiencing low to high attenuation.

A	T	d	Nature of Channel Transfer Function in dB		Value of SNR in dB at which error reduces to BER $<10^{-4}$
			$\|H_1(f)\|$(dB)	$\|H_2(f)\|$ (dB)	
0.1	0.1	1-10 m	-4.5	-4.5	3
0.1	0.1	1-10 m	-18.5	-18.5	13
0.1	0.1	1-10 m	-32	-32	19
0.1	0.1	1-10 m	-42	-32	19
0.1	0.1	1-10 m	-46	-32	19
0.1	0.1	1-10 m	-64	-32	19
0.1	0.1	1-10 m	-70	-32	19
0.1	0.1	1-10 m	-90	-32	17
0.1	0.1	1-10 m	-92	-32	19
0.1	0.1	1-10 m	-94	-32	21
0.1	0.1	1-10 m	-124	-32	21
0.1	0.1	1-10 m	-138	-32	21
0.1	0.1	1-10 m	-200	-32	19
0.1	0.1	1-10 m	-236	-32	21
0.1	0.1	1-10 m	-130	-46	25
0.1	0.1	1-10 m	-130	-60	Does not work even when SNR exceeds 25 dB

Table 4.5 Performance of error correction with channel 2 experiencing very high attenuation and channel 1 experiencing low to high attenuation.

A	T	d	Nature of Channel Transfer Function in dB Data size is $5x10^6$		Value of SNR in dB at which error reduces to BER < 10^{-4}
			$\|H_1(f)\|$ (dB)	$\|H_2(f)\|$ (dB)	
0.1	0.1	1-10 m	-4.5	-130	3
0.1	0.1	1-10 m	-18.5	-130	13
0.1	0.1	1-10 m	-28	-130	17
0.1	0.1	1-10 m	-32	-130	19
0.1	0.1	1-10 m	-40	-130	23
0.1	0.1	1-10 m	-58	-130	Does not work even when SNR exceeds 25 dB

From the results obtained in Table 4.4 and Table 4.5, following observations are made.

1. The advantage provided by use of diversity in power line in which the channel manifests frequency selective time variant behavior with corruption by added impulsive noise is verified. This means, if one path of the channel has high or very high attenuation, while the other path of the channel has less or medium attenuation, then meaningful information transfer is possible.

2. Table 4.3 and 4.4 also show that when both the paths suffer from very high attenuation, recovery is not possible.

3. BCH code with high error correcting capacity ($t = 21$), has assisted the performance improvement.

In Table 4.4 and Table 4.5, impulse noise case 1 is used and the distances d_i are fixed at 1, 3, 5, 8 and 10 (m). Many such tests are taken shown by the results tabulated in Table 4.6, in which different values for impulse noise parameters, data size, distance d and attenuation are used.

Table 4.6: Verification of space time diversity of two paths of power line channel.

Data size	A	T	$d(N)$	Nature of Channel Attenuation in dB		Value of SNR in dB at which error reduces to $< 10^{-4}$
				$\|H_1(f)\|$ (dB)	$\|H_2(f)\|$ (dB)	
10^4	0.1	0.1	1- 2.5 m (*N*=4)	Very High Constant for all bits	Low Constant for all bits	13
10^4	0.1	0.1	1- 2.5 m (*N*=4)	Very High Constant for all bits	Medium Constant for all bits	19
10^5	0.1	0.1	1- 2.5 m (*N*=4)	Medium	Low	9
10^5	0.1	0.1	1- 2.5 m (*N*=4)	Medium	High	13
10^5	0.1	0.1	1- 2.5 m (*N*=4)	Medium	Medium	11
10^4	0.1	0.1	1- 2.5 m (*N*=4)	Medium	High	13
10^6	0.1	0.1	1- 2.5 m (*N*=4)	Medium	High	15
10^6	0.1	0.001	1- 2.5 m (*N*=4)	Medium	High	13
10^5	0.1	0.1	1-200 m (*N*=6)	Very High	Medium	17
10^7	0.1	0.1	1-50 m (*N*=6)	High	Medium	11
10^5	0.1	0.1	1-5m (*N*=6)	Medium	Medium	15
10^5	0.1	0.01	1-5 m (*N*=6)	Medium	Medium	11
10^5	0.01	0.01	1-5 m (*N*=6)	Medium	Medium	9
10^6	0.01	0.01	1-50 m (*N*=11)	Medium	Medium	9
10^5	0.1	0.1	1-100 m (*N*=14)	High	Medium	13
10^5	0.01	0.01	1-100 m (*N*=14)	High	Medium	13
5×10^5	0.1	0.1	1-50 m (*N*=11)	High Constant for 5 bits	Medium Constant for 5 bits	11
5×10^5	0.01	0.01	1-50 m (*N*=11)	High Constant for 10 bits	Medium Constant for 10 bits	11
5×10^5	0.01	0.01	1-50 m (*N*=11)	High	Medium	13
5×10^5	0.1	0.1	1-50 m (*N*=11)	High	Medium	13
5×10^5	0.01	0.01	1-50 m (*N*=11)	Medium	Medium	11
10^5	0.01	0.01	1-200 m (*N*=22)	High	Medium	11
5×10^5	0.01	0.01	1-200 m (*N*=22)	High	High	17
10^6	0.1	0.1	1-1250 m (*N*=20)	Very High	High	21

Based on the Table 4.6, following observations are made:

1. Error performance of the order of 10^{-5} is observed within 25 dB of SNR.
   System is verified to work with impulsive environment of case 1 (A=0.1, T=0.1) and case 2 (A=0.1, T=0.01).

2. If distance is less, performance is better. This is expected as attenuation increases with line length. i. e. higher SNR is required to correct errors of the order 10^{-5}, with the increase in the distance.

3. If one of the channel is having low or medium attenuation, then high attenuation in the other channel can be tolerated.

4. If attenuation is very high in both the channels, system fails to correct the errors.

The observations in section 4.7 justify the use of the concatenated BCH-Alamouti arrangement for communicating data reliably on power line channels. In chapter 5, a partial hardware realization which leads to a semi-realistic implementation is explained. Performance results obtained using this approach have been compared with another scheme involving the use of Turbo coded OFDM.

Summary: In this chapter, models used to represent perturbations experienced by a propagating signal on a power line have been described. The channel is both time and frequency variant. There are two ways to represent power line channel using multipath model and using 2PN. Further, a study of relevant literature reveals that there are different ways of analyzing and modeling the impulsive noise.

This thesis has focused on the study, simulation and implementation of a few Channel coding and Modulation schemes designed to improve information integrity of power line channels carrying data. This work has been confined to channel coding for power line communication using medium voltage (1kV to 30 kV) power lines. The Power line channel is modeled as a multipath channel and simulated in MATLAB®. The frequency of operation is chosen as 200 kHz well within the specified limits of narrowband PLC (that is less than or equal to 500 kHz). For generation of impulse noise samples, Middleton's Class-A pdf has been employed.

Channel attenuation as a function of frequency, location, and distance has been computed and is found to exhibit time variant behavior. It is also observed that attenuation increases with frequency and distance between transmitter and receiver. Also impulse noise samples generated using Middleton Class-A noise pdf, are tested and verified to match with their description as per Table 4.2.

Using the simulated power line as channel, the performance of BCH coded Alamouti scheme has been determined. Results with a BER of 10-4 to 10-5 are achieved with SNR less than 25 dB. This observation implies that an efficient modem for power line channel should employ a suitable space time code, assisted with a powerful channel code.

OFDM is suggested by IEEE standard for narrowband PLC: IEEE 1901.2[Brian Evans 2012]. The use of a concatenated arrangement consisting of a Turbo code followed by OFDM has been investigated and the results of this study have been presented in Chapter 5.

In the next chapter, the performance of the two major schemes, namely the concatenated scheme consisting of Turbo code with OFDM as well as BCH coded Alamouti scheme will be presented. A partial hardware implementation of the second scheme has been performed and the results obtained therein for different channel conditions will be described.

Chapter 5

RESULTS AND DISCUSSION

The focus of this chapter is the comparison of the performance of two different types of channel coding and modulation schemes namely Turbo Coded OFDM and BCH coded Alamouti Space-Time code for preserving data integrity during communication on narrow band power lines. In section 5.1, the evaluation methodology used for the two schemes and the parameters used in the design are discussed. The performances of these schemes are described in sections 5.2 and 5.3 respectively. The communication medium is assumed to be medium voltage lines (1kV to 30 kV) and the frequency of operation is assumed to be 200 kHz (less than 450 kHz). It is further assumed that communication is being sought to be established in a substation environment. Therefore the distances between transmitter point and receiver points are of the order of a hundreds of meters to several kilometers. Under these conditions, the power line channel is affected by considerable channel attenuation and impulsive noise. Lines with attenuation classified as per Table 4.3 and impulse noise classified as per Table 4.2 have been used for testing the efficacy of channel coding and modulation strategies. A study of literature has revealed that the MV power line channel is mainly affected by multi-path propagation which results in frequency selective attenuation and signal fading. The noise affecting communication can be modeled as Impulsive noise.

An effective strategy to combat these effects is the use of a concatenated scheme comprising of BCH code combined with Alamouti's space time code. The arrangement used to couple Alamouti coded signal to the power line channel has been described in section 3.15. The performance of the concatenated arrangement consisting of BCH code with parameters $(n = 127, k = 22, t = 21)$ with Alamouti 2x1 code has been determined in Section 4.7. Successful data communication (with acceptable BERs) was observed and the details have been presented in section 4.7.

The BER specification gives a measure of the reliability of the channel in conveying data. To determine bit error rate (BER), binary input data and output data are

compared. A better understanding of the quality of the information transfer through the channel can be understood by verifying written text, audio or video data as input. Result in the output data file (received) is compared with the input file (transmitted). In this regard, a text written in .txt file was used as input. To achieve the transmission of this data over power line channel, in the first scheme, a BCH code with parameters $(n = 63, k = 36, t = 5)$ was synthesized using BCH code design procedure. Data from the BCH encoder was Alamouti coded by making use of Texas Instruments (TI) Digital Signal Processor TMS 320 C6713. The encoding and decoding block was implemented on the DSP platform. Encoded/decoded data from the DSP processor was communicated to the power line channel simulated on MATLAB® platform.

Figure 5.1 shows the block diagram schematic for the interface arrangement between MATLAB® and DSP kit.

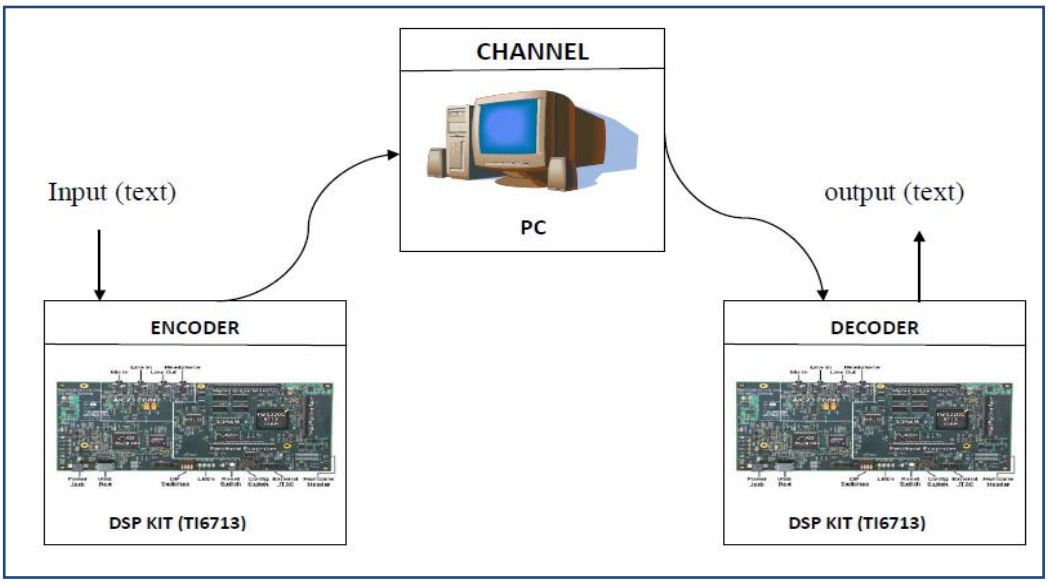

Figure 5.1 Block diagram showing the Interface of BCH encoder and decoder in DSP with channel in MATLAB®.

Specifications of DSP processor (TMS 320 C6713) have been provided in Appendix A with a brief introduction to Code Composer Studio (CCS).

The results obtained by this partial hardware arrangement are presented in section

5.3. In order to compare this with other channel coding /modulation schemes, a four state Turbo coded OFDM scheme was tested. OFDM is suggested by IEEE 1901.2, standard for narrowband PLC. These results are presented in section 5.2.

Thus results are categorized in to two sections as:

I. Simulation results of four state Rate 1/3 Turbo code concatenated with 32 carrier OFDM, presented in section 5.2.

II. Implementation results of $n = 63, k = 36, t = 5$ BCH code synthesized on Digital Signal Processor (TMS 320C6713) concatenated with Alamouti 2x1 space time code, presented in section 5.3.

5.1 Evaluation methodology of proposed schemes

In this section, the two schemes proposed for protecting data integrity over power lines are described with block schematic for implementation. Turbo coded OFDM is referred to as scheme 1 and BCH coded Alamouti space time code is referred to as scheme 2.

5.1.1 Turbo OFDM (Scheme 1)

The Block diagram used for this scheme is shown in Figure 5.12 In this scheme, a four state turbo convolutional code is used to encode the input data. A 32 subcarrier OFDM arrangement is used as the modulating entity. Text data written in a notepad is used as input.

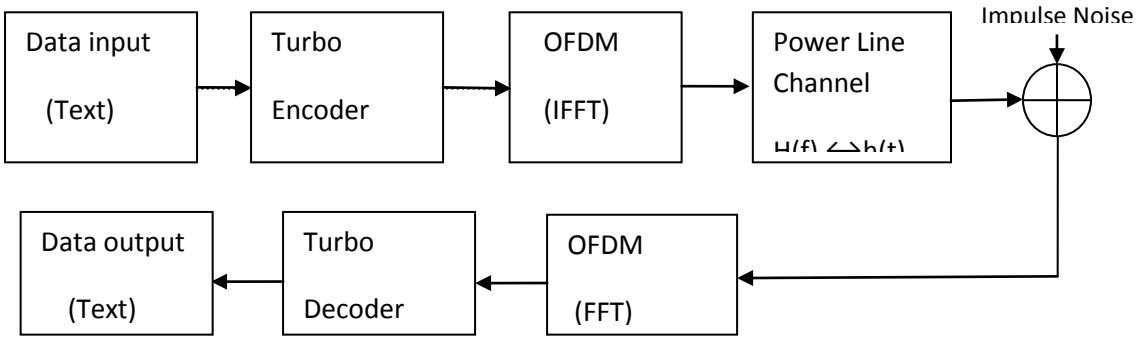

Figure 5.2 Block diagram for evaluating performance of Turbo coded OFDM for power line channel (scheme 1).

Power line is modeled as multipath channel. The transfer function $|H(f)|$ is designed to be time and frequency variant as explained in Chapter-4. Impulse noise samples are generated as per procedure explained in Chapter-4 and are added to the received signal, to recreate conditions expected during data transfer on power line. Output signal is suitably decoded and demodulated to recover binary data, which is written back in an output text file. Variance of noise is varied to vary the Signal to Noise Ratio (SNR) and plots of bit error rate (BER) vs. SNR are obtained for different operating conditions as-

(i) Gaussian noise channel (AWGN channel).

(ii) Impulsive noise channel (AWAN channel) as per Table 4.2, in the absence of channel attenuation.

(iii) Channel exhibiting attenuation with added impulsive noise.

(iv) Channel with medium/large distances between different loads, connected to power line.

(v) Channel with low/medium/high attenuation.

$|H(f)|$ is modeled using (4.10), with parameters

1. $a_0 = 0$
2. $0 < a_1 < 1$
3. $0 < k < 1$
4. $0 < g_i < \pm 1$
5. Two values of distances d_i are used
   (I) between 100 to 500 m (II) between 500 m to 2 km.
6. The number of reflections due to loads connected to the transmission line denoted by N is assumed to be equal to 5.
7. Frequency of operation f_c is chosen to be 200 kHz .

Discussion on results will be presented in section 5.2.

5.1.2 BCH coded space time code (Scheme 2)

The Block diagram used for this scheme is shown in Figure 5.3. In this scheme, a BCH code with parameters $n = 63, k = 36, t = 5$, is used for encoding the input data. The BCH encoded symbols are encoded a second time by employing Alamouti's 2x1 scheme. Power line channel and noise environment are created in the same manner as elaborated upon in Chapter-4 and parameters used for $|H(f)|$ are same as mentioned for scheme 1.

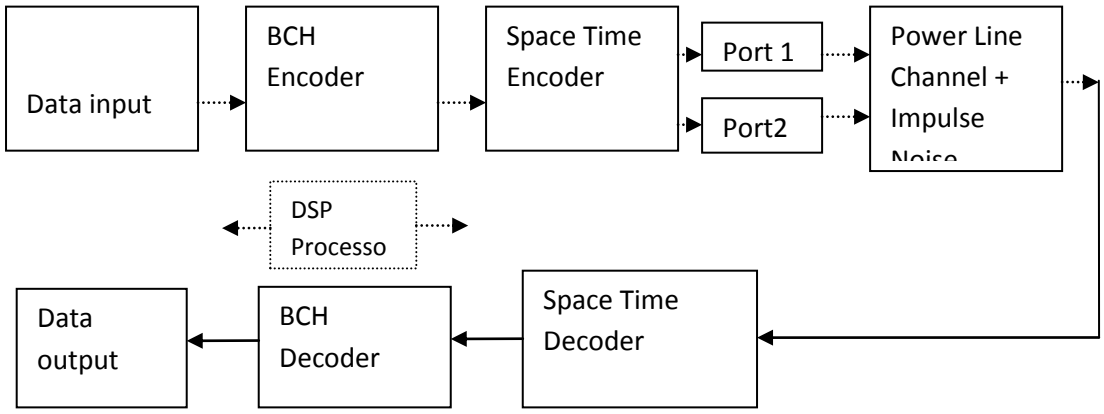

Figure 5.3 Block diagram for evaluating performance of BCH coded space time coding for power line channel (scheme 2).

Output signal is processed to recover binary data. Variance of noise is varied to vary the Signal to Noise Ratio (SNR) and plots of the bit error rate (BER) vs. SNR are obtained for different operating conditions. These may be classified as,

(i) Gaussian noise channel (AWGN channel)
(ii) Impulsive noise channel (AWAN channel) with parameters as per Table 4.2
(iii) Channel with frequency/time variant channel attenuation as well as impulsive effect with ideal CSI (Channel State Information)

The performance of the proposed scheme is verified for data sizes of 20 to 1000 frames with each frame having 63 bits.

Discussion on results will be presented in section 5.3.

5.2 Discussion on simulation results for Turbo OFDM (four state Rate 1/3 Turbo code concatenated with 32 carrier OFDM)

Four state Turbo code (RPCC) was designed using design procedure explained in section 3.7. Successful verification for encoding and decoding processes were performed on simulation platforms (MATLAB® and C). Similarly a 32 carrier OFDM was realized using 128 point IFFT and FFT. The Turbo code was then used as channel code in the concatenated arrangement with OFDM. The combination was employed as error control coding scheme and tested for different channel conditions as mentioned in section 5.1.1. These results are described and discussed in the following sections.

5.2.1 Performance of Turbo OFDM for white Gaussian noise

Concatenated arrangement of Turbo coded OFDM has been tested in a simulated AWGN (Additive White Gaussian Noise) channel. Variance of noise is computed from SNR specification and white Gaussian noise samples are determined, which are added to the signal as it passes through the channel. AWGN samples are shown in Figure 5.4(a). Plot of bit error rate (BER) vs. signal to noise ratio (SNR) in dB is shown in Figure 5.4(b).

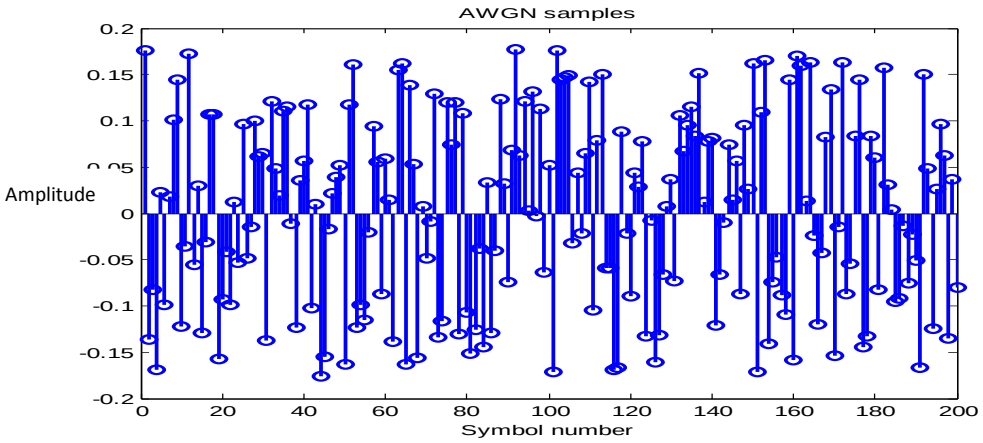

(a) AWGN samples at SNR = 12 dB

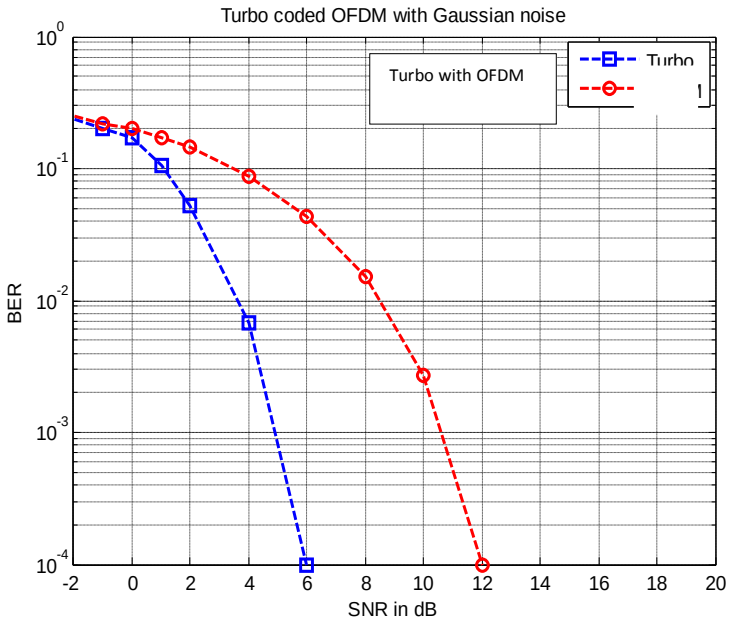

(b) BER performance of Turbo OFDM with white Gaussian noise

Figure 5.4 Turbo-OFDM with white Gaussian noise

In Figure 5.4 (a), Gaussian noise samples are depicted to demonstrate the random distribution (Gaussian) of noise amplitudes. Noise samples in Figure 5.4 (a) do not exhibit impulsive content. From the BER vs. SNR plot of Figure 5.4(a), for AWGN channel, Turbo code performs extremely well and there is a coding gain of nearly 6 dB over uncoded OFDM.

OFDM has reached performance of 10^{-4} at SNR =12 dB, for binary PSK transmission in Gaussian channel. With Turbo code, the combined scheme of Turbo coded OFDM, reaches the performance of 10^{-4} at SNR =6 dB. Thus there will be a coding gain of 6 dB between uncoded and coded OFDM.

5.2.2 Performance of Turbo OFDM for impulse noise, $A = 0.1, T = 0.1$

The concatenated arrangement of Turbo code with OFDM is tested in AWAN (Additive White Class-A Noise) channel. Impulse noise samples are determined using techniques described in Chapter-4 and added to the signal during propagation on the channel. $|H(f)|$ is assumed as 1 for all bits of transmission, to make the channel as AWAN channel. Plot of BER vs. SNR in dB, is shown in Figure 5.5. Snap shots of impulse noise samples are shown in Figure 5.6(a) and (b).

From BER vs. SNR plot of Figure 5.5, it is seen that Turbo code provides a coding gain of nearly 6 dBs over uncoded OFDM for $A = 0.1, T = 0.1$.

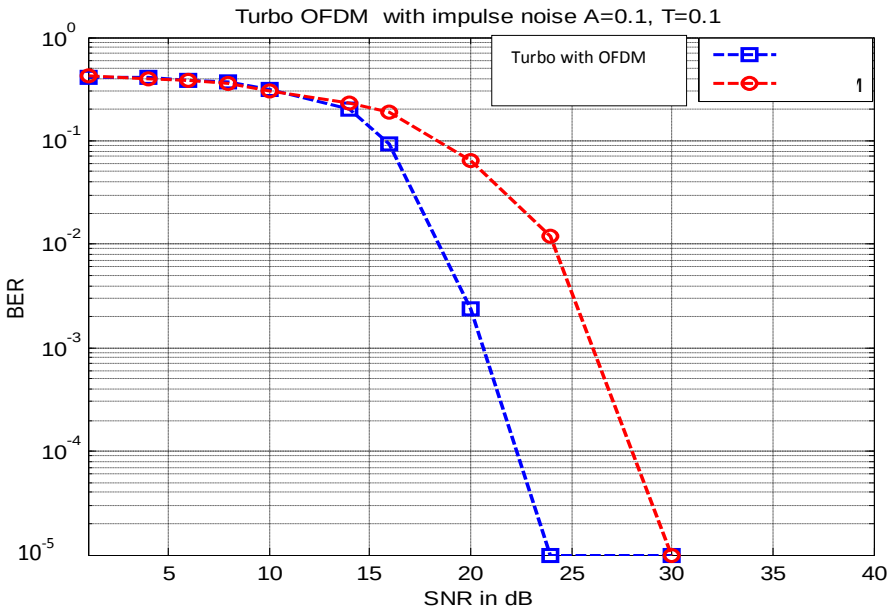

Figure 5.5 Turbo OFDM with impulse noise (AWAN channel): $A = 0.1, T = 0.1$(case-1)

Figures 5.6 (a) and (b) show the impulsive noise present in approximately 20 bits of noise samples, seen at different SNR, for the same impulse noise parameters

$A = 0.1, T = 0.1$. Since A and T have remained same, impulsive nature of the noise has remained the same as it is governed by the values of A and T. But the magnitude of noise level decreases with increase in SNR as per the definition of SNR,

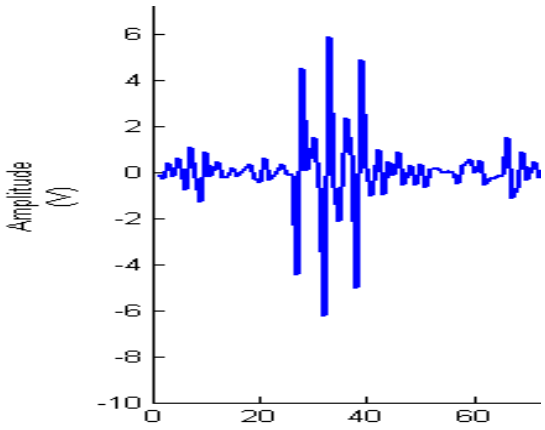

(a) $A = 0.1, T = 0.1$ at SNR = 12 dB

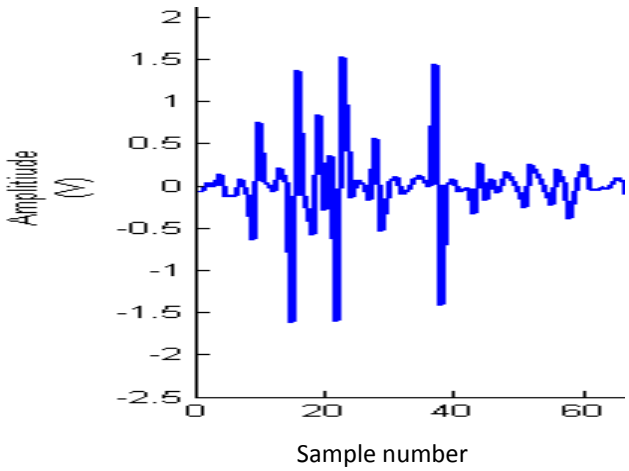

(b) $A = 0.1, T = 0.1$ at SNR = 16 dB

Figure 5.6 Impulse noise samples for $A = 0.1, T = 0.1$ (case-1) at two different values of SNR.

To observe impulse noise used to impair the data transmission more closely, impulse noise samples for 1000 noise samples are shown in the following figures. In Figures 5.7 (a) and (b), impulse noise parameters are set as $A = 0.1, T = 0.1$. Noise waveforms are shown for different SNR values.

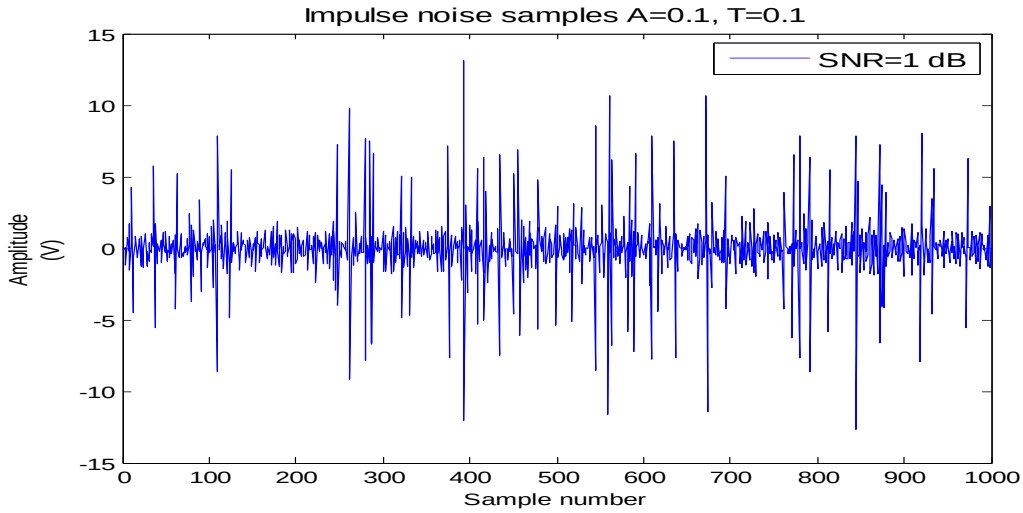

(a)

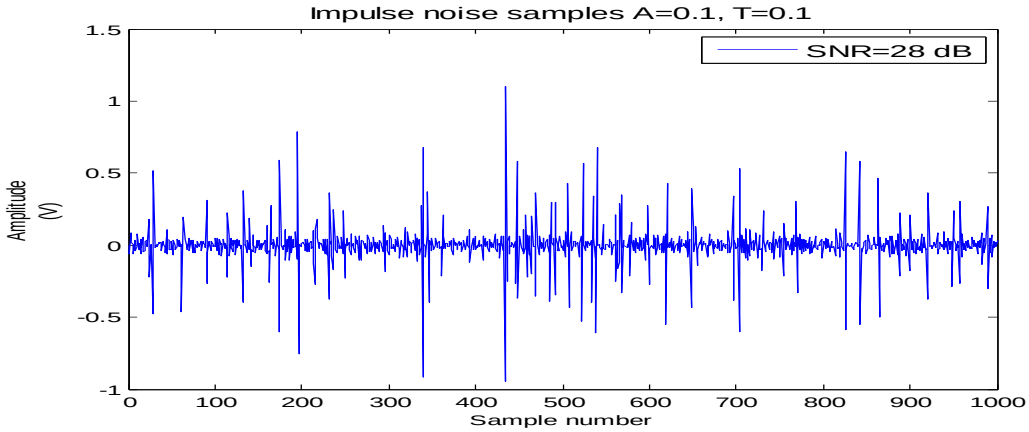

(b)

Figure 5.7 Impulse noise samples for $A = 0.1, T = 0.1$ (case-1) for 1000 bits, at different SNR (a) SNR=1dB (b) SNR=28 dB.

Since A and T are same for both cases (a) and (b) of Figure 5.7, only the strength of noise has reduced with SNR. The nature of the impulse noise in terms of number of peak impulses per unit time (A) and the proportion of impulsive noise power with respect to Gaussian noise power (T) are not affected.

At SNR=28 dB, impulses of the strength up to about 1.2 V have affected the system and for SNR value more than 24 dB (please refer Figure 5.5), the error that might occur due to this impulse noise are corrected.

In the following figures, Figures 5.8(a) and (b), impulse noise samples for

$A = 0.1, T = 0.01$ (case-2 of noise) for 1000 bits are shown for different values of SNR. Since T is reduced, strengths of impulse noise samples have increased. In general, this will increase the number of errors introduced by the channel during transmission.

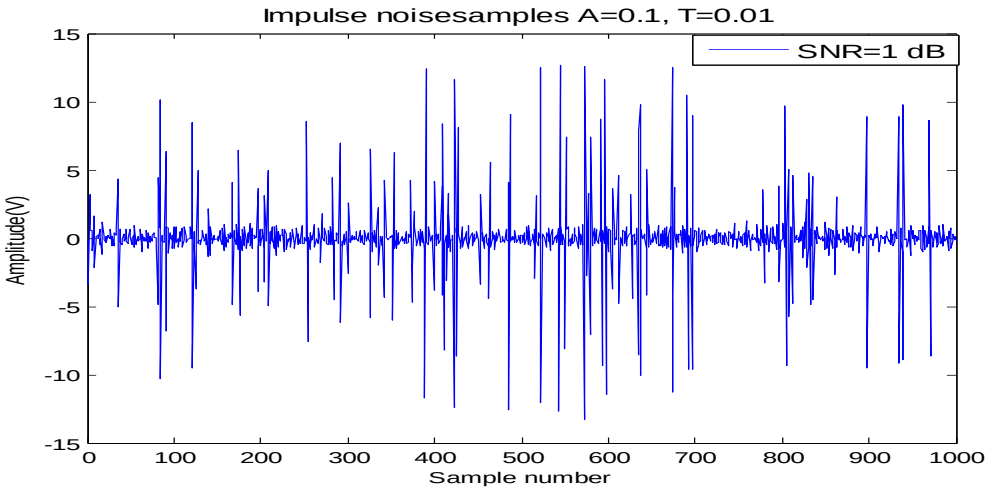

(a)

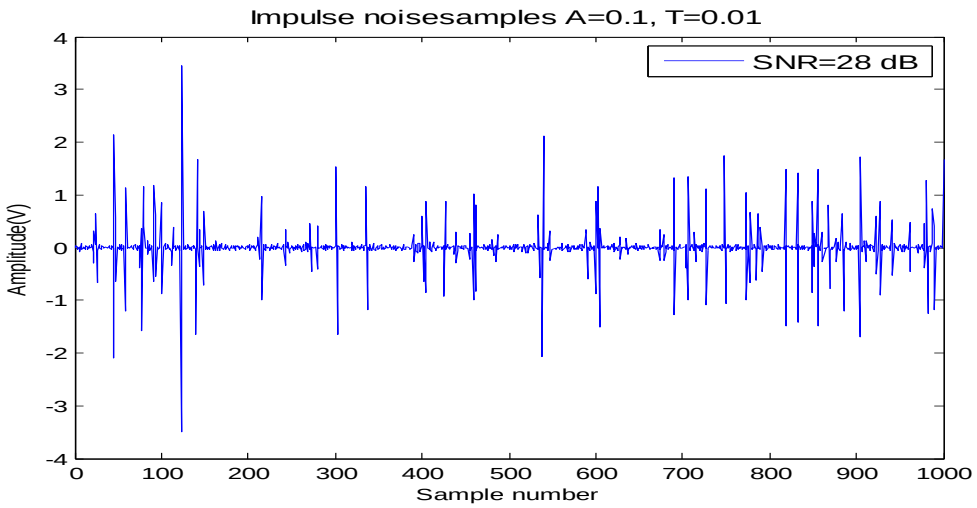

(b)

Figure 5.8 Impulse noise samples for $A = 0.1, T = 0.01$ (case-2 of noise) for 1000 bits, at different SNR.(a) SNR=1dB (b) SNR=28 dB.

In the following figures, Figures 5.9 (a) and (b), the parameters of impulse noise are specified as $A = 0.1, T = 0.001$ (case-3 of noise). The number of samples is chosen to be 1000. The noise waveforms are plotted for different SNR values. It is observed that there is an increase in the strength of impulse noise samples as shown in Figure 5.9 (b) for $T = 0.001$, compared to Figure 5.7 (b) for $T = 0.1$ and Figure 5.8 (b) for $T = 0.01$.

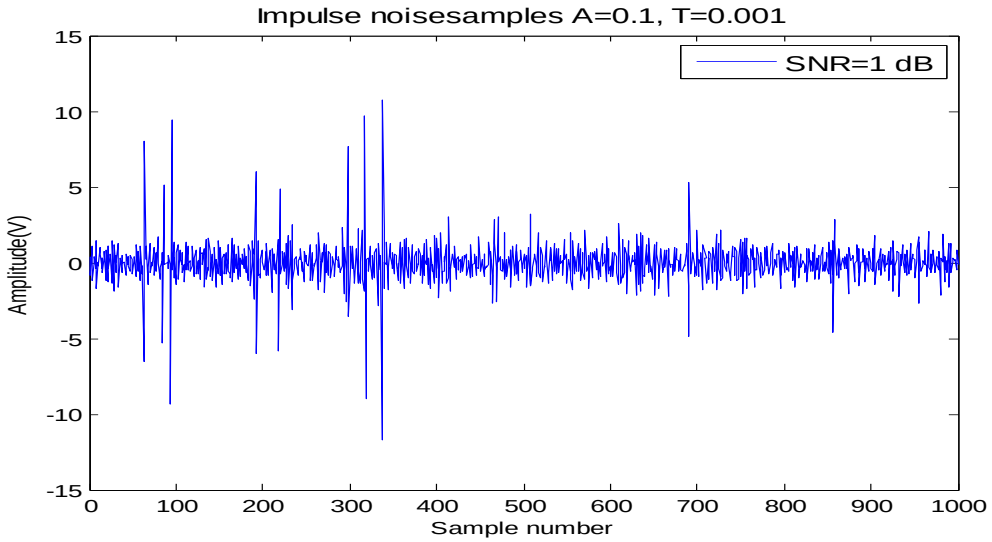

(a)

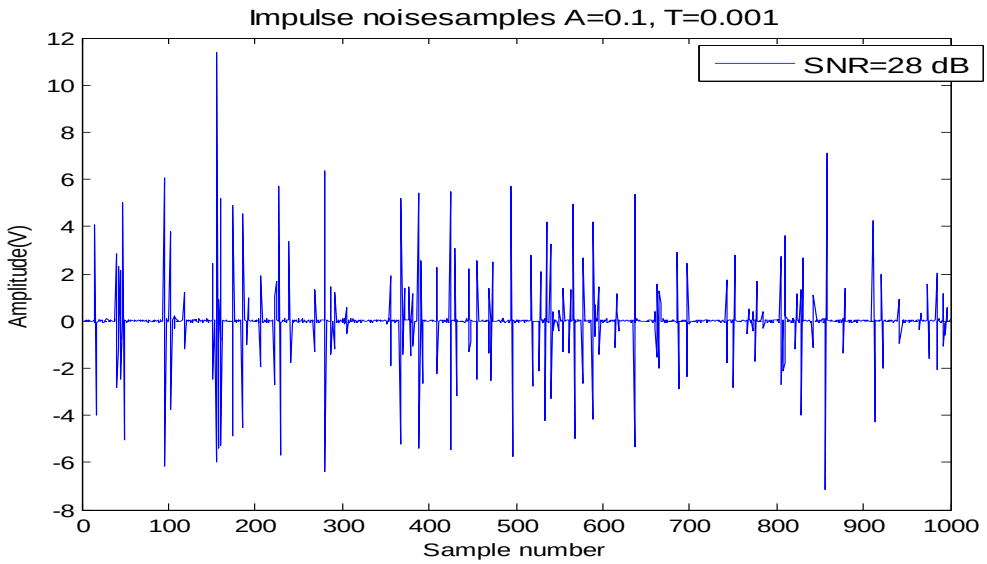

(b)

Figure 5.9 Impulse noise samples for $A = 0.1, T = 0.001$ (case-3 of noise) for 1000 bits, at different SNR. (a) SNR=1dB (b) SNR=28 dB.

5.2.3 Performance of Turbo OFDM for different values of T, with value of A fixed as $A = 0.1$

Figure 5.10 shows the comparison of performance of Turbo coded OFDM for $T = 0.1, T = 0.01, T = 0.001$, with value of $A = 0.1$ in each case.

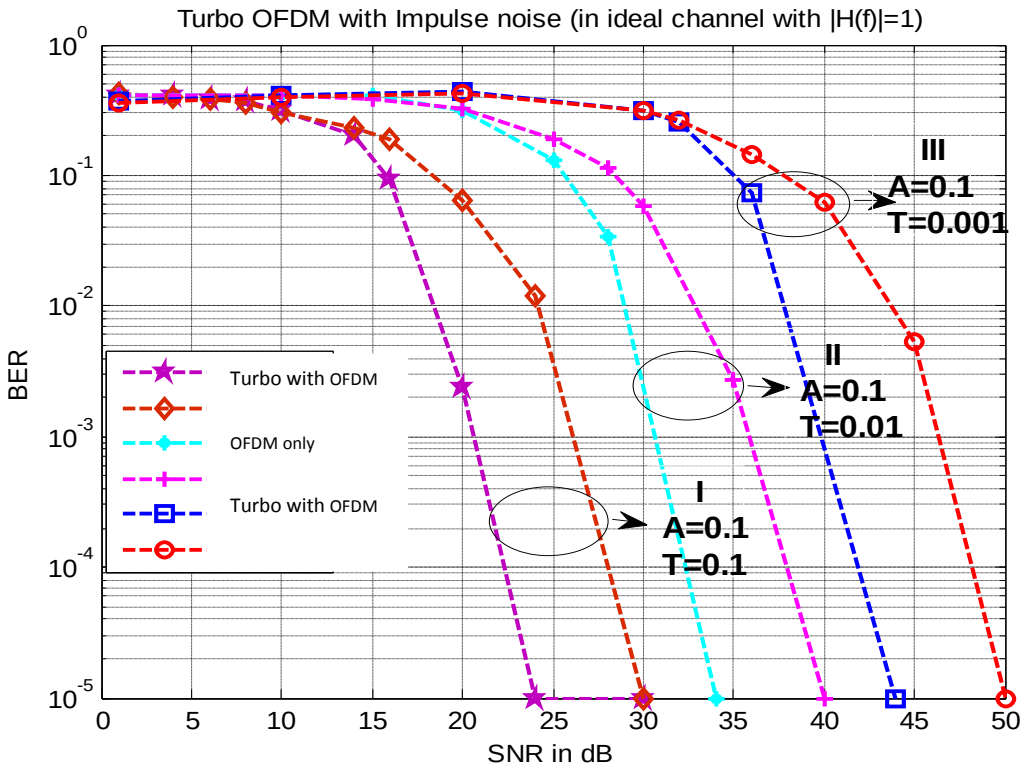

Figure 5.10 Performance comparison of Turbo OFDM for $A = 0.1$ and $T = 0.1, T = 0.01, T = 0.001$.

Table 5.1 Performance comparison of Turbo OFDM for $A = 0.1$ and $T = 0.1, T = 0.01, T = 0.001$.

	I (case-1 of noise)	II(case-2 of noise)	III(case-3 of noise)
A	0.1	0.1	0.1
T	0.1	0.01	0.001
Coding gain	6dB (24 dB to 30 dB)	6dB (34 dB to 40 dB)	6dB (44 dB to 50 dB)

As T decrease, the strength of impulsive noise component increases, which causes deterioration in the quality information transfer. Hence, a greater SNR is required to provide a specified BER requirement. Table 5.1 gives the values of A and T for the three cases of comparison. A coding gain of 6 dB is observed in each case.

5.2.4 Performance of Turbo OFDM for impulse noise parameters

$(A = 0.01, 0.1, 1, 10, T = 0.1)$

In this section, performance of concatenated arrangement of Turbo coded OFDM is observed keeping the value of T as equal to 0.1 and varying the parameter for impulse noise index T. A is allowed to take on values 0.01, 0.1, 1and 10.

The performances for $(A = 10, T = 0.1)$, $(A = 1, T = 0.1)$, $(A = 0.1, T = 0.1)$ and $(A = 0.01, T = 0.1)$ are shown respectively in figures 5.11, 5.12 and 5.13. and 5.14

Table 5.3 gives the comparison of performance for cases shown in Figure 5.11 to Figure 5.14. A coding gain of 6 dB is observed in each case.

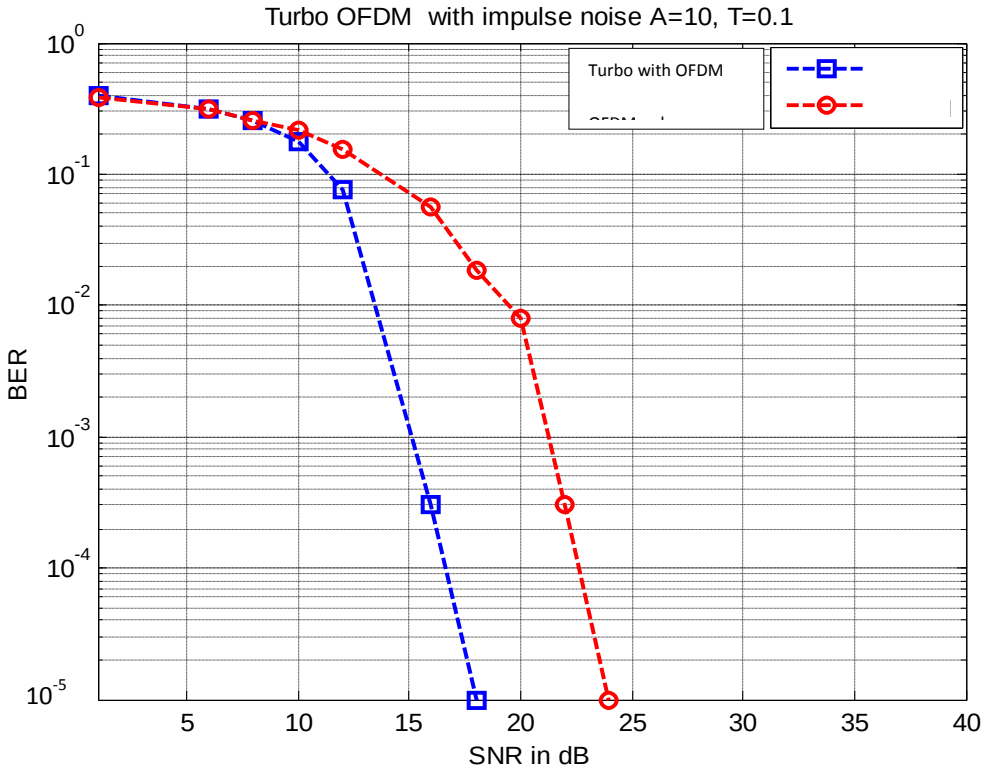

Figure 5.11 Performance of Turbo OFDM for $A = 10$ and $T = 0.1$

5.2.5 Performance of Turbo OFDM for $A = 1, T = 0.1$

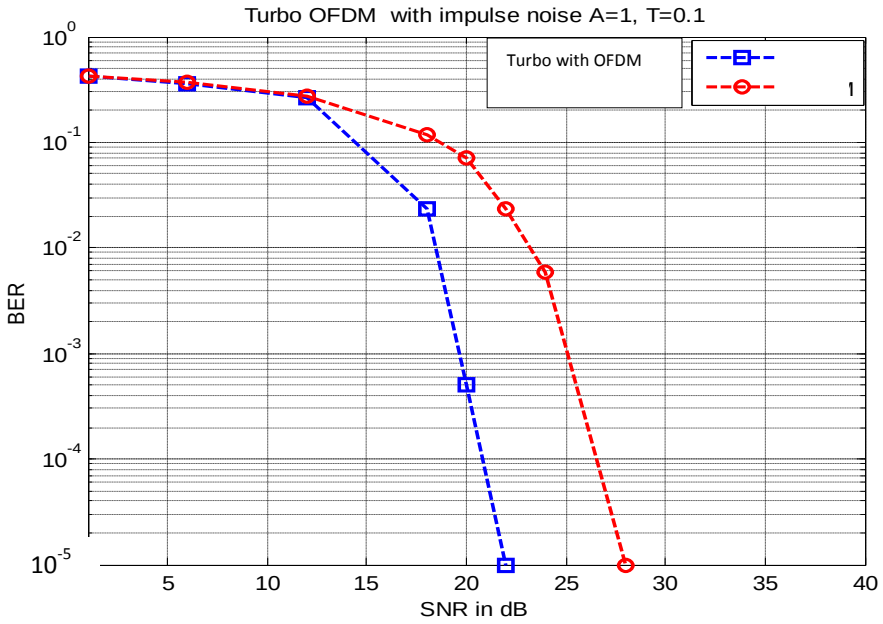

Figure 5.12 Performance of Turbo OFDM for $A = 1, T = 0.1$

5.2.6 Performance of Turbo OFDM for $A = 0.1, T = 0.1$

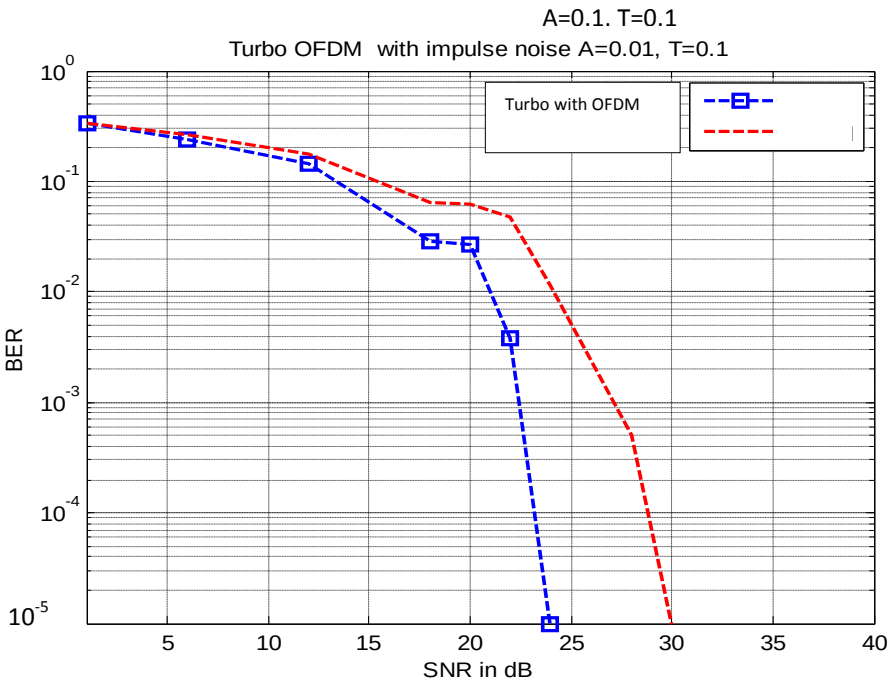

Figure 5.13 Performance of Turbo OFDM for $A = 0.1, T = 0.1$(case-1 of noise)

5.2.7 Performance of Turbo OFDM for $A = 0.01, T = 0.1$

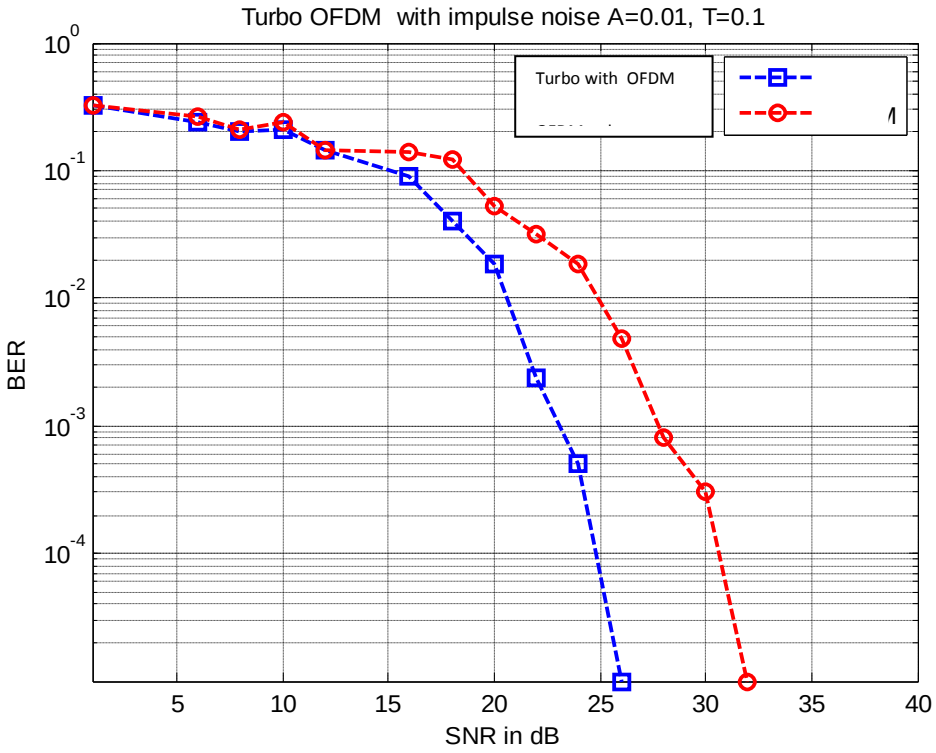

Figure 5.14 Performance of Turbo OFDM for $A = 0.01, T = 0.1$(case-4 of noise).

Table 5.2 Performance comparison of Turbo OFDM for $T = 0.1$ and with $A = 10, A = 1, A = 0.1, A = 0.01$

	I	II	III	IV
A	10	1	0.1	0.01
T	0.1	0.1	0.1	0.1
Coding gain with T-OFDM	6 dB (18 dB to 24 dB)	6dB (22dB to 28 dB)	6dB (24 dB to 30 dB)	6dB (26 dB to 32dB)

The relative performance of four different cases of study for different values of A, keeping the value of T fixed at $T = 0.1$, (refer BER plots obtained in Figures 5.11 to 5.14), have been tabulated in Table 5.2. It is seen that in each case, a coding gain of approximately 6 dBs can be obtained by using concatenated Turbo code-OFDM arrangement when compared to uncoded OFDM. As A increases, BER plots shift towards left, indicating a reduction in the impulsive nature of the channel.

5.2.8 Turbo OFDM with channel attenuation for different impulse noise conditions in power line channel: Effect of T

In this section, test results of effect of variation in the value of T, keeping value of A fixed at $A = 0.1$ is observed. The channel attenuation was varied between 10 to 50 dB. The nature of variation of channel attenuation remains the same in the three comparisons. BER plots were obtained for noise types (i) $A = 0.1, T = 0.1$ (ii) $A = 0.1, T = 0.01$ (ii) $A = 0.1, T = 0.001$ and have been plotted on same graph for comparison. This is shown in Figure 5.15. Table 5.3 gives the details of coding gain in each case.

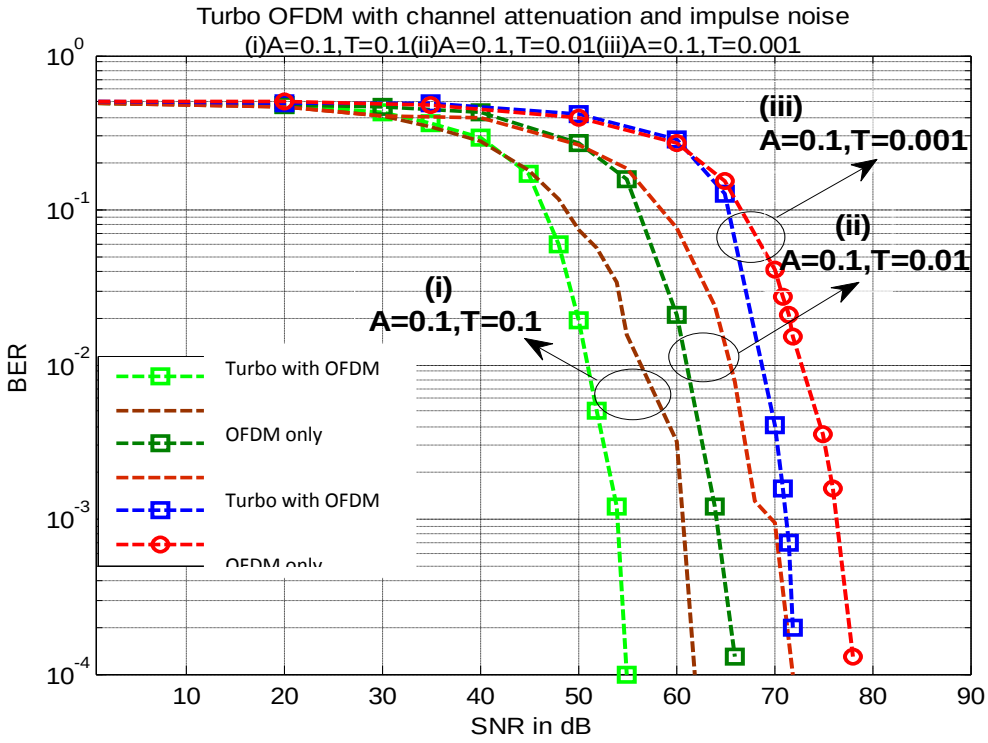

Figure 5.15 Performance comparison of Turbo OFDM with channel attenuation for

(i) $A = 0.1, T = 0.1$ (ii) $A = 0.1, T = 0.01$ (iii) $A = 0.1, T = 0.001$

Table 5.3 Coding gain for three cases shown in Figure 5.15.

	Impulse noise parameters			Attenuation
	$(i) A = 0.1, T = 0.1$ (case-1 of noise)	$A = 0.1, T = 0.01$ (case-2 of noise)	$A = 0.1, T = 0.001$ (case-3 of noise)	10 to 50 dB
coding gain	nearly 6 dB (56 dB to 62 dB)	nearly 6 dB (66 dB to 72 dB)	nearly 6 dB (72 dB to 78 dB)	

It is observed (from a comparison of Figures 5.10 and 5.15) that in the first case ($A = 0.1, T = 0.1$) the presence of channel attenuation, has resulted in an increase in the required SNR by nearly 30 dB to yield BER of the order of 10^{-4}. Similarly, in the second case ($A = 0.1, T = 0.01$), SNR required to yield BER of the order of 10^{-4} has been increased by nearly 32dB and nearly by 28 dB in the third case.

5.2.9 Turbo OFDM with channel attenuation and impulse noise in power line channel: Effect of load locations

In this section, test results of effect of variation of load locations along the distance between transmitter and receiver location for a specific noise scenario ($A = 0.1, T = 0.1$) are provided. BER plots for the two different distances are shown in Figure 5.16. Table 5.4 gives the details of distances used for load locations.

Two cases of distances are used for test. First case is referred to as d-I in Table5.4, for which the distance between transmitter and receiver points is assumed to be 500 m and along the length of the propagation over the line, loads being connected at distances shown for d-I. These loads will be responsible for setting multipaths in the channel. Similarly second case is referred to as d-II with distance between transmitter and receiver points is assumed to be 2km and with load locations as shown in Table5.4.

Table 5.4 Attenuation with different distances for BER vs. SNR in Figure 5.16

Distances of load locations in meters						Attenuation	SNR for which BER =10^{-4}
d-I	100	200	300	400	500	15 to 50 dB	55 dB
d-II	100	500	1000	1500	2000	18 to 60 dB	62 dB

Attenuation on the line for transmission of data bits is also shown in Table 5.4. When the channel is used for first case of load locations d-I, attenuation experienced by the data bits is 15 to 50 dB. Keeping all the other conditions for channel model unchanged, if distances of load locations now change to that of d-II, then attenuation experienced by the data bits increases to the level between 18 to 60 dB. Figure 5.16 gives the vs. SNR plot for the two cases d-I and d-II.

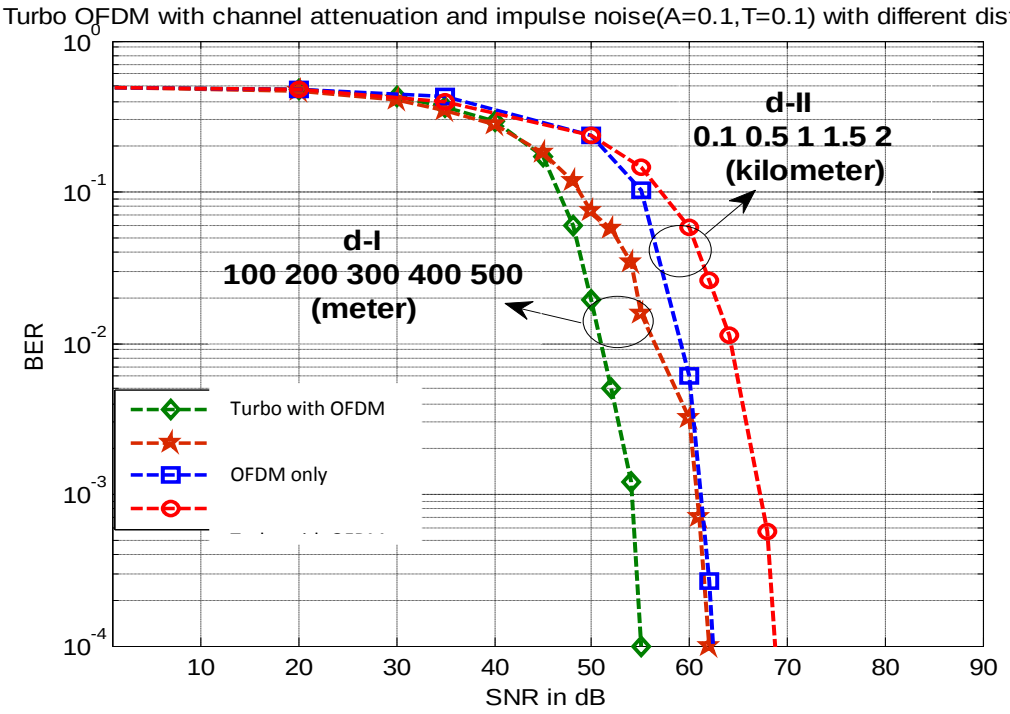

Figure 5.16 Effect of load locations to power line channel on performance of Turbo OFDM

It is observed that for the same operating conditions, attenuation has increased with distance which in turn requires the establishment of larger SNR values for effective correction of errors.

Increase in attenuation due to increased distance from case d-I to case d-II (as shown in Table 5.4), is shown in graphs of Figure 5.17 (a) and (b).

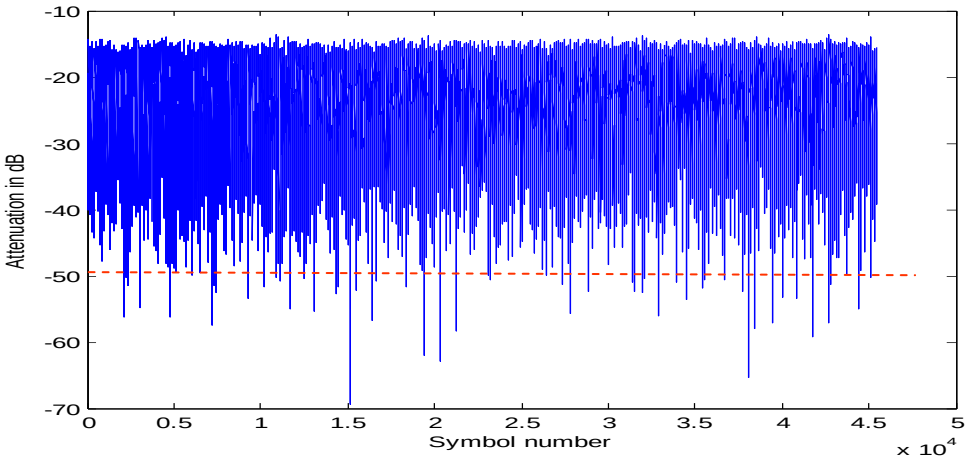

(a)

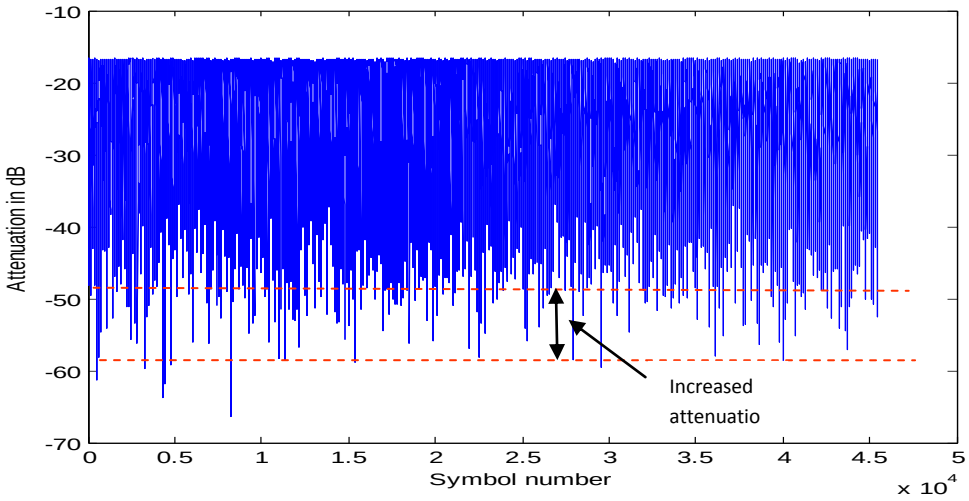

(b)

Figure 5.17 Attenuation for each symbol (bit) for different distances of load locations

(a) for case d-I (b) for case d-II

Figure 5.17(a) gives the values of attenuation suffered by each of the symbols for the first case of distances with locations of loads specified at: $d(\mathrm{m}) = (100, 200, 300, 400, 500)$ Most of the time, attenuation is confined to values between 10 dB to 45 dB. This is marked by the dashed line in Figure 5.17(a). Figure 5.17(b) gives the values of attenuations suffered by each symbols for the second case of distances of with locations of loads specified at $d(km) = (0.5, 1, 1.2, 1.5, 2)$. It is observed that in this case, attenuation exceeds the dashed line marked at 45 dB at many instances. Attenuation is now seen to be bounded between limits 18 dB to 60 dB. This is indicated by the two dashed lines in Figure 5.17(b).

It is seen that with increase in distance, there is consequent increase in attenuation. This has resulted in a greater SNR requirement to attain the same performance (BER value). It is observed that an increase of 7dB is required to attain a BER value of 10^{-4} in case –II. (Please refer Table 5.4).

5.2.10 Performance of Turbo OFDM with text data recovery for different SNR values

In this section, text output in .txt file is shown at different SNR values for case 1 of noise type (channel attenuation is 15 to 50 dB, Distance between transmitter and receiver is 500m). Observation of these results is to verify the process of error correction shown in the graph of Figure 5.15. Figure 5.18 shows the text present in input text file.

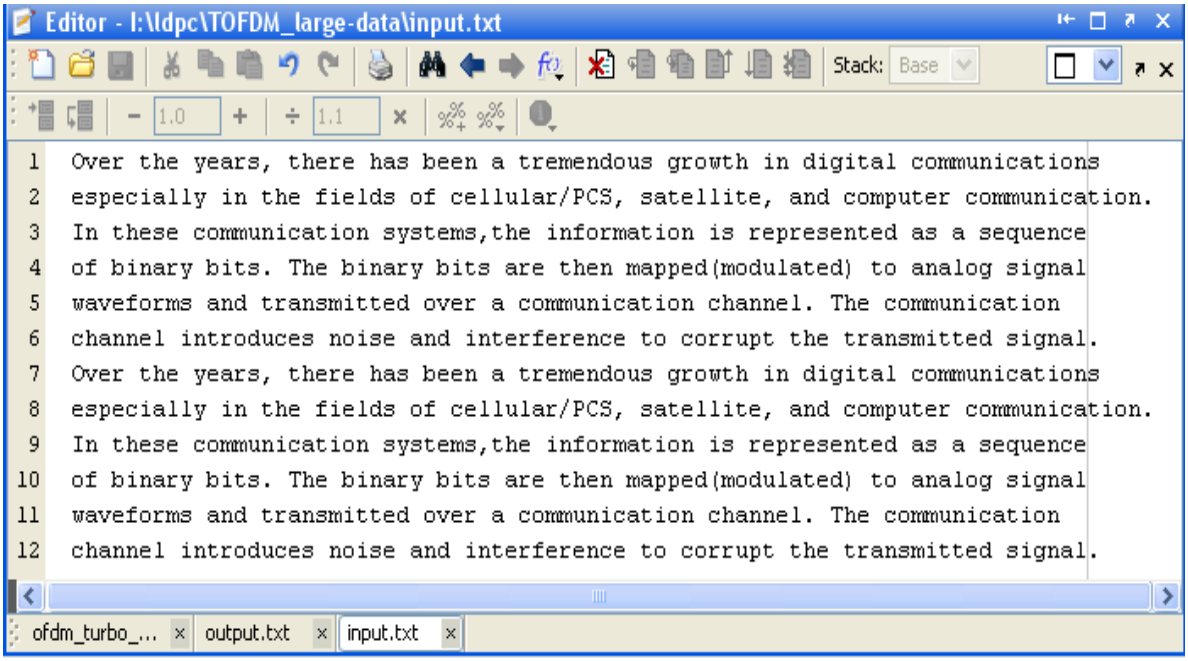

Figure 5.18 Text input to Turbo coded OFDM scheme in word format

Pictures of output text files are taken at different SNR and are shown in Figure 5.19 (a) to (d).

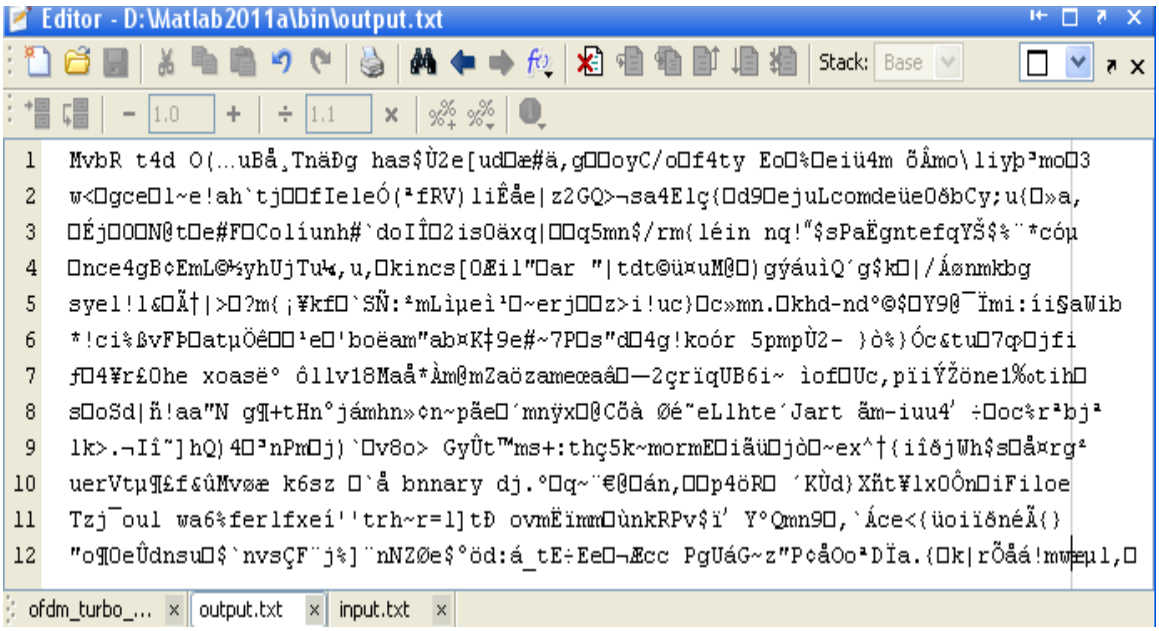

(a) Text output for $A = 0.1, T = 0.1$ at SNR=38 dB (1715 errors)

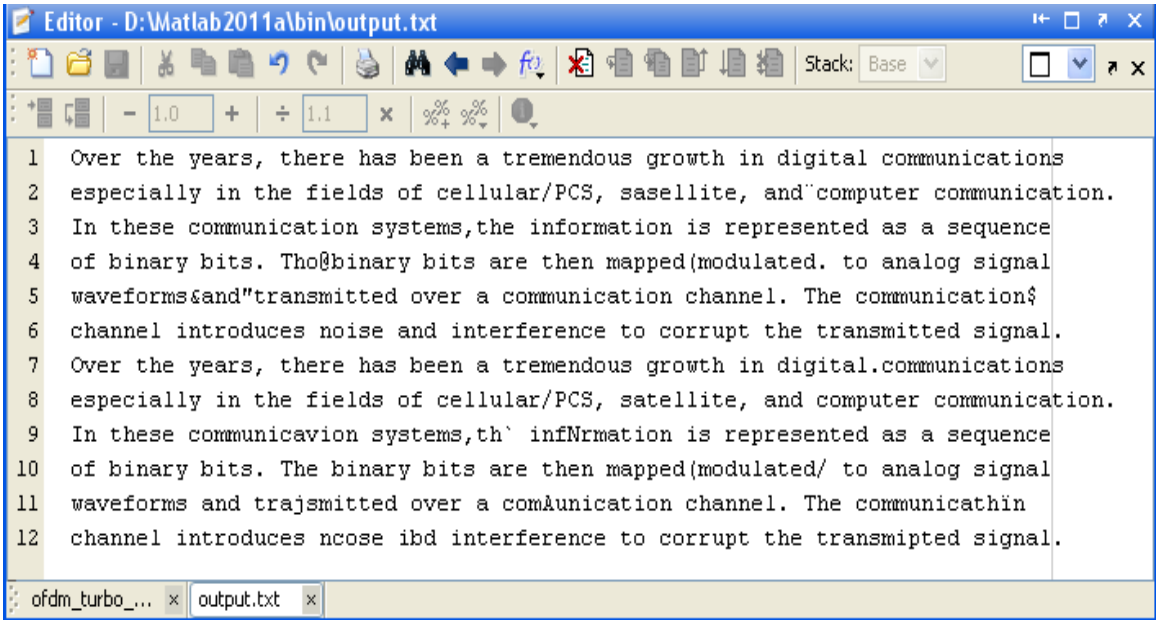

(b) Text output for $A = 0.1, T = 0.1$ at SNR=52 dB (44 errors)

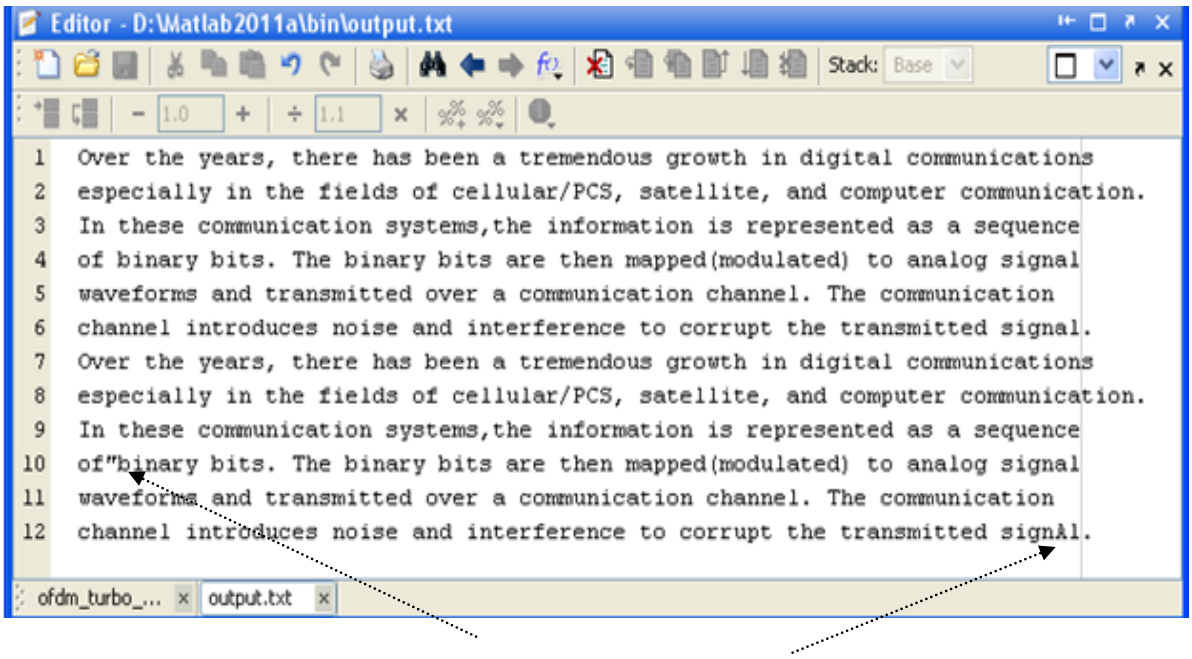

Two errors in text output

(c) Text output to Turbo coded OFDM scheme for $A = 0.1, T = 0.1$ at SNR=54 dB (2 errors)

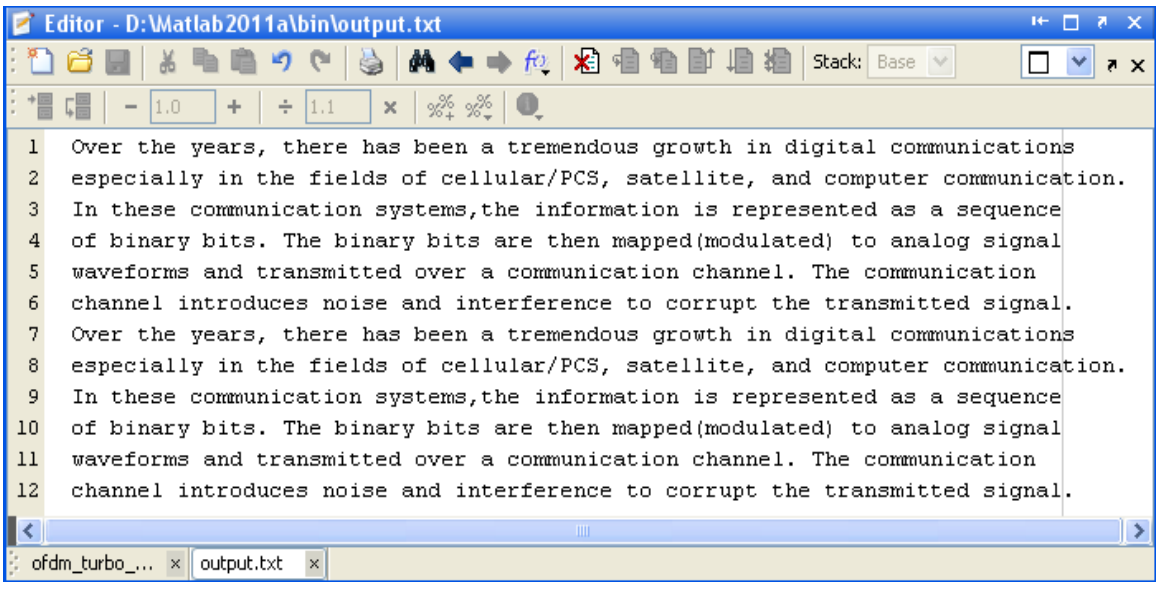

(d) Text output to Turbo coded OFDM scheme for $A = 0.1, T = 0.1$ at SNR=55 dB (no error)

Figure 5.19 Output text files for Turbo coded OFDM scheme for $A = 0.1, T = 0.1$ at different SNR

Observation of the pictures shown in Figure 5.18 (a) to (c) illustrates the effect of SNR on error correction. AT SNR= 55 dB, output available in output.txt file is free from errors and matches with input present in input.txt file shown in Figure 5.17.

Statistics of errors correction at different stages is shown in Table 5.5.

Table 5.5 Statistics of error correction at different stage for text output

	Number of letters=930 Total number of bits= Number of letters x 8 bits/letter=930 x 8=7440			
SNR (dB)	38	52	54	55
Number of errors	1715	44	2	0
BER	0.2305	0.0059	2.6882×10^{-4}	0

Statistics of error correction was also documented by observing the number of errors for 50 times. A bar graph for the same is shown in Figure 5.20. Values for number of errors documented during the tests are shown in Table 5.6 and were used to draw the graph of Figure 5.20. The uncorrected errors due to OFDM with Turbo are shown with blue in color.

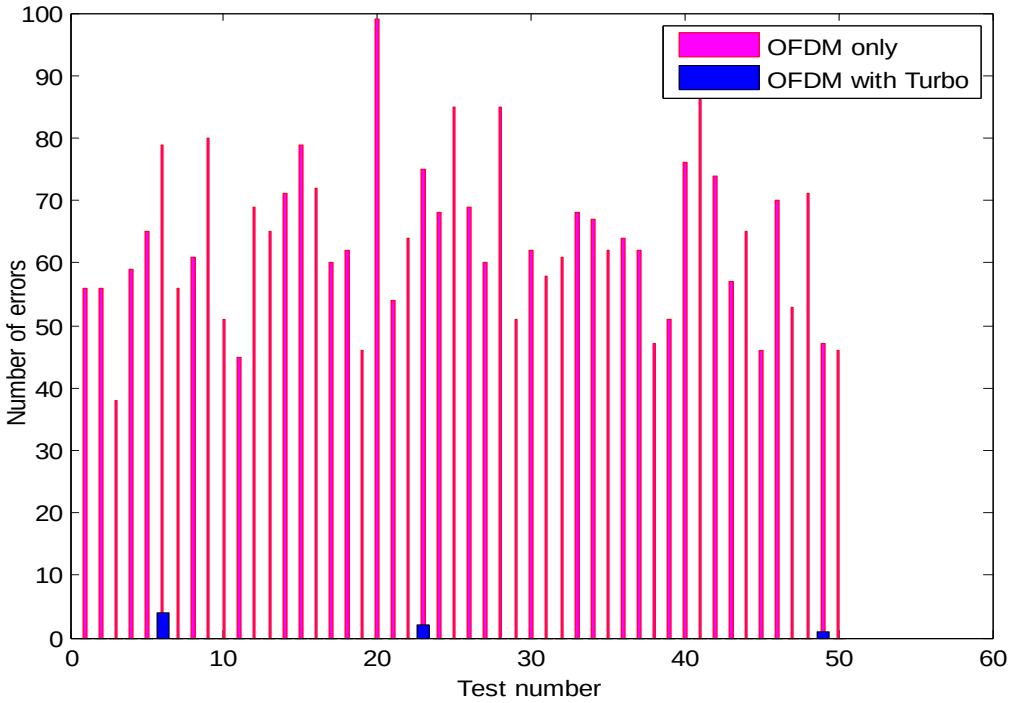

Figure 5.20 Bar graph for uncorrected errors at SNR= 55 dB, A=0.1, T=0.1

(case 1 of noise) by carrying repeated tests for 50 times.

From Figure 5.20, it is observed that at SNR= 55 dB, for A$A = 0.1, T = 0$, with attenuation of 10 to 50 dB, number of errors uncorrected by OFDM vary from 38 to 99. Simultaneously, OFDM with Turbo corrects the errors 47 times (94% of the time) and shows uncorrected errors for 3 times (6% of the time).

Table 5.6 Statistics of errors present at SNR = 55 dB for A=0.1, T=0.1 over 50 tests

SNR = 55 dB					
Number of letters=930 Total number of bits= Number of letters x 8 bits/letter=930 x 8=7440					
Test No.	Number of errors uncorrected with Turbo code	Number of errors uncorrected with OFDM	Test No.	Number of errors uncorrected with Turbo code	Number of errors uncorrected with OFDM
1	0	56	26	0	69
2	0	56	27	0	60
3	0	38	28	0	85
4	0	59	29	0	51
5	0	65	30	0	62
6	**4**	79	31	0	58
7	0	56	32	0	61
8	0	61	33	0	68
9	0	80	34	0	67
10	0	51	35	0	62
11	0	45	36	0	64
12	0	69	37	0	62
13	0	65	38	0	47
14	0	71	39	0	51
15	0	79	40	0	76
16	0	72	41	0	97
17	0	60	42	0	74
18	0	62	43	0	57
19	0	46	44	0	65
20	0	99	45	0	46
21	0	54	46	0	70
22	0	64	47	0	53
23	**2**	75	48	0	71
24	0	68	49	**1**	47
25	0	85	50	0	46

5.2.11 Turbo OFDM with channel attenuation and cyclostationary impulse noise

In this subsection, noise samples using cyclostationary noise given by (4.12) are derived using noise parameters as:

$$A_0 = 0.23, A_1 = 1.38, A_2 = 7.17, f_{ac} = 200 \text{ KHz},$$

$$\theta_0 = 0(\text{deg}),\ \theta_1 = 6 \text{ (deg)}, \theta_2 = -35(\text{deg}), \mathrm{n}_0 = 0, \mathrm{n}_1 = 1.91, \mathrm{n}_2 = 1.57 \times 10^5.$$

Noise samples with respect to time are plotted and are shown in Figure 5.21. It is observed that noise samples are broadly periodic with period (10 msec).

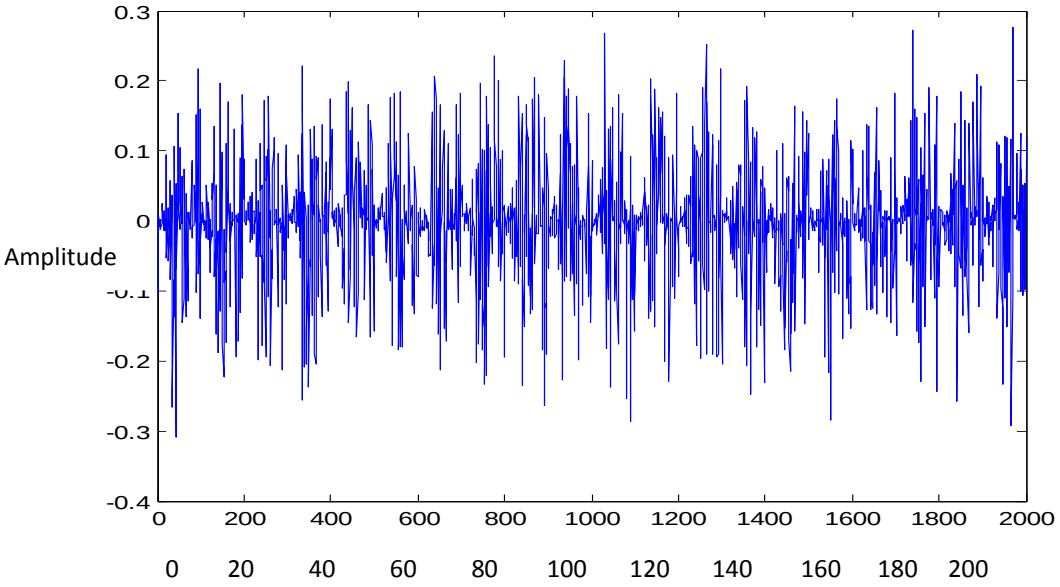

Figure 5.21 Noise samples of cyclostationary noise.

Attenuation on the data bits is between 15 dB to 50 dB. With this attenuation and cyclostationary noise (a sample function of which is shown in Figure 5.21), the plot of BER vs. SNR is shown in Figure 5.22.

As seen from the BER plot shown in Figure 5.22, text data shown in Figure 5.18 given as the input is recovered without errors at SNR =30 dB. This performance with cyclostationary noise is compared with performance with Middleton class-A noise shown in Figure 5.15.

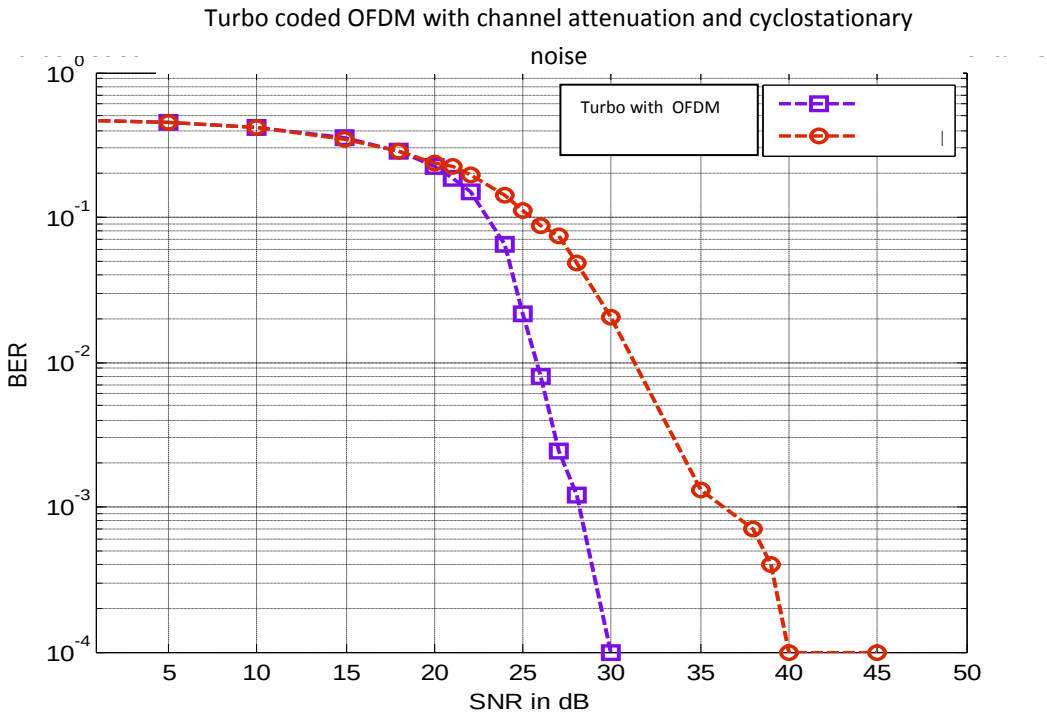

Figure 5.22 Performance of Turbo coded OFDM scheme for cyclostationary noise.

In Figure 5.15, with Middleton class-A noise, the performance of 10^{-4} is found at a much larger value of SNR (approximately 55 dB). This variation between the two results is due to class-A noise samples having more strength than cyclostationary noise samples.

5.2.12 Inferences from results of scheme 1:Turbo coded OFDM

Performance obtained by Turbo OFDM is reproduced in Table 5.7 as given below.

Two cases of distances for load locations along the length of transmitter and receiver points are considered ((i) 100 to 500 m and (ii) 0.5 km to 2 km). Channel attenuation of the value 10 to 50 dB is observed during these tests. Noise cases 1, 2 and 3 are individually tested.

Table 5.7 Performance of Turbo OFDM

Distance type of load locations	Attenuation	Noise case/type	BER=10^{-4}		Coding gain
			SNR(dB) for Turbo code	SNR(dB) for OFDM	
100-500m	low to high	case 1 (A=0.1,T=0.1)	56	62	6 dB
100-500m	low to high	case 2(A=0.1,T=0.01)	66	72	6 dB
100-500m	low to high	case 3(A=0.1,T=0.001)	72	78	6 dB
0.5-2 km	low to high	case 1(A=0.1,T=0.1)	62	68	6 dB
100-500m	low to high	cyclostationary	30	40	10 dB

Results in first to third row correspond to Middleton Class-A impulse noise and fourth row corresponds to cyclostationary noise. The behavior of error correction by Turbo code in providing coding gain over uncoded OFDM is observed to be by 6 dB, in case of different cases of Middleton Class-A impulse noise. For cyclostationary noise,

the system corrects at lower SNR values of nearly at 30 dB and provides a coding gain of approximately 10 dB. This behavior can be explained by observing the strengths of noise. As seen in Figure, noise samples for cyclostationary noise have lesser strengths than those for Middleton Class-A noise as seen in Figures 5.7, 5.8 and 5.9. This observation demonstrates that the proposed scheme will efficiently correct errors due to cyclostationary noise.

The overall observation of results has resulted in the following conclusions for the proposed scheme 1: Turbo coded OFDM:

1. Turbo code has given a coding gain of approximately 6 dB over uncoded OFDM in each case of noise type.
2. Turbo code has required SNR of approximately 6 dB for load location distance type (d-II) than for load location distance type (d-I).
3. Turbo code has given a coding gain of 10 dB over uncoded OFDM for cyclostationary noise.
4. Turbo coded OFDM approaches the performance of BER=10^{-5} at a much earlier SNR for cyclostationary noise (at SNR=30 dB), than that for impulse noise with Middleton Class-A noise with $A = 0.1, T = 0.1$ (at SNR=55 dB), for same channel attenuation.

In the next section, a discussion on the results for the performance of 'BCH coded Alamouti 2x1 space time coding' is presented.

5.3 Results of hardware implementation of BCH code synthesized on Digital Signal Processor (TMS 320C6713) concatenated with Alamouti code

A BCH code with parameters $n = 63, k = 36, t = 5$ was designed using the detailed explanation about the design procedure given in section 3.4 and 3.5. BCH code was synthesized on DSP processor TMS 320C6713 and tested for verification of encoding and decoding processes. Alamouti 2x1 space time code was tested independently in MATLAB platform for Gaussian channel. The two entities BCH encoder/decoder on processor and Alamouti scheme on MATLAB are then interfaced as per the block diagram shown in Figure 5.3. Results are documented for different channel conditions and presented in this section.

In the first part of this section, the performance of BCH code over channels perturbed by Gaussian noise and impulsive noise has been compared. Figure 5.23 shows this comparison.

5.3.1 Relative performance of BCH code (63, 36, 5) for Gaussian noise and impulse noise for $A = 0.1, \boldsymbol{T = 0.1}$.

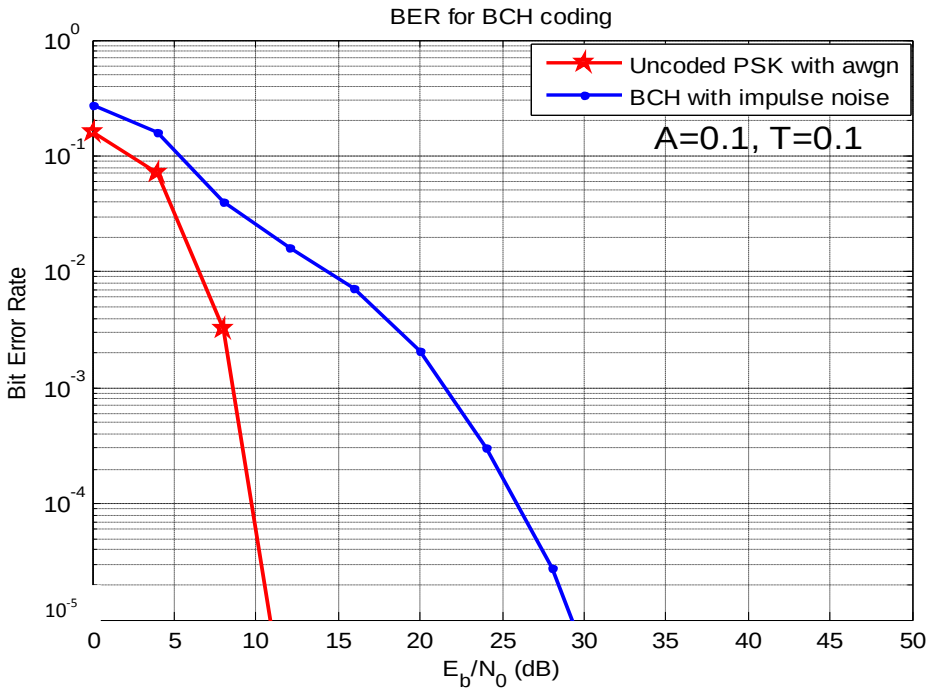

Figure 5.23 Comparison of performance of BCH code (63, 36, 5) for Gaussian noise and impulse noise for $A = 0.1, T = 0.1$ (case-1 of noise).

The parameters $A = 0.1, T = 0.1$ imply that strength of impulse noise power is 10 times that of Gaussian noise. Therefore, to obtain a BER of 10^{-5}, an increase of SNR by about 16 dB is required.

5.3.2 Performance evaluation of BCH code (63, 36, 5) for different values A and T

A performance comparison involving of BCH coded data $(n = 63, k = 36, t = 5)$ over channel perturbed by impulsive noise with different parameters (specified by values of A and T) in AWAN channel is shown in Figure 5.24. The input data comprises of 1000 frames with 63 bits in each frame.

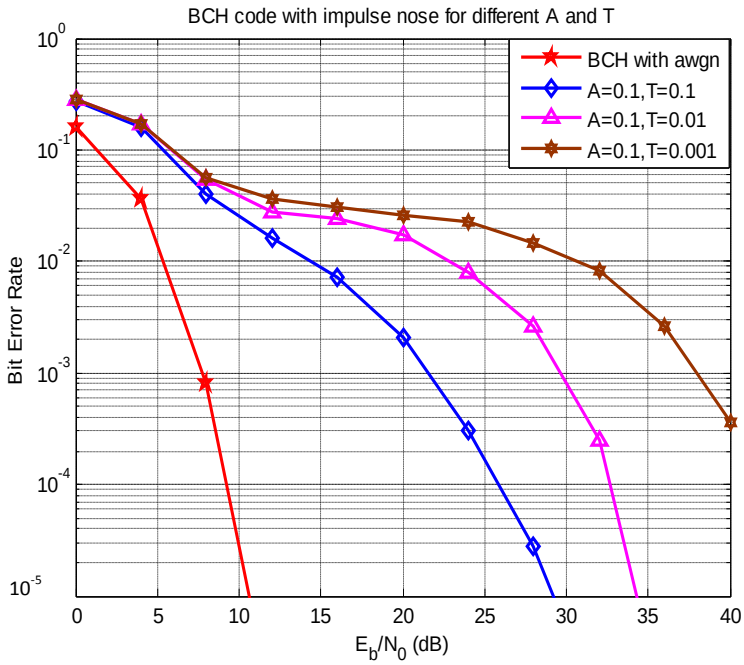

Figure 5.24 Relative performance of BCH code (63, 36, 5) for different cases of impulse noise

From Figure 5.24, following observations are made.

1. In the presence of impulse noise, the BCH code requires a higher value of SNR to deliver a given BER performance.

2. As T decreases, the strength of impulsive noise component increases and hence SNR requirement increases.

5.3.3 Implementation of DSP TMS320C6713 as BCH encoder and decoder.

In this subsection, block schematic shown in Figure 5.1 was implemented. Figure 5.25 shows the picture taken for the implementation of scheme 2. The encoder and decoder of BCH code with (63, 36, 5) were synthesized in Texas Instrument (TI)'s Digital Signal Processor TMS320C6713.

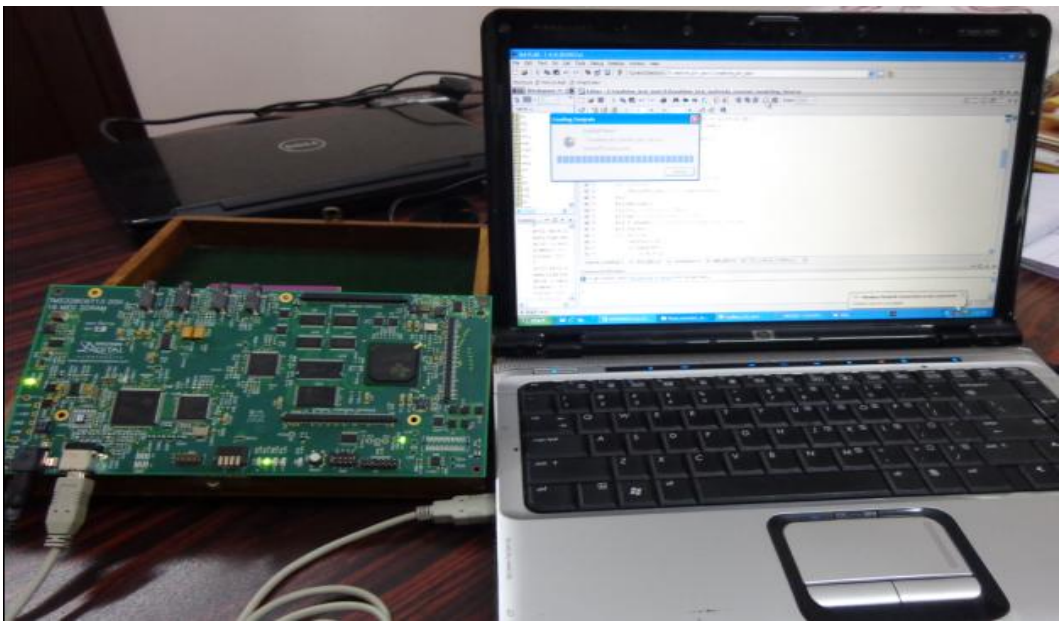

Figure 5.25 Picture showing the program for scheme 2 at work.

The sequence of operations performed in this exercise are listed below.

1. MATLAB® takes the text input and converts text into binary data.
2. BCH encoder takes the binary data from input file and encoding is performed in processor for one frame of bits.
3. Using the BCH encoded data as input, inner level coding is done. i. e., Alamouti's 2x1 space time coding for data propagation on two paths of the power line channel is configured in MATLAB®. Space time encoded signal (data) gets perturbed by power line channel attenuation and impulse noise, both modeled as explained in chapter 4. Estimates of data bits are made available using space time decoding procedure.
4. BCH decoder is fetches the space time decoded data as input and BCH decoding operation is done by the processor. Output is written in a text file.

Binary input and output are compared to find the number of uncorrected errors. The performance of BCH coded Alamouti space time code for protecting data integrity over power lines (scheme 2) is shown in section 5.2 and implemented as in Figures 5.25 is shown in Figure 5.26.

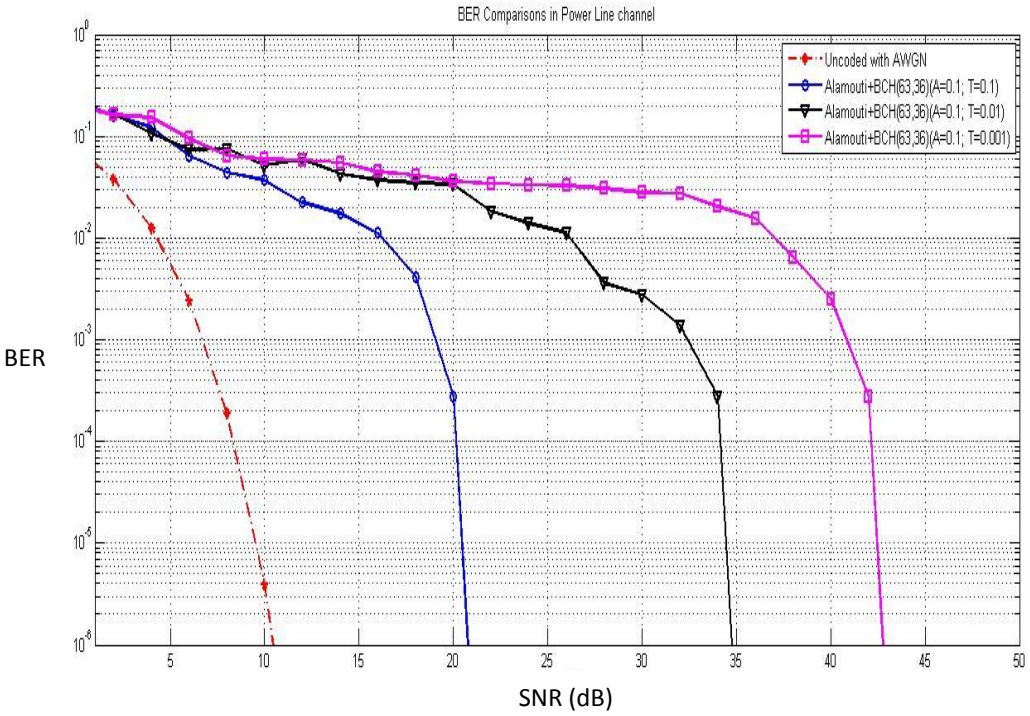

Figure 5.26 BER performance for (63, 36, 5) with different values of A and T.

Figure 5.26 shows the result of the steps 1 to 4 in which the performance of concatenated BCH coded Alamouti scheme is determined for different levels of impulse noise strength (quantified by values of T). These plots have been obtained with the following parameters quantifying the attenuation offered by the channel for a given frame:

- (i) $A = 0.1, T = 0.1$ (case-1) (ii) $A = 0.1, T = 0.01$ (case-2) (iii) $A = 0.1, T = 0.001$(case-3)
- channel state is fixed to be with 0 dB attenuation for first 32 bits and equal to 6 dB attenuation for the remaining 31 bits in each frame of 63 bits.

The text input used to obtain the results in Figure 5.26 is specified in Figure 5.27(a). Figures 5.27 (b) to (g) show the output at different SNR values for $A = 0.1$ and T taking on values 0.1, 0.01, 0.001.

Input Text file

Power line communication (PLC) is the communication over power line.
The main problem related to this is the interference with other communication system.
We proposed new technique to reduce the interference, using the powerful error control code (BCH+ Alamouti).

(a) Input Text file

Output Text files

Power line communication (PLC) is the communication ov**u2** power line.
The main problem related to this is the interference with □th**g**r communication syst**ug**.
We proposed new technique to reduce th**%** interference, usin**G** the powerful error control code (BCH+ Alamouti).

(c)

Power line communication (PLC) is the communication over power line.
The main problem related to this is the interference with other communication system.
We proposed new technique to reduce the interference, using the powerful error control code (BCH+ Alamouti).

Power line commu**fk**cation (PLC) is the communicatio~ ov**u2** power line.
The main problem related to this is the interference with other communication system.
We proposed new technique to reduce th**%** interference, usin**G** the powerful error control code (BCH+ Alamouti).

Fig 4.10 output Text file, A=0.1, T=0.01, SNR=30dB

Power line communication (PLC) is the communication over power line.
The main problem related to this is the interference with other communication system.
We proposed new technique to reduce the interference, using the powerful error control code (BCH+ Alamouti).

Fig 4.11 output Text file , A=0.1, T=0.01, SNR=36dB

(d) output Text file for A=0.1, T=0.01, SNR=20dB (e) output Text file for =0.1,T=0.01SNR=25dB

Power line0#ommunication (PLC) is the communication over power line.
Rie main problem related to th**iu** is **uð**e interference with other **}k**mmunication system.
We proposed new technique to reduce the inerference, using the powerfu**j** **ms**ror

Power line communication (PLC) is the communication over power line.
The main problem related to this is the interference with other communication system.
We proposed new technique to reduce the interference, using the powerful error control code (BCH+ Alamouti).

(f) output Text file for A=0.1,T=0.001, SNR=40dB (g) output Text file for A=0.1,T=0.001 SNR=45dB

Figure 5.27 Real-Time text files transmission (a) Input Text file (b) to (g) output files at different SNR.

Thus a text file (.txt) file is taken as the input, and the information contained therein is converted in to binary data stream. This data is encoded by using BCH code with parameters (*n*=63, *k*=36, *t*=5). Since the length of the code which is of 63 bits, is regarded as one frame. This encoded data is further encoded by Alamouti 2x1 scheme and the doubly-encoded data transmitted over the PLC channel. At the receiver, suitable decoding operations are carried out. The decoded binary data stream is converted into text (.txt) file in frame by frame manner for different A and T values.

Results in Figure 5.26 and 5.27, are obtained assuming that ideal channel state information (CSI) is known to the receiver. This is referred to as realizing space time coding with 'ideal CSI'. CSI knowledge is necessary for space time decoding used in this scheme. In a real communication channel, CSI is not known to the receiver and special attention in the decoding design needs to be given. This is referred to as realizing space time coding with 'derived CSI'. Thus the efficiency of scheme is directly dependent on availability of CSI. In practical implementation, when channel state information (CSI) is derived at the receiver, the performance is always less than that obtained for ideal CSI. This is because the estimated or derived CSI may not always be equal to real CSI values for a communication channel. The immediate inference that can be drawn from the results obtained for scheme 2 is that Alamouti space time (2x1) code can be successfully used to convey information over a power line channel for a wide variety of channel conditions provided accurate CSI is available at the receiver.

In computing the results shown in Figure 5.26, channel state is fixed to be equal to 1 for first 32 bits and equal to 0.5 (attenuation of 6 dB) for the remaining 31 bits in each frame of 63 bits. Therefore in order to verify the performance to a near realistic channel situation, performance was evaluated with a channel attenuation which was designed to change for every frame ($|H(f)|$<0 dB). Figure 5.28 shows the results of one of these tests.

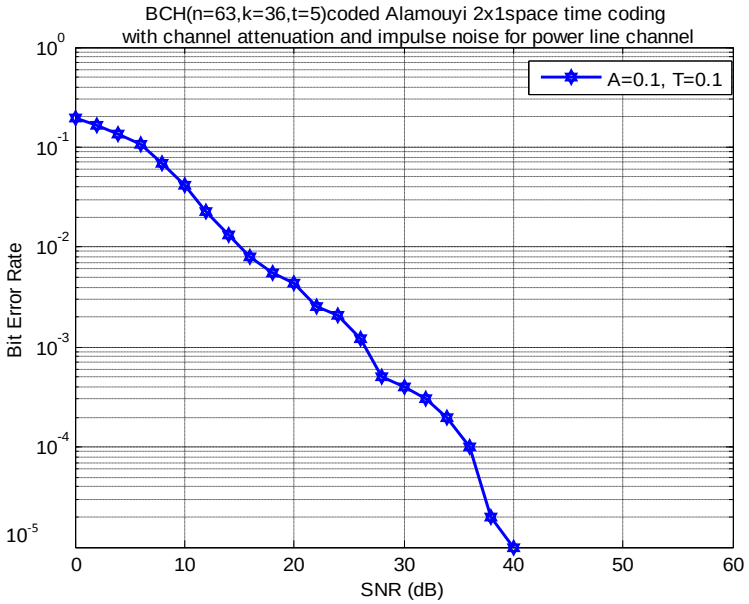

Figure 5.28 BER vs. SNR for $\mathrm{A} = 0.1, \mathrm{T} = 0.1$ (case-1) with channel attenuation.

Figure 5.28 shows BER vs. SNR plot for BCH coded space time code, with channel parameters specified by $A = 0.1, T = 0.1$(case-1 of noise) and channel attenuation changing with every transmitted frame. In Figure 5.29 (a) and (b), snap shots of attenuation along path-1 and path-2 are shown for one of the frames. In Figure 5.28, the system has been able to provide a BER of 10^{-5} at a SNR value of approximately of 40 dB. This performance can be compared with the plot shown in Figure 5.15 where the performance of Turbo OFDM (scheme-1) has been documented. It is seen that the Turbo-OFDM system requires an approximate SNR of

55 dB to yield similar BER results.

To observe the channel environment present when results of Figure 5.28 were obtained, channel attenuation and channel noise are plotted as shown in Figure 5.29 and in Figure 5.30 respectively. Both the paths-1 and 2 have low attenuation and the noise is characterized by parameters $A = 0.1, T = 0.1$(case-1 of noise).

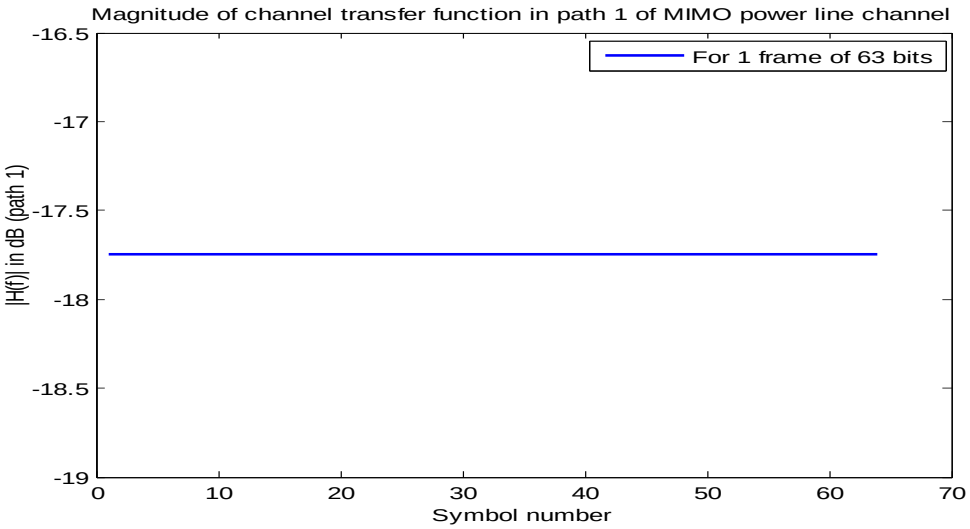

(a) For path 1

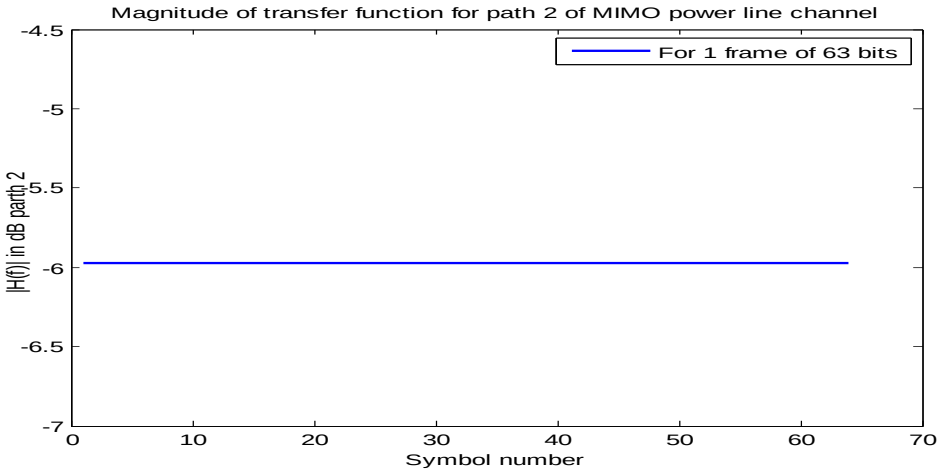

(b) For path 2

Figure 5.29 Atenuation in simulated 2x1 power line channel

for one of the frames seen at random instant.

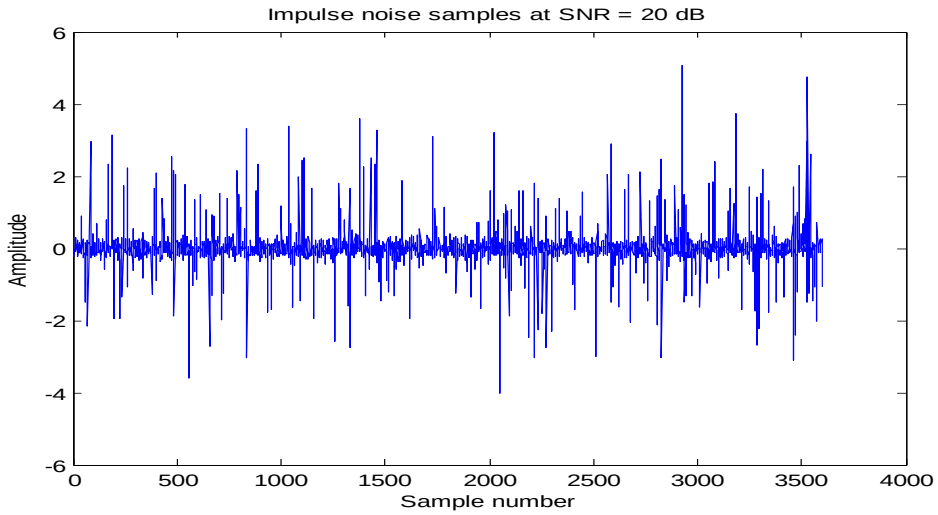

(a)

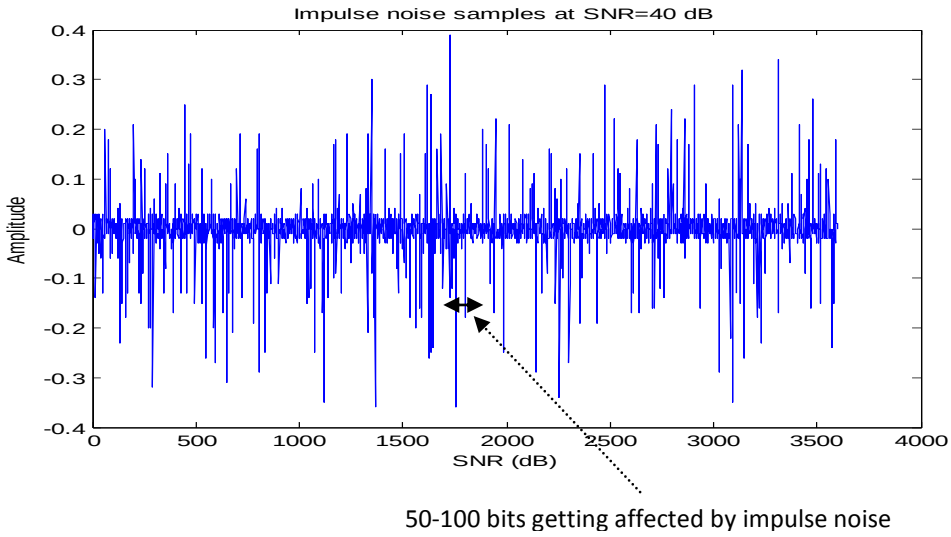

(b)

Figure 5.30 Impulse noise in simulated 2x1 power line channel for (case-1 of noise). (a) at SNR = 20 dB (b) at SNR=40 dB.

Figure 5.30 (b) shows that about a group of about 50 to 100 bits have got affected by impulse noise and the system takes these corrupted bits as input to decode. Part of correction to erroneous bits is performed by space time decoding and the remaining errors are corrected by BCH code.

In Figure 5.31, performance of Scheme-II for $A = 0.1, T = 0.01$ (case 2 of noise) is shown. Attenuation on two paths of the channel is same as that used for $A = 0.1, T = 0.1$ (please refer case-1:Figure 5.28). The two cases are shown in Figure 5.32 for comparison.

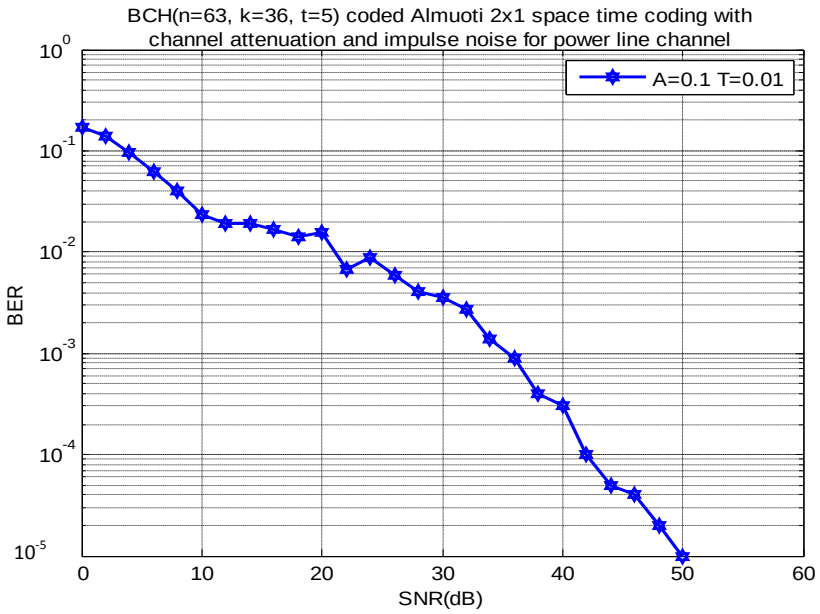

Figure 5.31 BER vs.SNR for A=0.1, T=0.01 (case-2 of noise), with channel attenuation.

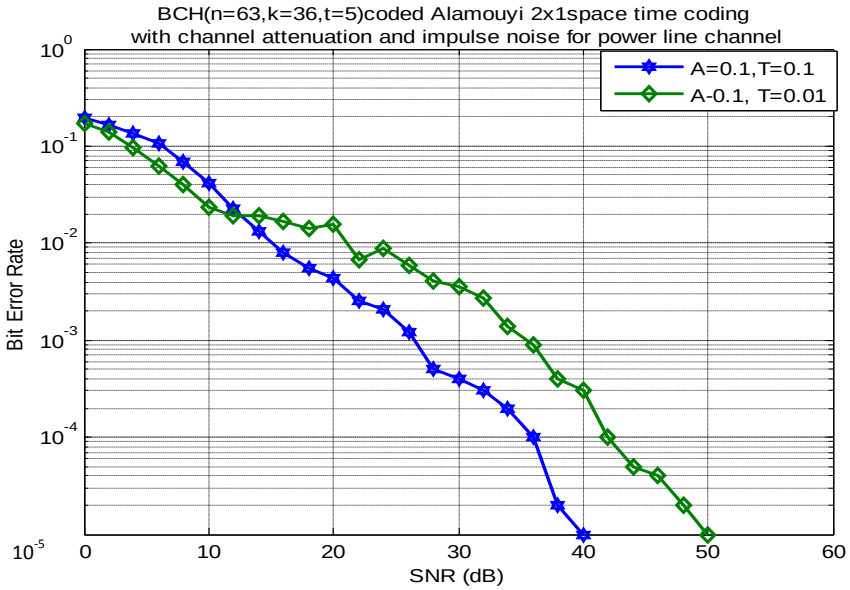

Figure 5.32 Comparison of BER vs.SNR with channel attenuation

for case 1 and case 2 impulse noise.

Figure 5.32 gives the performance of BCH coded Alamouti 2x1 space time coding for power line channel with parameters used in the channel model as per Table 5.8.

Table 5.8 Parameters used in the channel model for comparison graph in Figure 5.32.

Distance between transmitter and receiver point (m)	Number of disturbing load points between transmitter and receiver point and their distances(m)	Attenuation in path 1	Attenuation in path 2
500	5: 100 200 300 400 500	18 dB (low)	6 dB(low)

Referring to Figure 5.32, it is seen as the channel becomes more impulsive (T decreases from 0.1 to 0.01), SNR requirement increases by 10 dB.

Figure 5.33 gives the performance of BCH coded Alamouti 2x1 space time coding for power line channel with parameters used in the channel model as per Table 5.9. Channel attenuation levels have increased and range over values 16-34 dB.

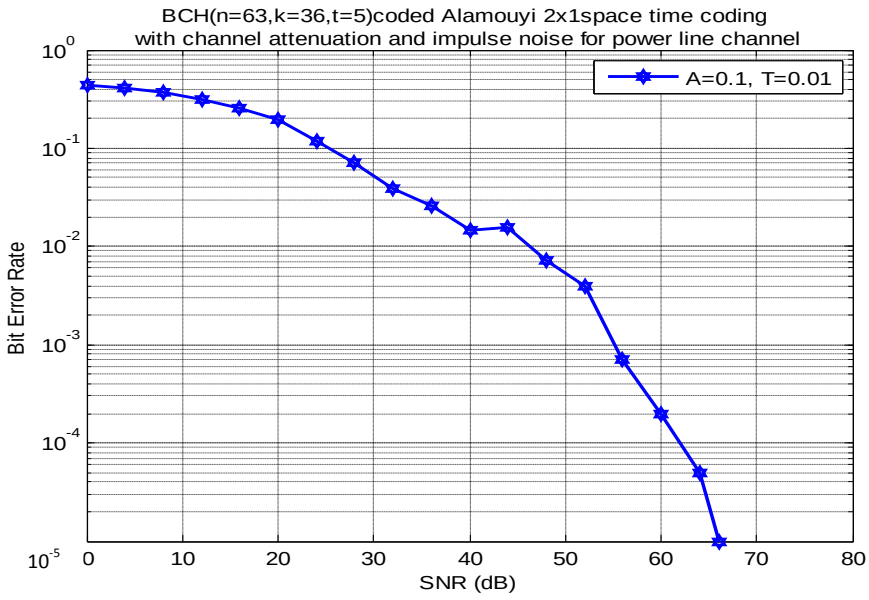

Figure 5.33 BER vs.SNR with channel attenuation as medium, with $A = 0.1, T = 0.01$.

Table 5.9 Parameters used in the channel model for the graph in Figure 5.33.

Distance between transmitter and receiver point (m)	Number of disturbing load points between transmitter and receiver point and their distances(m)	Attenuation in path 1	Attenuation in path 2
500	5: 100 200 3000 400 500	16 dB (low)	34 dB (medium)

Referring to Figure 5.31 and Figure 5.33, it is seen as the channel attenuation increases, the SNR requirement increases by nearly 16 dB (from 50 dB to 66 dB) even when the values of A and T remain unchanged.

5.3.4 Inferences and conclusions for results of scheme 2: BCH coded Alamouti 2x1 space time code

At this stage it is necessary to overview the results with those of scheme 1. Results seen in Figures 5.15 for Turbo coded OFDM (scheme1) and results shown in Figures 5.32 and 5.33 for BCH coded Alamouti space time code (scheme 2), are arranged in Table 5.10 as shown below.

Table 5.10 Overview of results for scheme 1 and scheme 2

	Distance between transmitter and receiver point (m)	Number of disturbing load points between transmitter and receiver point and their distances(m)	Attenuation in path 1	Attenuation in path 2	Noise case (A and T)	SNR at which BER=10^{-5}
Scheme 1	500	5: 100 200 300 400 500	10 to 50 dB (low to medium)	Not applicable	Case 1 (A=0.1, T=0.1)	56 dB
Scheme 2	500	5: 100 200 300 400 500	5 dB to 30 dB (low to medium)	5 dB to 30 dB (low to medium)	Case 1 (A=0.1, T=0.1)	50 dB
Scheme 1	500	5: 100 200 300 400 500	10 to 50 dB (low to medium)	Not applicable	Case 2 (A=0.1, T=0.01)	66 dB
Scheme 2	500	5: 100 200 300 400 500	5 to 20 dB (low)	5 to 35 dB (medium)	Case2 (A=0.1, T=0.01)	66 dB

The results tabulated in Table 5.10, have been obtained for scheme-I and scheme-II. While computing the parameters, it has been ensured that distances between transmitter and receiver point (500 m) are identical. Further, the number of disturbing load points (*N*) at located at distances 100m, 200m, 300m, 400m and 500m. Under these channel condition, inferences drawn from the comparison as per Table 5.10 are listed below:

- Scheme 1 has achieved BER of 10^{-5} at SNR=55 dB for $A = 0.1, T = 0.1$(case 1impulse noise), with 10dB to 50 dB channel attenuation. Scheme 2 has achieved BER of 10^{-5} at SNR=50 dB for $A = 0.1, T = 0.1$(case 1 impulse noise), with 18 dB and 6 dB channel attenuation on two paths.

- Both scheme 1 and scheme 2 have achieved BER of 10^{-5} at SNR=66 dB for $A = 0.1, T = 0.01$(case 2 impulse noise), with 10dB to 50 dB channel attenuation for scheme 1 and with 16 dB and 34 dB channel attenuation on two paths for scheme 2.

  Following remark can be made with reference to the discussion on results:

  Both schemes 1 and 2 have given equivalent performance under similar channel conditions (attenuation and noise), when the error correcting capacity of channel code used in scheme 2 is $t = 5$.

Relative merits of the two schemes can be stated in terms of specific features such as the need for equalization, need for channel state knowledge, number of check bits, bandwidth and complexity.

In the first scheme, a four state Turbo code with rate 1/3 is used. For a specific data stream of say 8 bits, Turbo code generates 30 bits (24 plus 6 tail bits) with 8 bits as information bits and 16 bits as parity or check bits. Assume a dummy 2 bits addition to make a stream of 32 bits. These 32 bits undergo OFDM modulation with binary PSK mapping. To configure the 32 carrier OFDM, a 128 point FFT is used, to allow the guard band between carriers. Thus stream of 32 bits stream from Turbo encoder will now take a length of 128 at OFDM output.

In the second scheme, a narrow sense binary BCH code is used with $k = 36$ and $n = 63$. This means 36 data bits get encoded into 63 bits. The second stage of scheme 2 is Alamouti space time code. And Alamouti scheme 2x1 or 2x2 are rate 1 codes. This means extra bits are not added.

Thus in the first scheme, for every 8 data bits there will be 128 bits on channel whereas in scheme 2, for every 36 data bits, there will be 63 bits on channel. This shows that scheme 2 can be arranged either to give more bit rate or to use less bandwidth than scheme 1.

Assuming that error correcting capacity of BCH code is doubled say by using $n = 63, k = 16, t = 11$ for BCH code. Then for every 16 data bits there will be 63 bits on the channel. Even with this arrangement of reduced number of data bits (k=16), the comparative length of bits

present in the channel for scheme 2 (length of 63 bits for 16 bits), will be still less than for scheme 1(length of 128 bits for 8 data bits). And further the use of $n = 63, k = 16,$ with enhanced error correction capacity($t = 11$), scheme 2 will require lesser SNR to give the same performance as scheme 1, under similar channel conditions. Thus requirement of less bandwidth or higher throughput will be the merits of scheme 2 over scheme 1.

In scheme 1, since OFDM is implemented using IFFT and FFT, equalization is not required and there is no essential requirement of channel state for OFDM decoding. But scheme 2 uses space time coding in which channel state estimation is essential for space time decoding.

Due to the availability of high speed processors, it is possible to implement Turbo code with complexity involved in decoding using BCJR algorithm and BCH code with complexity involved in decoding using Berlekamp Massey algorithm.

Thus with the availability of accurate channel state estimation schemes, space time coding application to PLC can be realized successfully.

Summary: In this chapter, the performance of two channel coding and modulation schemes for medium voltage power line channel have been discussed. Both the schemes are tested on a simulated power line channel experiencing attenuation and impulse noise. Text data was used as input to illustrate the correlation between BER specification and correct retrieval of data. It is found that both the schemes are capable of correcting errors induced by channel perturbations.

The first scheme comprising of a four state Turbo code used as an error correcting code concatenated with 32 carrier OFDM, with binary PSK modulation was designed. The performance was tested with simulated power line channel with two types of load locations (d) as-

(i) $\mathrm{d(m)} = (100,\ 200, 300, 400, 500)$ (ii) $\mathrm{d(km)} = (0.5, 1.0,\ 1.2,\ 1.5,\ 2.0)$

Impulse noise was used with case 1, case 2 and case 3 as per Table 4.2 described as:

(i) $A = 0.1, T = 0.1$(case 1) (ii) $A = 0.1, T = 0.01$ (case 2) (iii) $A = 0.1, T = 0.001$ (case 3)

Attenuation on line was classified as (i) very-low (ii) low (iii) medium as per Table 4.3. In this scheme, Turbo code was observed to give a coding gain of 6 dB over uncoded OFDM.

The second scheme comprised of a binary narrow sense BCH code with

$n = 63, k = 36, t = 5,$ synthesized as an error correcting code and concatenated with Alamouti 2x1 space time code with binary PSK modulation. The scheme was implemented to realize a near realistic approach of PLC, by realizing BCH encoder and BCH decoder in Texas Instrument's TMS 320 C 6713 Digital Signal Processor, which were interfaced using JTAG to MALAB® where simulated power line channel was configured for Alamouti 2x1 space time coding scheme. The performance was tested with the two types of disturbing load locations (d) as:

(i) $d(m) = (100,\ 200, 300, 400, 500)$ (ii) $d(km) = (0.5, 1.0,\ 1.2,\ 1.5,\ 2.0)$

Impulse noise was used with case 1 and case 2 as per Table 4.2 described as:

(i) $A = 0.1, T = 0.1$(case-1)(ii) $A = 0.1, T = 0.01$ (case-2)(iii) $A = 0.1, T = 0.001$ (case-3)

Attenuation on line was classified as (i) very-low (ii) low (iii) medium as per Table 4.3.

Channel State Information (CSI) was used as: ideal

Implementation of this scheme verified the data communication on MIMO power line channel.

Conclusions derived from results of the two are as follows:

Alamouti 2x1 space time code with BCH code with $t = 5$, has behaved equivalent to 32 carrier OFDM with four state Turbo code for similar channel attenuation and noise conditions.

Chapter 6

CONCLUSIVE REMARKS AND SCOPE FOR FUTURE WORK

The possible use of medium voltage power line as communication medium in a substation environment has gained attention of researchers in recent years. This is motivated by the fact that `Smart Grids' have to become a reality in the near future. As the power line channel is a harsh communication medium, the design of proper combination of error control code and digital modulation, form an important aspect of modem design. Medium voltage lines are characterized by large distances between transmitter and receiver points as compared to low voltage lines used for broadband application.

"Application of error control codes for data integrity over power lines" is the topic chosen for research work presented in this thesis. The necessity and significance of using medium voltage lines for narrow band data communication has been discussed in Chapter-1. A description of the state of the art along with extensive literature survey is provided in Chapter-2, in which an overview of major developments in recent years is enumerated. IEEE 1901.2 is the ongoing standard for narrowband PLC. IEEE 1901.2 standard has suggested the use of OFDM for modulation of digital data for narrowband PLC. An examination of this material has led to the conclusion that OFDM, BCH codes, Turbo codes and space time codes have the potential to be effective in correcting errors likely to be induced in PLC channels. Keeping these points in consideration, essential theoretical concepts and design procedures needed to appreciate and implement OFDM and Alamouti space time codes have been discussed in Chapter-3. A rate 1/3 Turbo code with a 4-state encoder has been used in this application. A BCH code with parameters $n = 63, k = 36$ and $k = 5$ was synthesized and was used as an outer code in the concatenated arrangement involving Alamouti Space-Time Code. In Chapter-4, power line channel was modeled using multipath model for channel attenuation and Middleton Class-A noise model to represent impulse noise. Two schemes (one involving Turbo coded OFDM and the other involving BCH coded Alamouti) were designed and deployed for verification of data integrity on power line in Chapter-5. Results demonstrating the efficacy of these schemes in preserving information integrity during propagation over Medium Voltage Power Line Channel has been presented in chapter-5.

6.1 Conclusions

1. Medium voltage power line channel can be employed for narrowband power line communication in a substation environment, by use of proper channel coding/ modulation in PLC modem.

2. Turbo code when concatenated with OFDM for the use of narrowband medium voltage PLC, gives coding gain of approximately 6 dB over uncoded OFDM. Impulse noise effects and attenuation effects on power line channel, distance between transmitter and receiver points, determine the performance.

3. The performance of BCH coded Alamouti and Turbo-coded OFDM schemes deployed in this application have been broadly similar.

6.2 Scope for further research

A few directions for further research are enumerated.

A 4-state rate 1/3 Turbo encoder employing uniform interleaver with 32 carrier OFDM arrangement has been used. To further improve performance, following approaches are suggested.

- A more complex Turbo code (higher number of states) can be employed.
- A suitably designed random interleaver can enhance the error correcting capability.
- The number of carriers in the OFDM arrangement can be enhanced.

In the arrangement employing BCH code with Alamouti space time code, BCH code with error correcting capacity $t = 5$ is used and Alamouti 2x1 scheme is used. To enhance the performance, the following modifications can be done.

- BCH code with higher error correcting capacity can be used.
- Other options of space time coding scheme can be tested.

The efficacy of the schemes critically depend on correct channel estimation. This requires knowledge of location and nature of loads because these parameters determine the nature of reflections (which induce multi-path fading) and attenuation offered by the channel. The availability of ideal CSI has been assumed in this thesis. But in the field, this information will have to be gathered by the receiver. The design of efficient algorithms to achieve this objective will be necessary for successful deployment. This can constitute a challenging problem for the researcher.

Using the availability of sophisticated measuring instruments, the average channel conditions for the location intended for use can be measured ahead and the statistics can be utilized to choose the optimum error control code to ensure data integrity. This implies that modem can be designed with the ability to choose the right error control strategy depending on channel conditions.

References

A. Cataliotti, A. Daidone, G. Tinè (2008). "Power line communications in Medium Voltage system: Characterization of MV cables", *IEEE Transactions on Power Delivery*, 23 (4), pp. 1896-1902.

A. Cataliotti, A. Daidone, G. Tinè (2009). "A Medium Voltage Cable model for Power Line Communication", *IEEE Transactions on Power Delivery*, 2009, 24(1), pp.129-135.

Aminuddin B A Kayani and Mohamad Y B (2011). "Performance of OFDM in the Variation of the Path Quantity in Power Line Communications", *International Journal of Mobile and Network Technologies*, 2 (1), pp 44-48.

Amirshahi, P, Navidpour S.M, Kavehrad M (2006). "Performance Analysis of Uncoded and Coded OFDM Broadband Transmission over Low Voltage Power Line Channels with Impulsive Noise", *IEEE Transactions on Power Delivery* 21(4), pp. 1927-1934.

Anna Papaioannou, George D. Papadopoulos and Fotini Niovi Pavlidou (2005). "Performance of Space-Time Block Coding in Powerline and Satellite Communications", *Journal of Communication and Information Systems*, 20(3), pp 174-181.

A J. Han Vinck (2000). "Coded Modulation for Power Line Communications", AEU Journal, pp. 45-49.

Alain Glavieux (2007). "Channel Coding in Communication Networks from Theory to Turbo codes", First South Asian Edition, ISTE Ltd.

Antonio Cataliotti, Dario Di Cara, Giovanni Tinè (2010). "Model of Line to Shield Power Line Communication System on a Medium Voltage Network", *IEEE Instrumentation Measurement Technology Conference Proceedings*, 2010, pp. 1459-1462.

A. Seddiki, A. Djebbari, J .M. Rouvaen, A. Taleb-Ahmed (2007). "Performance Evaluation of BCH correcting codes on a Fading channel using OFDM modulation", *Proceedings of the 11th WSEAS International Conference on Communications*, Agios Nikolaos, Crete Island, Greece, 11, pp. 340-346.

Alexandre Matov (2001). “Measurements and Modeling of Power Line Channel at High Frequencies”, *Proceedings of International Conference on Advances in Communications*, Rhodes, Greece, pp 118-123.

A. Purroy A. Sanz J. I. García Nicolás I. Urriza (2004). “Research Areas for Efficient Power Line Communication Modems”, *8th International Symposium on Power Line Communication*, Zaragoza, Spain.

Ahmed J. Jameel and You Xiaohu (2003). “Concatenation of Turbo Codes and Space-Time Block Codes for Fading Channels”, *Proceedings of ICCT*, 2, pp.1198-1201.

Anand Dabak, Han Kim, Badri Varadarajan, Tarkesh Pande [2012]. “Channel Modeling for MV/LV AMI Applications in the Frequency Range < 500kHz”, White paper, Texas Instruments.

Antti Kosonen (2008). “Power Line Communication in Motor cables of Variable speed electric drives − Analysis and Implementation, Ph. D. Thesis, Lappeenranta University of Technology, Lappeenranta, Finland.

Bamidele Adebisi, Saqib Ali and Braham Honary (2009). “Space-Frequency and Space- time Frequency M3FSK for Indoor Multiwire Communications”, *IEEE Transactions on Power Delivery*, 24 (4), pp. 2361 - 2367.

Bernard Sklar (1997). “Rayleigh Fading Channels in Mobile Digital communication Systems Part II: Mitigation”, *IEEE Communications Magazine,* pp.102-109.

Bertrand Muquet, Zhengdao Wang, Georgios B. Giannakis, Marc de Courville and Pierre Duhamel (2002). “Cyclic Prefixing or Zero Padding for Wireless Multicarrier Transmissions”, *IEEE Transactions on Communications*, 50(12), pp.2136-2148.

Bruce R. Trull (2006). “Overview of Broadband over Power line”, *River College Online Academic Journal*, 2(1), pp. 1-4.

Bernard Sklar (1988). “Digital Communications Fundamentals and Applications”, Prentice Hall.

Berrou, Alain Glavieux, and Thitimajashima (1993). “Near Shannon Limit Error-Correcting coding and Decoding: Turbo Codes”, *IEEE International Conference on Communications (ICC)*, Geneva May 1993, pp. 1064-1070.

C. E. Shannon (1948). “A mathematical theory of communications”, *Bell systems Technical. Journal*, 27, pp. 379 - 423.

Christine Hsu, Neng Wang, Wai-Yip Chan and Praveen Jain (2007). “Improving a Power Line Communications Standard with LDPC Codes”, *EURASIP Journal on Advances in Signal Processing*, pp. 1-9.

Claude Berrou, Joachim Hagenauer, Marco Luise, Christian Schlegel, Luc Vande ndorpe (2007). “Turbo Information Processing:Algorithms, Implementations & Applications”, *Proceedings of the IEEE*, 95(6), pp. 1146-1149.

C. Hensen, W. Schulz and S. Schwarze, (1999). “Characterisation, measurement and modeling of MV power-line cables for high data rate Communication”, *Proc. Int. Symp. Power-Line Commun. and Its Apps, (ISPLC’99)*, Lancaster, UK, April 1999, pp. 37-44.

Carlos L Giovaneli, Paddy Farrell, Bahram Honary (2003). “Application of Space Time Block Codes For Power Line Communication Channels”, *7th International Conference on Power line Communication and its application*, Kyoto, Japan, pp. 50-55.

Christian H. Calle Gustavsson, Mårten Sander, Peter Sidén, Roland S., Andreas Vedin (2001). “Full Duplex OFDM Modem Over a Frequency selective Channel”, Project Course in Signal Processing and Digital Communication Royal Institute of Technology, May 2001.

Cigre (2004). “Automation of new and existing substations: why and how”, The working group B5.07, report.

Daniel J. Costello and G David Forney (2007). “Channel Coding: The Road to Channel Capacity, *Proceedings of the IEEE*, 95(6), pp. 1150-1177.

D. Forney, "On decoding Bos-Choudhari-Hocquenghem codes(1965)”. *IEEE Transactions on Information Theory*, 11, pp. 549-557.

Donald G. Fink and H. Wayne Beaty (2000), Standard Handbook for Electrical Engineers, McGraw-Hill.

Dusan Matic (1999), JPL's wireless Communication Reference website. http://www.wirelesscommunication.nl/reference/chaptr05/ofdm/ofdmmath.htm

Ezio Biglieri, Politecnico di Torino (2003). "Coding and Modulation for a Horrible Channel", *IEEE Communications Magazine,* 41(5), pp. 92-98.

E. R. Berlekamp, "On decoding Bose-Chaudhuri-Hocquenghem codes (1965)". *IEEE Tranactions on Information Theory*, 11, pp. 577-580.

Eric Lawrey, (1997). "The suitability of OFDM as a modulation technique for wireless telecommunication, with a CDMA comparision".

http://www.skydsp.com/publications/index.htm

F. N. Pavlidou, A.J. Han Vinck, J. Yazdni, B. Honary (2003). "Power Line Communications: State of the Art and Future Trends", *IEEE Communications Magazine*, pp. 34 - 40.

Francis Berrysmith (2005), "A Multipath Model for the Power Line Channel", www.ele.auckland.ac.nz/archives/reports2005/pdfs/Telecommunications.

Federal Communications Commission, Rules – Part 15 (2005). Available at:

http://www.fcc.gov/oet/info/rules/part15/part15-91905.pdf

Göran N. Ericsson (2004). "Communication Requirements-Basis for Investment in a Utility Wide-Area Network", *IEEE Transactions on Power Delivery*, 19(1), pp. 92-95.

Gianaroli, F.; Barbieri, A.; Pancaldi, F.; Mazzanti, A.(2010). "Vitetta, G.M.; A Novel Approach to Power-Line Channel Modeling", *IEEE Transactions on Power Delivery*, Vol.25, No.1, pp. 132-140.

Hai Xu, Shiyuan Yang (2006). "A Loosely Synchronous-Coded OFDM System for Power-Line Communications in Home Networks", *IEEE Transactions on Power Delivery*, 21(4), pp. 1912-1918.

Halid Hrasnica et al. (2004). “Broad band Power line Communications Networks, Network Design “, John Wiley & Sons.

Haixia Zhang,Dongfeng Yuan, Feng Zhao, Dalei Wu (2004). “Performance Research Between Turbo and LDPC Coded WOFDM on Rayleigh Fading Channels”, *Proceedings of the 2nd International Conference on Information Technology for Application (ICITA).*

Hao, Lin; Guo, Jingbo (2007). “A MIMO-OFDM Scheme over Coupled Multi- conductor Power-Line Communication Channel, *IEEE International Symposium on* Power Line Communications and Its Applications, pp. 198-203.

Hua, Z.; Wu, J.; Mueller-Glaser, K.D.; Simon, O. (2006). “A Noise Analysis Based Channel Coding Technique for Multicarrier Channel of an Industrial PLC System”, *IEEE International Symposium on Power Line Communications and Its Applications (ISPLC)*, pp. 22-26.

Hank Wallace (2001). “Error Detection and Correction using BCH codes”. Phil Sutterlin and Walter Downey, (2000), “A Power Line Communication Tutorial –Challenges and Technologies”, Echelon Corporation.

J. I. Escudero, J. A. Rodríguez, M. C. Romero and S. Díaz (2005). “Deployment of Digital Video and Audio Over Electrical SCADA Networks”, *IEEE Transactions on Power Delivery,* 20(2), pp. 691-695.

J. Ebel, Member and William H Tranter (1995). “The Performance of Reed-Solomon Codes on a Bursty-Noise Channel”, *IEEE Transactions on Communications*, 43(2/3/4), pp. 298-306.

John G. Proakis (1995). “Digital Communications”, 3rd ed., McGraw-Hill.

John G. Proakis and Masoud Salehi (2006), “Communication Systems Engineering”. Prentice Hall, 2006.

John S. Barnes (1998). “A Phisical Multi-Path Model for Power Distribution Network Propagation”, ISPLC 1998.

Jin Young Kim (2004). “Turbo coded OFDM/QAM scheme for a high speed power line communication”, Zaragoza, 8th International Symposium on Power Line Communication, Zaragoza, Spain.

Jin Young Kim. “Turbo coded OFDM/QAM scheme for a high speed power line communication system”.

J. Curk, I. Kobal, G. Parkelj Iskra Sistemi Slovenia (2006). “Standard IEC 61850 opens possibility to develop new more efficient architectures of substation automation and protection systems”.

http : //www.cigre.org CIGRE 2006

Jordi Palet, “Power Line Integration, Executive Summary”, v0.5, 6 power Information Society Technologies.

Klaus M. Dostert (2003). “Telecommunication over the Power Distribution Grid Possibilities and Limitations”, *IEEE Transactions on Industry Applications*, 39, pp.

1-9.

Klaas De Craemer, Geert Deconinck. “Analysis of State-of-the-art Smart Metering Communication Standards”.
https://lirias.kuleuven.be/.../1/SmartMeteringCommStandards.pdf

Khalifa Saleh Al Mawali (2011). Techniques for Broadband Power Line Communications: Impulsive Noise Mitigation and Adaptive Modulation”, Ph. D. Thesis, RMIT University.

Leslie A. Berry (1981). “Understanding Middleton's Canonical Formula for Class-A Noise”, *IEEE Transactions on Electromagnetic compatibility*, 23(4), pp. 337 - 344.

Lampe L, Vinck AJHan (2011). “On cooperative coding for narrow band PLC networks”, *International Journal on Electronics and Communication*.

LiPing Lu, GangYan Li, YeQiong Song (2006). “Powerline Communication System for Monitoring and Supervision of Feeder Equipments for MV Substation Automation”, *International Symposium on Industrial Embedded Systems.*

L. Stadelmeier, D Schill (2008). “MIMO for Inhome Power Line Communications”, *IEEE Global Telecommunication Conference*, pp. 1-5.

Lotito A., Fiorelli R. Arrigo D. Cappelletti R.(2007), “A complete Narrow-Band Power Line Communication node for AMR, *IEEE International Symposium on PLC and applications*, pp. 161-166.

Luis F. Montoya (2006), “Power Line Communications Performance Overview of the Physical Layer of Available protocols”.
masters.donntu.edu.ua/2006/kita/avramenko/library/lib9a.pdf

E Lawrey (1997). “The suitability of OFDM as a modulation technique for Wireless telecommunications, with a CDMA comparison”, Ph. D. Thesis.

Matthias Götz, Manuel Rapp and Klaus Dostert (2004). “Power line channel characteristics and their effect on Communication System design”, *Communications Magazine*, IEEE, 42(4), pp. 78-86.

M. Zimmermann and K Dostert (2002). “A multipath model for the power line channel”, *IEEE Transactions on Communication*, 50(4), pp. 553-559.

M. Zimmermann and K. Dostert (2002). “Analysis and modeling of impulsive noise in broad-band power line communications,” *IEEE Transaction on Electronic Comp.*, 44, pp. 249-258.

Masaaki Katayama, H Okada (2006). “A Mathematical Model of Noise in Narrowband Power Line Communication Systems”. *IEEE Journal on Selected Areas in Communications* 24(7), pp. 1267.

M. M. Ahmed, W. L. Soo (2008). “Power Line Carrier (PLC) Based Communication System for Distribution Automation System”. *2nd IEEE International Conference on Power and Energy*, Johor Baharu, Malaysia.

Marcel Nassar, Jing Lin, Yousof Mortazavi, Anand Dabak, Il Han Kim, Brian L. Evans (2012). "Local Utility Powerline Communications in the 3-500 kHz Band: Channel Impairments, Noise, and Standards", *IEEE Signal Processing Magazine, Special Issue on Signal Processing Techniques for the Smart Grid.*

M. Nassar, A. Dabak, I. H. Kim, T. Pande and B. L. Evans (2012). "Cyclostationary Noise Modeling In Narrowband Powerline Communication For Smart Grid Applications", Proc. IEEE Int. Conf. on Acoustics, Speech, and Signal Proc. Kyoto, Japan., 25-30.

M. Zajc, N. Suljanović, A. Mujčić and J. F, "High voltage power line constraints for high-speed communications ", Tasič Laboratory for digital signal, image and video processing, University of Ljubljana, Slovenia.

N. Suljanovic, A. Mujcic, M. Zajc and J. F. Tasic (2004). "Integrated Communication Model of the HV power line channel, "*Proc. IEEE International Symposium o Power Line Communications and Its Applications*, Zaragoza, Spain, pp. 79-84.

Noura Al-Hinai1, Amin Z. Sadik and Zahir M. ussain (2009). "Performance of BCH Coding on Transmission of Compressed Images over PLC Channels", *International Conference on Advanced Technologies for Communiations*.

Noura Yahya Al-Hinai (2010). "Transmission of Compressed Images over Power Line Channel", Ph. D. Thesis, RMIT University.

Open meter, Open Public (2009). Extended Network metering Energy Theme; Grant Agreement No 226369.

www.openmeter.com

O. Ohno(1998). "A Simple Model of Cyclostationary Power-lin Noise". www.isplc.org/docsearch/Proceedings/1998/pdf/0461_001.pdf

http://www.answers.com/topic/power line communication #wp_note-1

Patrick J. Langfeld (2001). "The Capacity of typical Power line Reference Channels and Strategies for System Design", Proceedings of International Symposium on Power line communication and its applications, pp. 271-278.

Phil Sutterlin and Walter Downey, “A Power Line Communication Tutorial –Challenges and Technologies”.

www.viste.com/LON/tools/PowerLine/pwrlinetutoral.pdf

Phil Sutterlin and Walter Downey. “A Power Line Communication Tutorial –Challenges and Technologies”.

www.viste.com/LON/tools/PowerLine/pwrlinetutoral.pdf

Riccardo Pighi and Riccardo Raheli (2007). “Linear Predictive Detection for Power Line communications Impaired by Colored Noise”, *EURASIP Journal on Advances in Signal Processing*.

Ralph Chassaing (2002). “DSP Applications Using C and the TMS320C6xDSK”, John Wiley & Sons.

Robson, Manu Haddad, Huw Griffiths(2009). “Simulation of Narrowband Power Line Communication using ATP-EMTP*”, North American Power Symposium (NAPS).

RSGB EMC Committee for the PLC Workshop in Brussels (2001). “Compatibility between Radio communications services and Line communication systems”, A position paper.

S.M. Alamouti (1998). "A simple transmit diversity technique for wireless communications". *IEEE Journal on Selected Areas in Communications,* 16(8), pp. 1451-1458.

Sinem Coleri, Mustafa Ergen, Anuj Puri and Ahmad Bahai (2002). “Channel Estimation Techniques Based on Pilot Arrangement in OFDM Systems”, *IEEE Transactions on Broadcasting*, 48(3), pp. 223-229.

Shu Lin, D. J. Costelo (2003). “Error Control Coding Fundamentals & Applications”, Second edition, Prentice Hall.

Stephen Robson, Manu Haddad, Huw Griffiths (2009). “Simulation of Narrowband Power Line Communication using ATP-EMTP*”, *North American Power Symposium (NAPS)*.

Serena M. Zabin(1989). “Identification of Impulsive Interference Channels”, Coordonated Scienc Laboratory, Ph.D. Thesis, College of Engineering, University of Illinois.

Theodore S. Rappaport (2002). Wireless Communications Principles and Practice, Second Edition, Pearson Education.

T. Banwell and S. Galli (2001). “A new approach to the modeling of the transfer function of the power line channel”, *Proc. International Symposium on Power Line Communication and Its Applications*, pp. 319–324.

TMS320C67x/C67x+ DSP CPU and Instruction Set, Reference Guide.

Malayasian Communication and Multiledia Commission (2005). Deployment of Power Line Communications Systems in Malaysia.

V. Tarokh, N. Seshadri, and A. R. Calderbank (1998). “Space-time codes for high data rate wireless communication: Performance criteria and code construction,” *IEEE Transactions on Inform. Theory*.

William Y. Zou Yiyan Wu (1995). “COFDM: An Overview”, *IEEE Transactions on Broadcasting*, 41(I), pp.1-8.

William J. Ebel and William H. Tranter (1995). “The Performance of Reed-Solomon Codes on a Bursty-Noise Channel”, *IEEE Transactions on Communications*, 43(2/3/4), pp. 298-306.

W. W. Peterson (1960). “Encoding and error-correction procedures for the Bose-Chaudhuri codes," *IEEE Transactions on Inform. Theory*, IT-6, pp. 459-470.

W. Baass et al. (2004). “Automation of new and existing substations: why and how”', Cigre working group B5.07, report.

Yu-Ju Lin Latchman, H.A Minkyu Lee, Katar S. (2002). “A Power Line Communication Network Infrastructure for the Smart Home”, *IEEE Transactions on Wireless Communications*, 9(6), pp. 104-111.

Yihe Guo, Zhiyuan Xie and Yu Wang (2009). “A Model for 10kV Overhead Power Line Communication Channel”, *Symposium on International Computer Science and Computational Technology*, Huangshan, China, pp. 289-292.

APPENDIX A

INTRODUCTION TO TMS32067xx DIGITAL SIGNAL PROCESSOR

TMS320 DSP FAMILY OVERVIEW

The TMS320 DSP family consists of fixed-point, floating-point and multiprocessor digital signal processors (DSPs). TMS320 DSPs have an architecture designed specifically for real-time signal processing and support complex applications that often require multiple operations to be performed simultaneously. The C6x notation is used to designate a member of the Texas Instruments (TI) TMS320C6000 family of digital signal processors. The architecture of the C6x digital signal processor is very well suited to numerically intensive calculations. Based on a very long instruction word (VLIW) architecture, the C6x is considered to be TI's most powerful processor family.

The Texas Instrument TMS320C6713 Digital Signal Processing Starter Kit is low cost development platform for real time digital signal processing application. It comprises a small circuit board containing TMS320C6713 floating point digital signal processor and a TLV320AIC23 analog interface circuit (codec) and connects to a host PC via USB port. PC software Code Composer Studio (CCS) is provided in order to enable software written in C or assembly language to be compiled and/or assembled, linked, and downloaded to run on the DSK.

Digital signal processors are used for a wide range of applications, from communications and control to speech and image processing. Overall, DSPs are concerned primarily with real - time signal processing. Real - time processing means that the processing must keep pace with some external event; whereas non real - time processing has no such timing constraint. The external event to keep pace with is usually the analog input. While analog based systems with discrete electronic components including resistors and capacitors are sensitive to temperature changes, DSP based systems are less affected by environmental conditions such as temperature. DSPs enjoy the major advantages of microprocessors. They are easy to use, flexible and economical.

'TMS320C67x/C67x+ DSP CPU and Instruction Set Reference Guide' gives technical information about: The C6000 Central Processing Unit (CPU), TMS320C6713 DSP, The General Purpose Register File, Integer and Floating-Point Word Formats, The Multiplier, Interrupts,

Memory Organization for the TMS320C6713 DSK, Enhanced Direct Memory Access Controller (EDMA), Serial Ports, Other Internal Peripherals, TMS320C6000 Instruction Set, Pipelining etc.

C6713 DSK BOARD

The DSK packages are with the necessary hardware and software support tools for real time signal processing. The DSK boards, which measure approximately 5 × 8 inches, include either a 225 MHz C6713 floating point digital signal processor or a 1 GHz C6416 fixed point digital signal processor and a 16 bit stereo codec TLV320AIC23. The DSK boards each include 16 MB (megabytes) of synchronous dynamic RAM (SDRAM) and 512 kB (kilobytes) of flash memory.

CODE COMPOSER STUDIO

Code Composer Studio (CCS) provides an integrated development environment (IDE) for real time digital signal processing applications based on the C programming language. It incorporates a C compiler, an assembler and a linker. It has graphical capabilities and supports real time debugging. The C compiler compiles a C source program with an extension .c to produce an assembly source file with an extension *.asm*. The assembler assembles *.asm* source file to produce a machine language object file with extension *.obj*. The linker combines object files and object libraries as input to produce an executable file with extension *.out*. This executable file can be loaded and run directly on the digital signal processor.

A Code Composer Studio project comprises all of the files (or links to all of the files) required in order to generate an executable file. A variety of options enabling files of different types to be added to or removed from a project are provided. In addition, a Code Composer Studio project contains information about exactly how files are to be used in order to generate an executable file. Compiler/linker options can be specified. A number of debugging features are available, including setting breakpoints and watching variables, viewing memory, registers, and mixed C and assembly code, graphing results, and monitoring execution time. One can step through a program in different ways (step into, or over, or out).

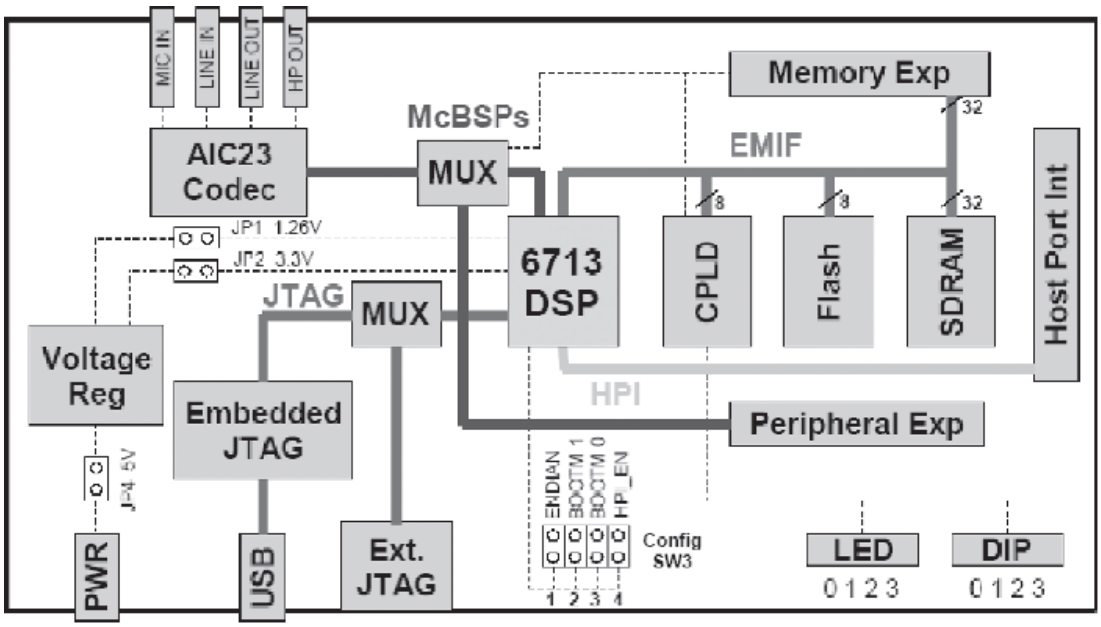

Figure A.1:TMS320C6713 - based DSK board: Block diagram.

INTERFACE BETWEEN DSK AND MATLAB

Realization of BCH encoding/decoding in real time environment is accomplished by making use of TMS320C6713 DSK. Data transfer between the encoder/decoder (DSK) with the power line channel simulated in MATLAB® can be done through Real Time Data Exchange (RTDX) interfacing technique. This is shown using a blockdiagram.

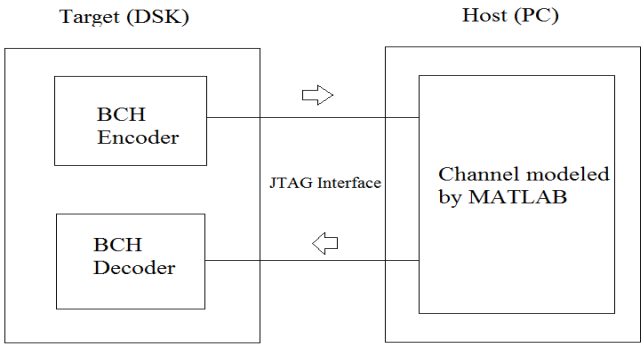

Figure A.2: Block diagram showing the real time data exchange using JTAG interface.

Real Time Data Exchange

RTDX enables real-time, asynchronous exchange of data between the target and the host, without stopping the target application. In essence, the RTDX data link provides a "data pipe" between DSP application and the host. The bidirectional capability allows developers to access data from the application for real-time visibility or to simulate data input to the DSP, perhaps before real time hardware is available. This shortens development time by giving developers a realistic view of the way their systems operate. RTDX is available on XDS510 and XDS560 class of emulators.

Data is analyzed and visualized on the host using the COM interface provided by RTDX. Clients such as Visual Basic, Visual C++, Excel, LabView, MATLAB and others may easily use the COM interface.

Data can be sent from the target application to the host client and vice versa. We can visualize this as a collection of one or more channels, through which the data travels. This tags the data as belonging to a particular channel to distinguish various data. These channels are unidirectional; Data can be input into a channel asynchronously, that is, at any time.

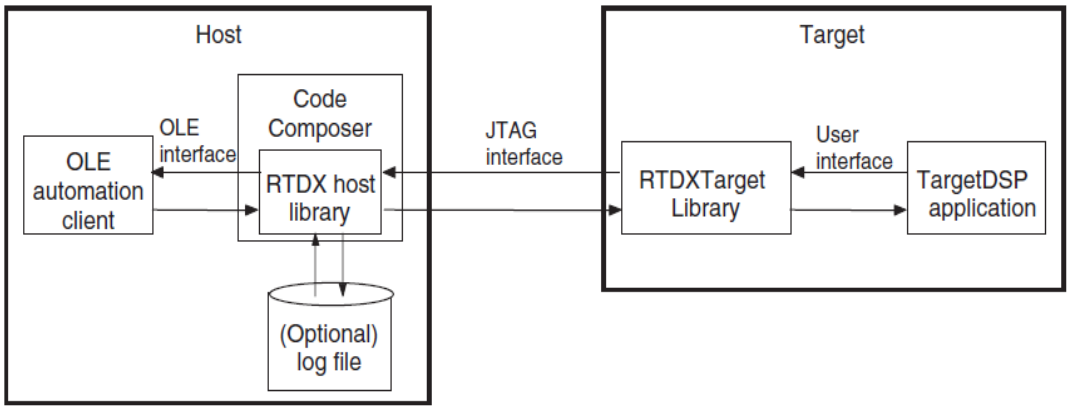

Figure A.3: RTDX interfacing between host (computer system) and target (DSK)

The target application sends data to the host by calling functions in the RTDX Target Library. These functions immediately buffer the data and then return. The RTDX Target Library then transmits the buffered data to the host without interfering in the target application. The host records the data into either a memory buffer or a RTDX log file, depending on the specified RTDX host recording mode. The recorded data can be retrieved by any client host application of the RTDX host interface. Windows™ platform computers provide a COM

interface for the RTDX host interface.

Similarly, a host client can send data to the target. The RTDX Host Library buffers all data sent to the target. If the RTDX Host Library receives a data request from the target application with sufficient data in the host buffer to satisfy the request, it sends the data to the target. The data is written to the requested location without interfering with the target application. The host notifies the RTDX Target Library upon operation completion.

To review its key benefits, RTDX:

- Provides continuous bi-directional data exchange without halting an application
- Functions in real time with minimal perturbation on the application
- Uses TI's universal JTAG data path and TI's debugger
- Displays data using your favorite OLE-enabled visualization package
- Is easy to program on both target and host
- Is a capability offered at no additional cost.

Problems faced during interfacing and debugging techniques

During interfacing one may face several kinds of problems. The communication between DSK and PC (Personal Computer) may not start only or even if it starts it is one way communication. In such a case one should verify first whether the necessary header files are included in the project file or not. The problem also can occur if the necessary RTDX channels are not defined in the source file or even if they are defined, if they are not enabled at the time of data transfer. Sometimes the communication may start naturally at the right time as expected but can get aborted showing the error like "RTDX timed out waiting for confirmation". In such problems one should verify whether the variables defined or registers used for holding the sent/accepted data are of required length or not. During the "target to host" data transfer one should also verify whether the processor is made to WAIT until the write operation is complete. This is important because if the processor does not wait while the data are being written into PC the data transfer may get terminated prematurely and RTDX host library will expect all the required amount of data, when this does not occur within the specified time interval it terminates stating the error as "RTDX failure". Despite of the above precautions sometimes the execution of source program in the DSK enters an infinite loop. At such situations MATLAB® may not possess any bugs and problem occurs usually if there are bugs in the source program.